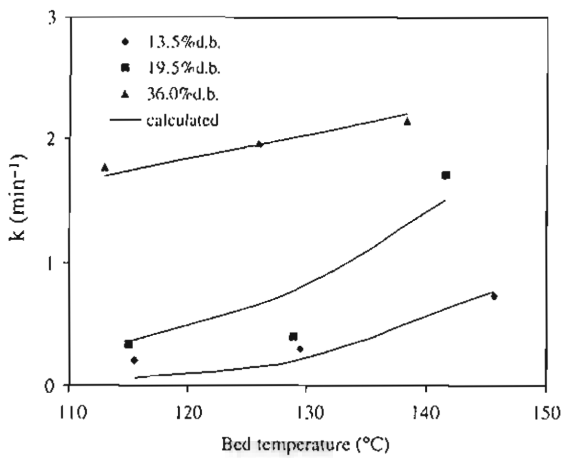

Figure 8. Apparent rate constant for inactivating urease enzyme at different temperatures and initial moisture contents.

increase in the reaction rate constant from 0.43 to 1.7 min^{-1} when the corresponding bed temperature rises from 113 to 140°C. This effect turns into lesser importance for the higher initial moisture content, as indicated by a linear increase in the apparent reaction rate constant with increasing temperature for soybean sample at 36% d.b. At such high initial moisture content, the prevalent contribution of moisture initially present in soybeans induces the rapid inactivation in the first 2 min of drying, by which the residual urease activity lies between 15 and 17% after soybeans are treated with temperature in the range studied.

The rate constant and equilibrium activity are empirically correlated with the initial moisture content and bed temperature, and their relationships are given by the following equations:

$$k = \left(5.7696 \times 10^{-18} + 1.3531 \times 10^{-16} M_{\text{in}} - \frac{8.59758 \times 10^{-15}}{T}\right) \times \exp(-0.245571 T M_{\text{in}} + 97.7304 M_{\text{in}} + 0.09702 T) \quad (9)$$

$$C_{\text{eq}} = \left(-0.047523 + 0.071742 M_{\text{in}}^2 + 0.000122 T\right) \times \exp\left(-\frac{978.15 M_{\text{in}}}{T} + \frac{3227.286}{T}\right) \quad (10)$$

As shown in Fig. 7, the kinetic model of urease inactivation proposed, along with its constant parameters in Eqs. (9) and (10), can reasonably predict the experimental data.

Color Changes

The changes in color of a product reflect a sensation to human eye and the visual examination is often used to evaluate product color. The *L*-, *a*- and *b*-values of soybean at the beginning are respectively 85.71, 0.38 and 24.33, presenting yellow color. Figure 9 shows the change in the behaviors of *L*-, *a*- and *b*-values for soybeans dried at various steam temperatures, with a progressive decrease of the *L*-value whilst the increase of the *a*- and *b*-values with the increased drying time are evident. The decrease in *L*-value upon heating is attributed to the formation of brown pigments, as a result of Maillard reaction. The linear behaviour of the lightness suggests a zero-order kinetic model.

In addition to the *L*-value, *a*- and *b*-values are also used to indicate characteristics of brown pigments formed by heat treatment. The change of *a*-value is initially slow and followed by a rapid raise of the level of redness. To explain the whole range of redness, the change of a-value follows the Monod kinetic reaction. For the *b*-value, it exponentially increases according to the first-order reaction kinetics. The reaction rate constants of the *L*-, and *b*-values were determined by a linear regression technique whereas the rate constant of the *a*-value was determined by a nonlinear regression because of nonlinearity of Eq. (6). The experimentally determined reaction rate constants are presented in Fig. 10 to show the effect of temperature on their reaction rate constants. The results indicate that the reaction speeds of the color parameters increase with increased temperature. The increase in the reaction speed of the individual color parameters has a difference of magnitude in which the fast reaction speed is the lightness followed by the redness, and the slowest speed is the yellowness. From this figure, it can be seen that the initial moisture content has some effect on the color of soybeans during heat treatment. This influence on the color change is different to that found with the urease inactivation in a way that the higher moisture content slows down the rate of brown pigment formation, as interpreted by lower reaction rate constants of both lightness and redness shown in Figs. 10a and b. The moisture content is not influential to the yellowness change for soybeans. The slow development of brown color is attributed to the fact that the lower concentration of the reactive compounds inside the food material retards the browning rate and this lower concentration

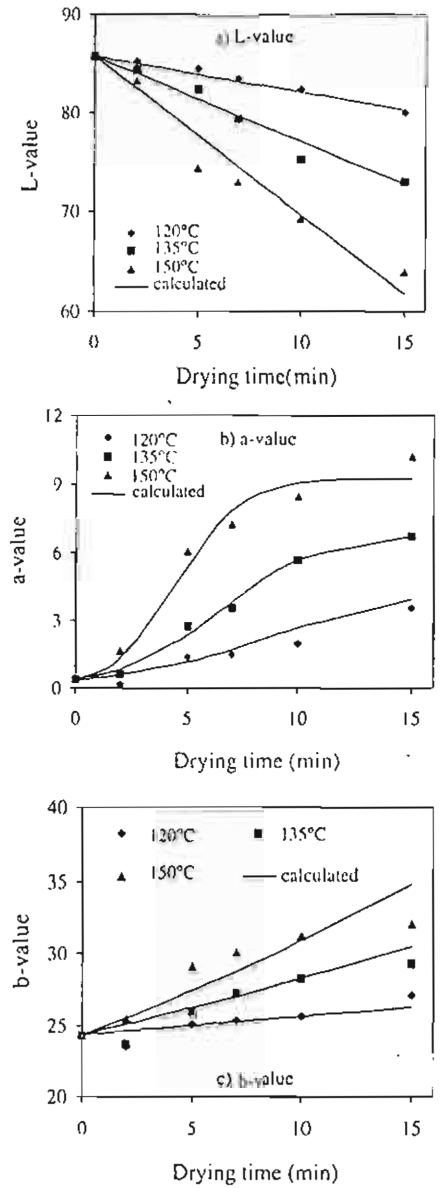

Figure 9. Changes in colour parameters versus drying time for different inlet superheated steam temperatures (initial moisture content of 13.5% d.b.).

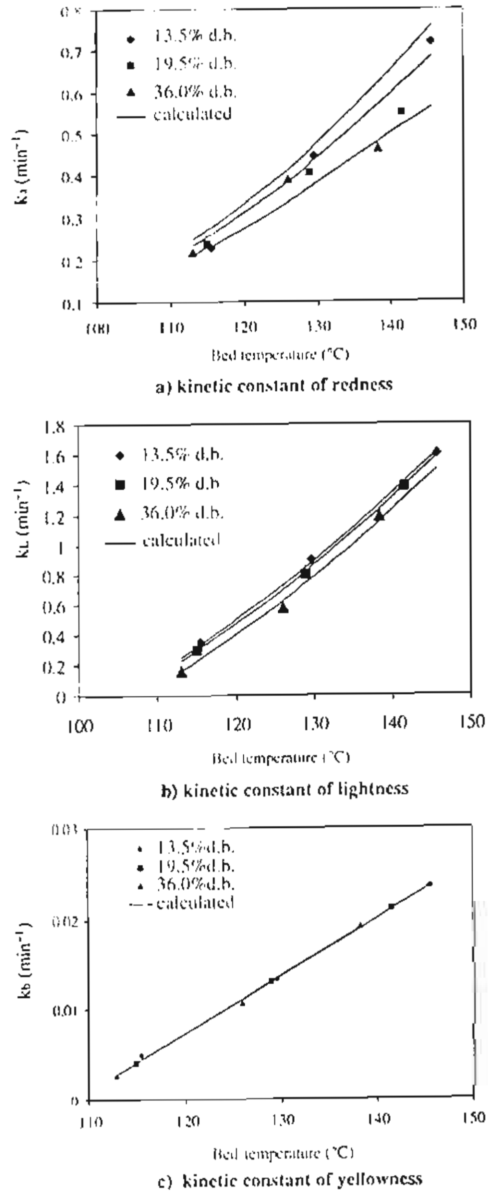

Figure 10. Effect of initial moisture content on colour parameters at various bed temperatures.

effect seems to be more dominant than the effect of reactant mobility, which has higher motivation at elevated initial moisture contents. The effect of water content on the browning rate for food materials has been reported by several workers.[20,23] The results found from their investigations were similar to this finding.

According to the experimental results, such reaction rate constants of the L-, a- and b-values were empirically correlated with the relevant parameters by the following equations:

$$\text{For } L\text{-value} \quad k_L = (-200.35 - 6.8356M_{in} + 0.53253T)\exp\left(-\frac{1087.66}{T}\right)$$
$$R^2 = 0.99, \quad RSS = 0.004 \tag{11}$$

$$\text{For } b\text{-value} \quad k_b = (-0.2435 + 6.4 \times 10^{-4}T)\exp\left(-\frac{5.3 \times 10^{-5}}{T}\right)$$
$$R^2 = 0.99, \quad RSS = 0.0127 \tag{12}$$

$$\text{For } a\text{-value} \quad k_a = [1.5 \times 10^9 - 1.1343 \times 10^8 M_{in} - 3.2052 \times 10^6 T]\exp\left(-\frac{8019}{T}\right)$$
$$R^2 = 0.96, \quad RSS = 0.007 \tag{13}$$

$$c = \left(-66.6919 + 0.181201T + \frac{3417.06M_{in}}{T}\right) \times \exp\left[1.5M_{in} - \frac{898.370M_{in}}{T}\right]$$
$$R^2 = 0.95, \quad RSS = 0.2267 \tag{14}$$

The result for the changes of L-, a- and b-values, calculated by using Eqs. (11)–(14), with drying time are depicted in Fig. 9, suggested that the proposed models can predict the color parameters in a good agreement with the experimental results over a wide range of drying condition.

Protein Solubility

For determining the amount of soluble proteins, some treated soybean samples that contain the level of urease activity lower than the required standard limit were analysed. Changes in protein solubility of soybeans treated at different operating conditions are shown in Table 1. The protein solubility is about 94.3% for raw soybeans and it is decreased faster when the soybeans were subjected to contact with steam at higher temperatures and for longer times. The reduction in protein solubility is caused by the destruction of helical regions of the proteins and subsequent disulfide bond, which links between amino acid groups. Consequently, the proton of hydrogen in water molecules inside proteins will react with the sulfur of disulfide to form as sulfhydryl. However, the formation of sulfhydryl is not stable and protein molecules will aggregate with the neighbouring molecules by disulfide bond, leading to the larger molecules of protein and the subsequent reduction in their dispersability in water.

As shown in Table 1, for the low initial moisture content of 13.5% d.b., the inlet steam temperature of 120°C is sufficiently high enough to inactivate the urease enzyme and the treating time is taken only 7 min, which is four times shorter than the use of the same technique but the hot

Table 1. Protein solubility and lysine content of soybeans treated with superheated steam at various temperatures.

Initial moisture content (%d.b.)	Inlet steam temperature (°C)	Treating time (min)	Moisture content after treatment (%d.b.)	Protein solubility (%)	ΔpH	Lysine content (mg/g of soybean)
Raw soybeans	---		---	94.3	1.9	2.85
13.5	120	7	14.0	85.7	0.2	2.80
	135	5	12.4	71.7	0.03	2.76
	150	5	10.7	54.9	0.04	NA
19.5	120	5	18.3	85.2	0.04	2.67
		15	16.7	75.3	0.005	NA
	135	5	16.5	82.3	0.01	2.71
		7	14.8	76.7	0.005	NA
	150	2	18.9	83.8	0.02	NA
		5	14.1	72.9	0.015	2.82
36	120	2	38.9	80.6	0.05	NA
	135	2	34.1	81.4	0.025	NA
		15	14.7	59.4	0	NA
	150	2	31.6	75.3	0.02	NA
		10	11.4	53.6	0	NA

air replaced the superheated steam.[7,8] Using this temperature, the protein solubility and lysine content maintain at the satisfactory levels of 85% and 2.80 mg/g soybean, respectively. In addition, the color of treated soybeans does not changed much from the beginning, with the values of 83, 1.45, and 25 for the respective lightness, redness, and yellowness related parameters. However, the higher temperature of 120°C is not recommended because of lower protein solubility than the desirable range.

When the superheated steam was introduced to the moist soybeans, it beneficially provides shorter time for inactivation together with high protein solubility and lysine content. Unfortunately, their moisture contents at that treating time are still higher than the level for the extended storage. They therefore need to further dry to the safe moisture content. As can be seen from Table 1, the superheated steam can comply with both requirements, drying and urease inactivation, for soybeans at initial moisture content of 19.5% d.b. while preserving their nutritional value and yellow color as long as the inlet steam temperature varies between 120 and 135°C. At elevated initial moisture content, two-stage drying, where the soybean is treated with superheated steam at such a temperature range for a certain time to inactivate the urease enzyme and then followed with low-temperature hot-air drying to prevent the denaturation of protein and brown color development, should be applied.

CONCLUSION

Soybean treatment using superheated-steam fluidized-bed technique was examined. Steam was initially condensed onto the kernel surface which enables grains to adsorb it. An amount of condensed steam related to steam temperature and initial moisture content in a way that high steam inlet temperature and high initial moisture content reduced the quantity of condensing steam. During evaporation period, the transport of water is governed by internal diffusion and the rate of water removal depends on the temperature and moisture content, the first factor being the most important. During its operation, the urease activity and the color of soybeans, described by three Hunter parameters *L*-, *a*- and *b*-values, are also changed. The rates of urease inactivation and brown pigment formation, corresponding to the decrease of *L*-value and increases of *a*- and *b*-values, were enhanced by increasing temperature. In addition, the inactivation rate was faster whereas the change rates of *L*- and *a*-values became slower with higher initial moisture content, except for the *b*-value which showed an insignificant change. To inactivate

the urease enzyme while maintaining soybean qualities in terms of protein solubility, lysine and color, inlet steam temperature should not exceed 135°C; with 120°C being the minimum required for treating dry soybean. Furthermore, this technique can be acted as the simultaneous operation of inactivating urease and removing water in a single operation for the moist soybean at a certain level.

ACKNOWLEDGMENT

The authors would like to thank the Thailand Research Fund for supporting this work.

REFERENCES

1. Rackis, J.J.; Wolf, W.J.; Baker, E.C. Protease inhibitors in plant foods: content and inactivation. In *Nutritional and Toxicological Significance of Enzyme Inhibitors in Foods*; Friedmann, M., Ed.; Plenum Press: New York, 1986.
2. Abd El-Hady, E.A.; Habiba, R.A. Effect of soaking and extrusion conditions on antinutrients and protein digestibility of legume seeds. Lebensm-Wiss. U.-Technol. **2003**, *36*, 285–293.
3. Alonso, R.; Grant, G.; Dewey, P.; Marzo, F. Nutritional assessment in vitro and in vitro of raw and extruded peas (Pisum sativum). Journal of Agricultural and Food Chemistry **2000**, *68*, 2286–2290.
4. Cheong, Y.L. Fullfat soybean meal production and utilization. *Technical Bulletin of American Soybean Association*, Singapore, 1997.
5. Raghavan, G.S.V.; Harper, J.M. Nutritive value of salt-bed roasted soybeans for broiler chicks. Poultry Science **1974**, *53* (2), 547–553.
6. Valle, F.R. Nutritional qualities of soya protein as affected by processing. Journal American Oil Chemists' Society **1981**, *58* (3), 419–429.
7. Soponronnarit, S.; Swasdisevi, T.; Wetchacama, S.; Wutiwiwatchai, W. Fluidised bed drying of soybeans. Journal of Stored Products Research **2001**, *37*, 133–151.
8. Osella, C.A.; Gordo, N.A.; González, R.J.; Tosi, E.; Ré, E. Soybean heat-treated using a fluidised bed. Lebensm. Wiss u.-Technology **1997**, *30*, 676–680.
9. Salin, J.G. Steam drying of wood for improved particle board and lower energy consumption. Paper and Timber **1988**, *9*, 806–810.

10. Heinrich, S.; Krüger, G.; Mörl, L. Modelling of the batch treatment of wet granular solids with superheated steam in fluidised beds. Journal of Chemical Engineering Processing **1999**, *38*, 131–142.
11. ASA. *Fullfat Soybeans Handbook of American Soybean Association*; Singapore, 1990.
12. Baker, E.C.; Mustakas, G.C. Heat inactivation of trypsin inhibitor, lipoxgygenase and urease in soybeans: Effect of acid and base additives. Journal of the American Oil Chemists' Society **1973**, *50*, 137–141.
13. AACC. *Approved method of the American Association of Cereal Chemist*, 9th ed.; AACC: St. Paul, MN, 1995.
14. Rasmussen. 2002, Determination of residual urease activity. http://www.analytichem.com/Applications/Kjeldah/.
15. American Oil Chemists' Society (AOCS). Protein solubility index. AOCS Official method BA **1979**, 10–63.
16. AccQ-Tag Instruction Manual. *Lysine determination*. Manual no. WAT052874, Revo April, 1993.
17. Saravacos, G.D.; Raouzeos, G.S. Diffusivity of moisture in air drying of raisins. In *Drying'86*; Mujumdar, A.S., Ed.; McGrawHill: Hemisphere, 1986; Vol. 2, 487–491.
18. Ramesh, M.N. Moisture transfer properties of cooked rice during drying. Lebensm. Wiss u.-Technology **2003**, *36*, 245–255.
19. Crank, J. *The Mathematics of Diffusion*, 2nd ed.; Oxford University Press: Oxford, 1975.
20. Rapusas, R.S.; Driscoll, R.H. Kinetics of non-enzymatic browning in onion slices during isothermal heating. Journal of Food Engineering **1995**, *24*, 417–429.
21. Krokida, M.K.; Tsami, E.; Urbricain, M.J. Kinetics on colour changes during drying of some fruits and vegetables. Drying Technology **1998**, *16* (3–5), 667.
22. Avila, I.M.L.B.; Silva, C.L.M. Modeling kinetics of thermal degradation of colour in peach puree. Journal of Food Engineering **1999**, *39*, 161–166.
23. Prachayawarakorn, S.; Sawangduanpen, S.; Saynampheung, S.; Poolpatarachewin, T.; Soponronnarit, S.; Nathakarakule, A. Kinetics of colour change during storage of dried garlic slices as affected by relative humidity and temperature. Journal of Food Engineering **2004**, *62*, 1–7.

Available online at www.sciencedirect.com
SCIENCE DIRECT•
Journal of Stored Products Research 41 (2005) 333–351
Journal of STORED PRODUCTS RESEARCH
www.elsevier.com/locate/jspr

Quality maintenance and economy with high-temperature paddy-drying processes

Somkiat Prachayawarakorn[a,*], Nattapol Poomsa-ad[b], Somchart Soponronnarit[c]

[a]*Faculty of Engineering, King Mongkut's University of Technology Thonburi, Suksawat 48 Road, Bangkok 10140, Thailand*
[b]*Faculty of Engineering and Computer Science, Mahasarakham University, Mahasarakham 44150, Thailand*
[c]*School of Energy and Materials, King Mongkut's University of Technology Thonburi, Suksawat 48 Road, Bangkok 10140, Thailand*

Accepted 25 May 2004

Abstract

Drying processes result in some loss of product quality. Three drying systems for paddy were investigated for their effects on head-rice yield and whiteness. Fluidised-bed drying, tempering and ambient air ventilation units were the main components, but they were arranged differently in each drying system. Heat- and mass-transfer equations were applied to predict the change in moisture content for each drying system. Both the experiments and simulations indicated that the two sub-drying systems (system No. 2) with tempering and ventilation as elements of each stage yielded higher drying capacity and thermal efficiency than the single drying system (system No. 1), in which paddy was treated with the drying, tempering and ventilation units only once. The proportion of full kernels and value of the whiteness obtained from both drying systems were not significantly different. System No. 3, where grains after the first tempering were dried immediately by the second fluidised-bed dryer with no ventilation unit, produced poor head-rice yield and colour and was unacceptable for producing white rice.

Keywords: Dehydration; Fluidisation; Grain; Head rice; Mathematical model

*Corresponding author. Tel.: +662-4270-9221; fax: +662-428-3534.
E-mail address: somkiat.pra@kmutt.ac.th (S. Prachayawarakorn).

0022-474X/$ - see front matter © 2004 Elsevier Ltd. All rights reserved.
doi:10.1016/j.jspr.2004.05.001

Nomenclature

C_a	specific heat of dry air, kJ/kg °C
C_v	specific heat of water vapour, kJ/kg °C
C_{pw}	specific heat of moist paddy, kJ/kg °C
D_{eff}	effective diffusivity, m^2/s
h_{fg}	latent heat of water, kJ/kg
I_c	tempering index, decimal
M	moisture content, dry-basis decimal
M_{eq}	equilibrium moisture content, dry-basis decimal
$M_{i,av}$	average inlet moisture content, dry-basis decimal
$M_{i,n}$	inlet moisture content at nth element, dry-basis decimal
$M_{f,n}$	outlet moisture content at nth element, dry-basis decimal
$M_{s,t}$	surface moisture content at time t, dry-basis decimal
$\dot{m}_i$	mass flow rate of dry fresh air, kg/s
$\dot{m}_p$	mass flow rate of dry matter, kg/s
$\dot{m}_{mix}$	mass flow rate of dry air, kg/s
$\dot{m}_{rc}$	mass flow rate of dry air in the recycle line, kg/s
l	half length of cylinder axis, m
$\dot{Q}$	thermal energy consumption, kJ/s
P	pressure drop across fan, Pa
R	ratio of dry mass of grain to mass of air, kg dry matter/kg dry air
R_t	ratio of dry mass of grain to mass of air at ventilation unit, kg dry matter/kg dry air
r	distance in radial direction, m
r_o	radius of paddy, m
SHC	specific thermal energy consumption, MJ/kg water evaporated
SPC	specific electrical energy consumption, MJ/kg water evaporated
T_{abs}	absolute temperature, K
T_b	temperature at the fan exit, °C
$T_{f,n}$	exhaust temperature at nth element, °C
T_{fl}	exhaust temperature, °C
T_{ft}	outlet air temperature at ventilation unit, °C
T_{mix}	inlet air temperature, °C
T_x	temperature at the fan inlet, °C
t	time, s
V_p	particle volume, m^3
$W_{f,n}$	humidity ratio at nth element exit, kg water/kg dry air
W_{fl}	humidity ratio at fluidised-bed dryer exit, kg water/kg dry air
W_i	humidity ratio of fresh air, kg water/kg dry air
W_{mix}	humidity ratio at fluidised-bed dryer inlet, kg water/kg dry air
W_{ft}	outlet humidity ratio at the ventilation unit, kg water/kg dry air
z	distance along the axis direction, m

θ_{in}	grain temperature, °C
ρ_{air}	air density, kg/m^3
ϕ	relative humidity, fraction
η_{fan}	fan efficiency, decimal

1. Introduction

The drying process involves transfers of heat and mass between media and solid materials, in which heat from the media is convected to the particles present in the dryer vapourising the water inside the particles. This phenomenon is very complicated and causes irreversible change in the physical and chemical properties of food materials such as colour, cracking and viscosity (Ávila and Silva, 1999; Peplinski et al., 1994; Wiset et al., 2000). Such changes give lower quality and reduce price. For rice, whole kernels, one of the most important qualities, have a higher commercial value than broken ones. Therefore, industry requires milled rice with a larger proportion of full kernels.

Numerous studies on breakage in paddy kernels have reported that kernel breakage is dependent on a number of factors such as grain properties, environmental conditions for milling grains, and drying approaches (Kunze, 1972; Nguyen and Kunze, 1984; Siebenmorgen et al., 1998; Inprasit and Noomhorm, 2001). Breakage is a result of the development of stress cracks inside kernels, causing grains to have lower resistance to milling. Stress cracks are induced by non-uniform distribution of temperature and moisture. Thermal stresses usually occur during the heating period and become smaller afterwards. Subsequently, stresses from the moisture gradient are increasingly important. Paddy kernels that experience large moisture differences between their interiors and exteriors are prone to cracking. Conditions most favourable for stress cracking occur when the grain is subjected to high heat- and mass-transfer rates.

Fluidised-bed techniques, where solid particles and fluid media are in a good contact over the entire bed, can generate a large amount of broken rice (Sutherland and Ghaly, 1990; Soponronnarit and Prachayawarakorn, 1994). This problem motivated us to investigate the approach of taking the moisture content of paddy down to 16.5% dry basis while maintaining head-rice yield. The other two important factors, grain colour and energy consumption, were also explored as the fluidised-bed dryers are operated at high temperatures to accelerate moisture movement inside kernels. High temperatures may encourage change in the colour of paddy from white to yellow and may consume a large amount of energy if the management or the drying process is inappropriate. In the present study, experiments and mathematical simulation were conducted to determine the process for paddy drying that meets the requirements for high quality and less energy consumption.

2. Materials and methods

In the experimental work, paddy was dried using three different configurations of the drying process, each of which consisted of three main units, a fluidised-bed dryer, a tempering unit and ambient-air ventilation. The tempering unit was responsible for grain relaxation after drying. Previous studies had shown that if drying was operated in a single step without tempering, very low yields of whole kernels would result (Steffe and Singh, 1980; Soponronnarit et al., 1999). During the tempering stage, it is believed that moisture distribution inside kernels becomes almost uniform, resulting in high yields of full kernels.

The ambient-air ventilation cooled the grain to stop formation of yellow pigment. Yellowing can be a severe problem in rice drying because temperature stimulates the development of rice yellowness, a non-enzymatic browning reaction (Taweerattanapanish et al., 1999; Soponronnarit et al., 1998; Yap et al., 1988). Ventilation was stopped when the grain temperature approached or was slightly above ambient-air temperature.

Details of the proposed drying systems are shown in Fig. 1. System No. 1 was the simplest system, in which paddy was first dried in the fluidised-bed dryer and then held temporarily in the tempering unit, after which it was ventilated with ambient air. System No. 2 contained two sub-drying systems, in each of which the components were arranged as in system No. 1. The two sub-drying systems were connected in series with a tempering unit between the sub-systems to equalise the moisture content inside the kernels before they passed through the second fluidised-bed dryer. In system No. 3, grains after relaxing in the first tempering unit were dried immediately by the second fluidised-bed dryer without ambient-air ventilation. To prevent water condensation in the grain bulks, grains were ventilated by ambient air before taking them to the storage area as shown in Fig. 1 for each drying system. This is an additional advantage to that mentioned in the above section.

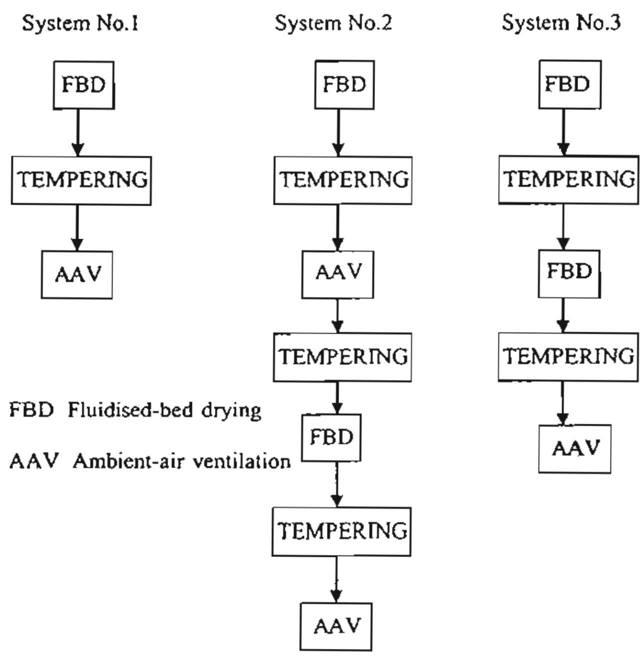

Fig. 1. Plan of three paddy-drying systems.

Details of experimental conditions for each drying system are presented in Tables 1–3. Paddy qualities in terms of head-rice yield and whiteness were determined quantitatively after treatment with the drying systems.

2.1. Equipment

2.1.1. Paddy preparation

Paddy was freshly harvested from the central region of Thailand with an average moisture content of 20% dry basis. The paddy was rewetted, mixed and kept in a cool storage at a temperature of 3–5 °C for 5–7 days. Two initial moisture contents of 30% and 35% dry basis were used. Before starting the experiment, the cooled paddy was placed in the ambient atmosphere until its temperature was close to that of ambient-air temperature.

2.2.2. Fluidised-bed drying

Experiments on quality were carried out with a batch fluidised-bed dryer. Drying conditions for all systems involved a superficial air velocity of 2.3 m/s, a bed thickness of 10 cm and temperatures of 130 and 150 °C. The inlet temperature was controlled by a proportional integral derivative controller with an accuracy of ± 1 °C. Drying time, i.e., residence time in the dryer, varied from 1 to 4 min, depending on the drying system.

2.2.3. Tempering

During tempering, the paddy was held in a completely sealed glass bottle with a diameter of 12 cm and a height of 10 cm and kept in an oven at the grain temperature obtained from the previous stage between 15 and 45 min. When tempering was complete, the samples were ventilated by ambient air or passed through the second fluidised-bed dryer depending on the drying system being investigated. For the second drying, the paddy was dried at the same temperature as the first one.

2.2.4. Ambient-air ventilation

The fixed-bed ventilator used in this study consisted of a cylindrical chamber with an inner diameter of 20 cm with a paddy bed height of 3 cm. The paddy was ventilated for at least 20–30 min using ambient air at a velocity of 0.125 m/s.

2.2. Measurement of moisture content

Samples were collected before and after passing through each process and the moisture content was determined from the weight loss of samples held in a hot-air oven at 103 °C for 72 h.

2.3. Quality of paddy

After completion of each drying system, the paddy was kept in a plastic bag for a week in a cool storage room at a temperature of 3–5 °C. A 125 g sample was then dehusked, milled and the whole kernels separated from the broken rice by a screen device. The head-rice yield was defined as the mass of unbroken rice kernels (a length longer than 80% of the whole kernel length was

Table 1
Experimental conditions and results of moisture content, relative head-rice yield and whiteness for drying system No. 1

Run No.	Initial moisture content (% dry basis)	Fluidised-bed drying conditions		Tempering time (min)	Ventilation time (min)	Moisture content after ventilation (% dry basis)	Relative head-rice yield (%)	Whiteness (%)
		Temperature (°C)	Time (min)					
1	35	150	3	0	20	19.5	1.5	40.6
2	35	150	3	15	20	18.5	80.5	41.6
3	35	150	3	30	20	18.3	110.2	40.1
4	35	150	3	45	20	18.4	108.3	39.5
5	35	130	4	0	20	19.7	3.0	41.2
6	35	130	4	15	20	18.5	60.5	40.6
7	35	130	4	30	20	18.4	103.2	40.3
8	35	130	4	45	20	18.4	105.3	39.8
9	30	150	2.5	0	20	18.5	3.5	41.5
10	30	150	2.5	15	20	17.8	95.3	41.2
11	30	150	2.5	30	20	17.5	108.2	41.3
12	30	150	2.5	45	20	17.6	106.4	40.8
13	30	130	3	0	20	18.9	5.0	41.8
14	30	130	3	15	20	17.8	73.8	41.3
15	30	130	3	30	20	17.7	101.2	41.9
16	30	130	3	45	20	17.6	105.3	38.2

Note: reference head-rice yield, 46.3%; reference whiteness, 44.0.

Table 2
Experimental conditions for drying system No. 2

		Reference code			
		a	b	c	d
Initial moisture content (% dry basis)		35	30	35	30
Fluidised-bed drying					
The first stage	Temperature (°C)	150	150	130	130
	Time (min)	1.5	1.5	2.0	2.0
	Bed thickness	10	10	10	10
	Tempering time (min)	15	15	20	20
	Ventilation time (min)	30	30	30	30
The second stage	Temperature (°C)	150	150	130	130
	Time (min)	1.0	1.0	1.5	1.5
	Bed thickness (cm)	7.5	7.5	7.5	7.5
	Tempering time (min)	15	15	20	20
	Ventilation time (min)	30	30	30	30

Table 3
Experimental results of moisture content, relative head-rice yield and whiteness for different reference codes in Table 2

Drying strategy	Tempering time between the first and the second stage (min)	Moisture content after passing the second FBD (% dry basis)	Relative head-rice yield (%)	Whiteness
	0	19.6	107.6	40.2
	15	19.5	109.6	39.5
a	30	19.6	102.5	40.0
	60	19.6	107.6	39.6
	120	19.4	106.4	39.2
	0	18.5	100.0	40.1
	15	18.3	102.6	39.8
b	30	18.3	104.4	39.6
	60	18.5	110.4	39.4
	120	18.2	98.7	39.6
	0	20.4	104.7	40.5
	15	20.6	108.9	40.2
c	30	20.5	103.4	39.8
	60	20.2	98.8	39.7
	120	20.3	103.9	40.0
	0	19.6	94.5	40.3
	15	19.4	98.2	39.9
d	30	19.3	95.8	40.0
	60	19.5	93.2	39.7
	120	19.2	96.4	40.0

Note: Reference head-rice yield, 47.6%; reference whiteness, 43.5; FBD, fluidised-bed drying.

acceptable) after milling, divided by the mass of paddy before milling. The control sample was prepared by drying paddy from its initial moisture content to 16% dry basis using ambient temperature. This took around 16 h. The results were presented as relative head-rice yield, defined as the ratio of head rice obtained from each system to that from the control sample.

A commercial whiteness meter (Kett C-300) was used for measuring the colour. Before measuring, it was standardised with pure white magnesium oxide powder which had a value of 86.3. The whiteness values of samples before treating were between 46.8 and 47.6.

2.4. Mathematical model for drying system

The state of moist grains present in each unit of the drying process such as drying, tempering and ventilation was different. A mathematical model for each unit was formulated to describe its behaviour. The models developed in conjunction with the head-rice equation allowed estimation of the energy consumption for each drying treatment.

2.4.1. Dryer unit

The first unit involved simultaneous heat and mass transfer in which air was used to convey heat to the grains to evaporate their moisture and then take the water vapour away. In the fluidised-bed dryer, there was dispersion of grain. The simplified analysis used in the present study assumed that the grain movement along the axial direction was a plug flow and the subsequent moisture content of paddy was reduced following this direction. To describe such results, the grain bed was divided into a series of N small sets. Two governing equations, Eqs. (1) and (2), for a differential volume as shown in Fig. 2, along with a theoretical diffusion equation for a single kernel as given by Eq. (3), were used in the model. Eqs. (1) and (2) were written based on energy and mass balances for a small interval of time Δt and a single compartment:

$$W_{f,n} = R(M_{i,n} - M_{f,n}) + W_{mix}, \tag{1}$$

where $W_{f,n}$ was the humidity ratio at nth element exit (kg water/kg dry air), R was the ratio of dry mass of grain to mass of air (kg dry matter/kg dry air), $M_{i,n}$ was the inlet moisture content at nth element (dry-basis decimal), $M_{f,n}$ was the outlet moisture content at nth element and W_{mix} was the humidity ratio at the fluidised-bed dryer inlet.

$$T_{f,n} = (C_a T_{mix} + W_{mix}(h_{fg} + C_v T_{mix}) - W_{mix} h_{fg} + RC_{pw}\theta_{in})/(C_a + W_{f,n} C_v + RC_{pw}), \tag{2}$$

where $T_{f,n}$ was the exhaust temperature at nth element (°C), T_{mix} was the inlet air temperature, C_a was the specific heat of dry air (kJ/kg °C), C_v was the specific heat of water vapour, C_{pw} was the specific heat of moist paddy, h_{fg} was the latent heat of water (kJ/kg) and θ_{in} was the grain temperature. The moisture transport inside the paddy, assuming a cylindrical shape, can be described by

$$\frac{\partial M}{\partial t} = D_{eff}\left[\frac{\partial^2 M}{\partial r^2} + \left(\frac{1}{r}\right)\frac{\partial M}{\partial r} + \frac{\partial^2 M}{\partial z^2}\right], \tag{3}$$

where M was the moisture content, D_{eff} was the effective diffusivity (m^2/s), t was the drying time (s), r was the distance in a radial direction (m) and z was the distance along the axis direction

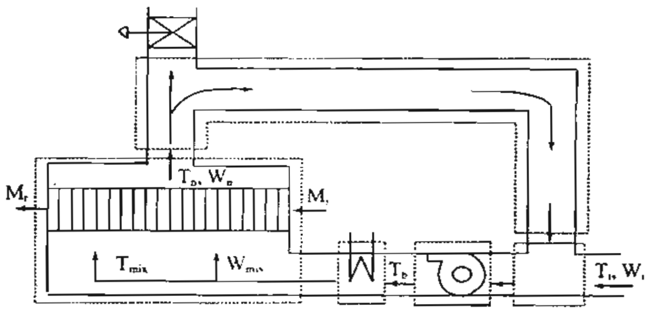

Fig. 2. Schematic diagram of continuous fluidised-bed dryer. *Note*: M_i, inlet moisture content of paddy; M_f, outlet moisture content of paddy; T_b, temperature at the fan exit; T_{f1}, exhaust air temperature; T_i, ambient air temperature; T_{mix}, inlet air temperature; W_i, humidity ratio of ambient air; W_{f1}, humidity ratio of exhaust air; W_{mix}, humidity ratio of inlet air.

(m).The effective diffusion coefficient for paddy was given by Poomsa-ad et al. (2002):

$$D_{eff} = 5.41141 \times 10^{-6} \exp\left(-\frac{28436.4}{T_{abs}}\right), \tag{4}$$

where T_{abs} was the absolute temperature (K). Eq. (4) was obtained from the experiments that were carried out at a thin bed depth of 3 cm. Using this bed depth, the inlet-air temperature was slightly reduced and thus Eq. (4) was statistically fitted with the inlet-air temperature. The equilibrium moisture equation of Laithong (1987) used in the present study was

$$1 - \phi = \exp\{(-4.584 \times 10^{-6}) T_{abs} (100 M_{eq})^{2.397}\}, \tag{5}$$

where ϕ was the relative humidity (fraction) and M_{eq} was the equilibrium moisture content. In order to solve Eq. (3), the following conditions were assumed: (1) the initial moisture content was uniform throughout the kernel; (2) the air was at equilibrium with the moisture content at the surface and both ends of the solid particle over the drying time; and (3) the moisture content of paddy had a maximum value at the central region during drying. The average temperature between inlet- and outlet-air temperatures was used as the input parameter for calculating the effective diffusion coefficient because the temperature of the inlet air entering the drying chamber dropped due to the relatively thick bed depth used in the experiments (10 cm). If the outlet or inlet temperature was used, the relatively large differences between the calculated moisture contents and experimental values were obvious. The outlet temperature can be calculated by Eq. (2), assuming thermal equilibrium between the kernels and exhaust air.

To obtain the moisture distribution in a paddy kernel, the finite difference was applied to solve Eq. (3). The grain shape was divided into a constant number of elements with 80 nodes of length and 10 nodes of radius. The average moisture content, M_{av}, throughout the kernel at time t was determined by the following equation:

$$M_{av} = \frac{1}{V_p} \iint 2\pi r M(r, z, t)\, \mathrm{d}r\, \mathrm{d}z, \tag{6}$$

where V_p was the particle volume (m^3). The algorithm for solving the set of equations (Eqs. (1)–(6)) followed an iteration procedure commencing with an assumed absolute humidity ratio at the drying chamber inlet. This procedure was similar to that developed by Soponronnarit et al. (1996). After obtaining the set of solutions for each compartment, the average outlet absolute-humidity ratio, W_{f1}, and exhaust-air temperature, T_{f1}, were then calculated by arithmetic means. Time steps for paddy movement through a small element in the dryer were calculated from the residence time of paddy divided by N.

By conservation of mass around the hypothetical volume where the recycled air and fresh air are mixed together, the humidity ratio at the inlet was calculated by

$$W_{mix} = (1 - \frac{\dot{m}_{rc}}{\dot{m}_{mix}})W_i + \frac{\dot{m}_{rc}}{\dot{m}_{mix}} W_{f1}, \tag{7}$$

where $\dot{m}_{rc}$ was the mass flow rate of dry air in the recycle line (kg/s), $\dot{m}_{mix}$ was the mass flow rate of dry air at the fluidised-bed dryer inlet, W_i was the humidity ratio of fresh air and W_{f1} was the humidity ratio at the fluidised-bed dryer exit.

The amount of energy consumed for heating the moist air to the desired temperature was calculated by

$$\dot{Q} = \dot{m}_{mix}(C_a + C_v W_{mix})(T_{mix} - T_b), \tag{8}$$

where $\dot{Q}$ was the thermal energy consumption (kJ/s) and T_b was the temperature at the fan exit. Before determining the thermal energy consumption, T_b must be known. To accomplish this, the conservation of energy was applied around the hypothetical volume and the temperature at the fan inlet was

$$T_x = \frac{\dot{m}_i(C_a + C_v W_i)T_i + \dot{m}_{rc}(C_a + C_v W_{f1})T_{f1}}{\dot{m}_{mix}(C_a + C_v W_{mix})}, \tag{9}$$

where T_x was the temperature at the fan inlet and T_i was the temperature of fresh air. Thus, the temperature at the fan exit, T_b, was given by

$$T_b = T_x + \frac{P\dot{m}_{mix}}{\rho_{air}\eta_{fan} C_a}, \tag{10}$$

where P was the pressure drop across the fan (Pa), ρ_{air} was the air density (kg/m^3) and η_{fan} was the fan efficiency (decimal).

In the case of no air recycling, T_x was replaced by T_i. In the present study, the amount of energy consumed was represented by the specific energy. The specific heat consumption was given by

$$SHC = \frac{\dot{Q}}{\dot{m}_p(M_{i,av} - M_{f,av})1000}, \tag{11}$$

where SHC was the specific thermal energy consumption (MJ/kg water evaporated), $M_{i,av}$ was the average inlet moisture content and $M_{f,av}$ was the average moisture content at the dryer outlet. The specific electrical energy for the fan was given by

$$SPC = P\left(\frac{\dot{m}_{mix}/\rho_{air}\eta_{fan}}{\dot{m}_p(M_{i,av} - M_{f,av})1000}\right), \tag{12}$$

where SPC was the specific electrical energy consumption (MJ/kg water evaporated), $\dot{m}_p$ was the mass flow rate of dry matter (kg/s) and η_{fan} was the fan efficiency. η_{fan} was about 0.8.

2.4.2. Tempering unit

The drying processes shown in Fig. 1 were interrupted when the partially dried grains were in the tempering unit. In this temporary stop, the grains were not subjected to contact with hot air and the subsequent moisture and temperature gradients inside the individual kernels had less variation.

During tempering, the moisture in the interior of grains will move to the exterior surface, but it does not evaporate to the environment. The transport of moisture can be described by the moisture diffusion equation, which is similar to Eq. (3). In order to solve this equation, the initial and boundary conditions must be known:

$$t = 0, \quad M = M(r, z), \tag{13}$$

$$t > 0, r = r_0, \quad \frac{\partial M}{\partial r} = 0, \tag{14}$$

$$z = \pm l, \quad \frac{\partial M}{\partial z} = 0, \tag{15}$$

$$t > 0, \quad r = 0, \quad \frac{\partial M}{\partial r} = 0. \tag{16}$$

where r_0 was the radius of paddy (m) and l was the half length of cylinder axis (m). Eq. (13) was the initial condition obtained from the end of the previous section. Eqs. (14) and (16) were similar but did not have the same physical meaning: Eq. (14) showed the maximum moisture content at the centre whilst the other represented the state of water that cannot vapourise through the exterior surface.

When the grains were in the tempering unit, time was an important parameter for uniformly distributed moisture content. Theoretically, the uniform distribution of moisture, corresponding to the tempering index of unity, required infinite time. The tempering index was defined by several workers (Steffe and Singh, 1980; Zhang and Litchfield, 1991; Tolaba et al., 1999) as

$$I_c = \frac{M_{s,t} - M_{s,t=0}}{M_{s,t=\infty} - M_{s,t=0}}, \tag{17}$$

where I_c was the tempering index (decimal) and $M_{s,t}$ was the surface moisture content at time t. This index strongly affected the next drying stage: the lower the tempering indices, the smaller the drying rates. Poomsa-ad et al. (2002), however, found that the drying rate at an index higher than 0.95 was almost the same as that at unity. It is thus reasonable to say that an index of 0.95 was an appropriate value for tempering the paddy.

2.4.3. Ambient-air ventilation unit

In the tempering section, the grains were tempered at the temperature of the outlet grain temperature from the dryer, usually higher than 80 °C where the fluidised-bed dryer was operated at a temperature higher than 100 °C. At such temperatures, it was necessary to reduce the grain temperature to ambient temperature before storage or passing to the following step. First, if not ventilated, the moisture around the grain surface would have evaporated to the air space and the grain temperature dropped. This situation would have encouraged water vapour flow in the bin which could have condensed when it came into contact with cooler surfaces. This in turn could cause wet spots during storage, which could induce the growth of microorganisms. The second reason was to inhibit the development of yellow pigment and to avoid the paddy becoming darkened.

While air was passed through the heated grains, there was simultaneous heat and mass transfer from the grain to air, making the air slightly warmer and more humid. The heat-transfer phenomenon in this unit was opposite to that occurring in the dryer section. Assuming that the air flowed through a thin bed in the cross-flow dryer, the outlet-air temperature, T_{ft}, was given by

$$T_{ft} = (C_a T_i + W_i(h_{fg} + C_v T_i) - W_i h_{fg} + R_t C_{pw}\theta_{in})/(C_a + W_{ft} C_v + R_t C_{pw}), \tag{18}$$

where R_t was the ratio of dry mass of grain to mass of air in the ventilation unit (kg dry matter/kg dry air) and W_{ft} was the outlet humidity ratio of the ventilation unit. Using such a simplified assumption, the properties of air changed insignificantly along the bed height, thereby providing economic computation by a single-step approach. The moisture transport was calculated by using Eq. (3) again, with the following initial and boundary conditions:

$$t = 0, \quad M = M(r, z), \tag{19}$$

$$t > 0, r = r_0, \quad M = M_{eq}, \tag{20}$$

$$z = \pm \ell, \quad M = M_{eq}. \tag{21}$$

In the determination of moisture reduction, the grain temperature was used in Eq. (4), instead of the inlet-air temperature, because the grain temperature at the beginning of ventilation was 50 °C higher than the ambient-air temperature.

3. Results and discussion

3.1. Experimental results of the drying performance and final quality

The experimental results from system No. 1 are shown in Table 1. In this system, the outlet moisture content after fluidised-bed drying was limited to approximately 22% dry basis. At this moisture level, the drying times varied from 2.5 to 4 min depending upon the inlet temperature and moisture content. The system that did not have tempering after drying gave very low relative head-rice yields. Values were between 1.5% and 5% as shown in Table 1 for run Nos. 1, 5, 9 and 13 despite the time in the fluidised-bed dryer being very short. This result emphasised the necessity for tempering in the drying system. Such low head-rice yields were caused by the combined effects of moisture and temperature gradients, with the latter being dominant because of the thermal stresses set up when the heated grain contacted cooler air. The significant improvement in head-rice quality with tempering, however, became evident. Higher head-rice yields related to higher tempering times as illustrated for run Nos. 2 and 3 for the tempering times of 15 and 30 min, which produced 80.5% and 110.2% relative head-rice yield, respectively. Similar results were found at other temperatures and initial moisture contents. The high head-rice yield is attributed to less moisture stresses after tempering and the partial formation of gel in paddy kernels when the moist grains were tempered at temperatures higher than 80 °C.

Table 1 illustrates that tempering for longer than a certain period does not increase head-rice yield, but does result in milled rice becoming darker. A tempering time of 30 min was enough for redistribution of moisture inside individual kernels, while luminosity and whiteness of the milled rice were still acceptable. The values of whiteness for paddy tempered at such a recommended tempering time were higher than 40.

It is interesting to note that the final moisture content after ventilation was lower for the tempered paddy than for paddy not tempered. This resulted from the moisture gradient produced inside the paddy in the drying unit becoming less variable after tempering and consequently the water was removed more easily when the paddy was ventilated. This is an advantage of tempering and can accordingly provide more economic energy utilisation. This drying system is now used in some rice industries.

Paddy dried by system Nos. 2 and 3 exhibited different qualities from that dried by system No. 1 as presented in Tables 3 and 4, respectively. The two sub-drying processes in system No. 2 provided premium quality, with high values of head-rice yield and whiteness, while system No. 3, with ambient-air ventilation only in the last step, gave poor quality. The colour of the milled rice had relatively more yellowness and darkness with the values falling in the range of 35–37, compared with a reference value of 45.5 for the gently dried paddy. Milled rice with a colour below 40 is not preferred by the domestic market. This result indicates that the grain should be ventilated immediately as otherwise the colour becomes a severe problem.

The colour of the milled rice in system No. 2 was similar to that from system No. 1. For whole kernels, the values of head-rice yield obtained from both systems were not significantly different if the grains treated with system No. 1 were tempered for longer than 30 min.

Table 3 illustrates that after ambient ventilation in the first drying stage of system No. 2, further tempering did not significantly affect the head-rice yield. The relative head-rice yield obtained from the experiments varied from 94% to 110%. These results indicated that the forces between compression and tension acting on the kernels during ventilation were not significantly different because of the relatively small moisture reduction which resulted in less shrinkage at the exterior surface. System No. 2 thus yielded sound quality paddy and a tempering period between the two drying stages was not necessary.

3.2. *An appropriate drying system*

The experimental data from Soponronnarit et al. (2001) were compared with those obtained here. In their work, the experimental results were obtained from a continuous fluidised-bed dryer operated in the rice industry under different drying conditions. Results are presented in Table 5 showing that each predicted parameter such as outlet moisture content and energy consumption was in good agreement with the experimentally determined values.

Table 4
Experimental conditions and results of relative head-rice yield and whiteness for drying system No. 3

Run no.	Initial moisture content (% d.b.)	The first FBD drying condition Temperature/ time (°C/min)	Tempering time (min)	The second FBD drying condition Temperature/ time (°C/min)	Tempering time (min)	Ambient air ventilation(min)	Relative head-rice yield (%)	Whiteness
1	35	150/2.0	15	150/1.0	15	30	77.9	35.4
2	35	150/2.0	30	150/1.0	30	30	77.1	35.4
3	35	150/2.0	15	130/1.5	15	30	84.3	37.0
4	35	130/2.5	15	130/1.5	15	30	80.9	36.8
5	35	130/2.5	15	130/1.5	30	30	83.3	35.4
6	30	150/2.0	15	150/1.0	15	30	82.3	35.2
7	30	150/2.0	30	150/1.0	30	30	81.2	34.3
8	30	130/2.0	15	130/1.5	15	30	78.3	37.8
9	30	130/2.5	30	130/1.5	30	30	77.9	36.1

Note: Reference head-rice yield, 47.6%; reference whiteness, 45.5; FBD, fluidised-bed drying.

Table 5
Comparison between experiments and simulations for industrial-scale fluidised-bed dryer (after Soponronnarit et al., 2001)

Run no.	Drying temperature (°C)	Feed rate (tonnes/h)	Bed height (m)	M_{in} %dry basis	M_f (%d.b.)		SHC (MJ/kg of water)		SPC (MJ/kg of water)	
					Exp.	Sim.	Exp.	Sim.	Exp.	Sim.
1	130	3.12	0.115	25.9	22.5	22.1	6.45	5.31	0.9	0.88
2	140	4.72	0.147	26.7	23.3	23.6	4.83	4.05	0.73	0.81
3	150	6.42	0.119	25.9	23.3	23.0	4.93	4.83	0.7	0.55
4	150	6.09	0.15	25.9	23.7	22.8	6.7	5.01	0.85	0.69
5	150	5.1	0.15	26.1	23.4	22.9	6.01	5.02	0.79	0.72
6	130	4.82	0.115	26.8	23.7	23.7	5.47	4.68	0.77	0.74
7	140	4.82	0.115	24.1	20.7	20.9	4.69	5.15	0.66	0.74
8	150	4.82	0.115	28.0	23.0	24.0	3.8	4.78	0.48	0.56

Note: *SHC* = Specific thermal energy consumption; *SPC* = Specific electrical energy consumption; M_{in} = Initial moisture content; M_f = Final moisture content

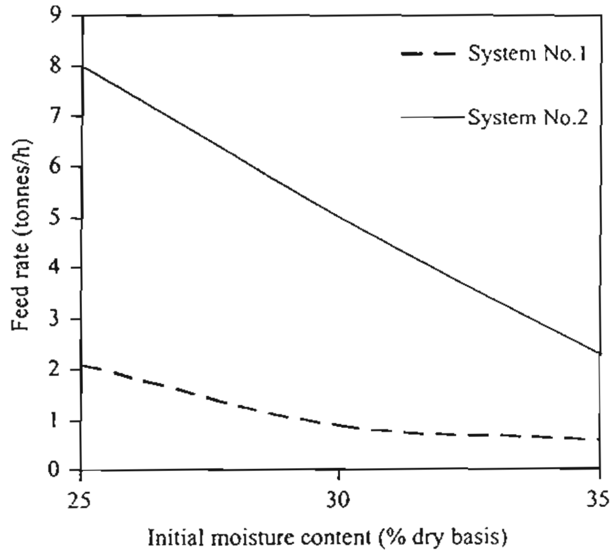

Fig. 3. Feed rates at different initial moisture contents for system Nos. 1 and 2.

Simulations were then made with the drying system Nos. 1 and 2 to determine the most suitable drying process. System No. 3 was not considered, as it did not reach the standard for producing white rice. In simulating system No. 2, the tempering step between the two sub-drying systems was not included. The criteria quantifying performance were energy consumption and drying capacity. In the simulations, drying temperature was limited to 150 °C, bed depth was fixed at 10 cm corresponding to the holding capacity of 60 kg, superficial air velocity was 2.3 m/s and ratio of recycled air was 0.85. The tempering index of 0.95 was chosen for the required time to represent idealised moisture equalisation inside kernels. In addition to such constraints, grains must be cooled to room temperature in the ventilation unit and the final moisture content at the last unit of each system must be lower than 17.5% dry basis.

Trial and error was used to estimate the feed rate needed to acquire the desired moisture level at process end. Fig. 3 shows the results of calculated feed rates at different initial moisture contents. Feed rate reduced with increase in initial moisture content as the drying time took longer with a higher initial moisture content. The feed rate for system No. 2 was at least 4 times higher than that for system No. 1, implying more potential for water removal. The higher drying capacity was due to the tempering units that enabled the remaining moisture after drying to move towards the grain surface. The surface moisture could therefore be removed quickly when the grains reached the next stage. The advantage of the tempering units complies not only with high drying capacity, but also with energy saving, in particular, the thermal energy that is consumed in the thermal dehydration process. The total specific heat consumption for system No. 2 was, for example, 4.75 MJ/kg water evaporated at 35% dry basis whilst it was 7.32 MJ/kg water evaporated for system No. 1. The energy consumption at the other moisture contents for system Nos. 1 and 2 are shown in Tables 6 and 7, respectively. It can be seen that the thermal energy utilisation of system

Table 6
Simulation results of drying system No. 1

	Case 1	Case 2	Case 3
Initial moisture content (% dry basis)	25	30	35
Feed rate (tonnes/h)	2.1	0.9	0.6
The FBD drying condition			
Drying temp (°C)	150	150	150
Bed height (m)	0.1	0.1	0.1
Air velocity (m/s)	2.3	2.3	2.3
Moisture content after the FBD (% dry basis)	18.3	18.5	18.7
Grain temperature after the first FBD (°C)	107.5	112.5	120.6
The tempering time (min)	19	20	22
The ventilation time (min)	30.0	26.5	25.2
Moisture content after the ventilator (% dry basis)	17.2	17.0	17.3
Energy consumption			
For the FBD			
SPC (MJ/kg)	1.37	1.48	1.63
SHC (MJ/kg)	6.89	7.57	7.95
For the ventilator			
SPC (MJ/kg)	1.59	1.43	1.42
Total energy consumption			
SPC (MJ/kg)	1.40	1.47	1.61
SHC (MJ/kg)	5.91	6.67	7.32

Note: *SPC*, specific electrical energy consumption in term of primary energy (conversion factor 2.6); *SHC*, specific heat consumption; FBD, fluidised-bed drying.

Table 7
Simulation results of drying system No. 2

	Case 1	Case 2	Case 3
Initial moisture content (% dry basis)	25	30	35
Feed rate (tonnes/h)	7.9	5.0	2.3
The FBD drying condition			
Drying temperature (°C)	150	150	150
Bed height (m)	0.1	0.1	0.1
Air velocity (m/s)	2.3	2.3	2.3
Moisture content after the first FBD (% dry basis)	21.9	24.8	26.7
Grain temperature after the first FBD (% dry basis)	81.2	89.6	97.7
The first tempering time (min)	22	26	19
The first ventilation time (min)	19.5	22.5	24.0
Moisture content after the second FBD (% dry basis)	18	18.4	18.2
Grain temperature after the second FBD (% dry basis)	95.1	96.5	106.5
The second tempering time (min)	20	27	20
The second ventilation time (min)	25	27	32
Moisture content after the second ventilator (% dry basis)	16.7	17.0	16.9
Energy consumption			
For the first FBD	0.61	0.84	1.02
SPC (MJ/kg of water evap.)			
SHC (MJ/kg of water evap.)	5.36	5.07	5.55
For the second FBD			
SPC (MJ/kg of water evap.)	0.73	1.09	1.39
SHC (MJ/kg of water evap.)	5.36	6.15	6.89
For the first ventilator			
SPC (MJ/kg of water evap.)	1.37	1.45	1.57
For the second ventilator			
SPC (MJ/kg of water evap.)	1.54	1.56	1.68
Total energy consumption			
SPC (MJ/kg of water evap.)	0.92	1.10	1.36
SHC (MJ/kg of water evap.)	3.64	3.96	4.75

Note: *SPC*, specific electrical energy consumption in term of primary energy (conversion factor 2.6); *SHC*, specific heat consumption.

No. 2 is relatively economical over the range of moisture contents compared with system No. 1 whilst the electrical energy utilisation for both systems is relatively comparable.

4. Conclusions

Three paddy-drying processes were examined for energy consumption and paddy qualities in terms of head-rice yield and whiteness. Paddy dried through the system Nos. 1 and 2 yielded the highest quality. The colour of paddy had the most intense yellowness when treated with system No. 3. In system No. 2, the tempering section between two sub-drying systems was not necessary.

Heat and mass-transfer equations for each unit enabled us to estimate the moisture content and energy consumption. The simulation results have shown that the process with tempering and ventilation as important elements of each stage provided superior performance, with a high drying capacity and less energy consumption. In the first stage, paddy at initial moisture content of 25–35% dry basis should be dried to the corresponding range of 21.9–26.7% dry basis at the first fluidised-bed dryer followed by tempering for 22 down to 19 min and ventilating for 19 up to 24 min. In the second stage, the moisture content at the outlet of the second fluidised-bed dryer was approximately 18% dry basis and the required time ranged between 20 and 27 min for tempering and between 25 and 32 min for ventilation.

Acknowledgements

The authors would like to express their sincere thanks to the Thailand Research Fund for financial support and The Division of Agricultural Engineering, Department of Agriculture, Thailand for test milling.

References

Ávila, I.M.L.B., Silva, C.L.M., 1999. Modelling kinetics of thermal degradation of colour in peach puree. Journal of Food Engineering 39, 161–166.

Inprasit, C., Noomhorm, A., 2001. Effect of drying air temperature and grain temperature of different types of dryer and operation on rice quality. Drying Technology 19, 389–404.

Kunze, O.R., 1972. Moisture adsorption related to tensile strength of rice. Cereal Chemistry 49, 684–696.

Laithong, C., 1987. Study of thermo-physical properties of rough rice. Masters Thesis, King Mongkut's Institute of Technology Thonburi, Bangkok.

Nguyen, C.N., Kunze, O.R., 1984. Fissures related to post drying treatments in rough rice. Cereal Chemistry 61, 63–68.

Peplinski, A.J., Paulis, J.W., Bietz, J.A., Pratt, R.C., 1994. Drying of high-moisture corn: changes in properties and physical quality. Cereal Chemistry 71, 129–133.

Poomsa-ad, N., Soponronnarit, S., Prachayawarakorn, S., Terdyothin, A., 2002. Effect of tempering on subsequent drying of paddy using fluidisation technique. Drying Technology 20, 195–210.

Siebenmorgen, T.J., Nehus, Z.T., Archer, T.R., 1998. Milled rice breakage due to environmental conditions. Cereal Chemistry 75, 149–152.

Soponronnarit, S., Prachayawarakorn, S., 1994. Optimum strategy for fluidised bed paddy drying. Drying Technology 12, 1667–1686.

Soponronnarit, S., Prachayawarakorn, S., Sripawatakul, O., 1996. Development of cross-flow fluidised bed paddy dryer. Drying Technology 14, 2397–2410.

Soponronnarit, S., Srisubati, N., Yoovidhya, T., 1998. Effect of temperature and relative humidity on yellowing rate of paddy. Journal of Stored Products Research 34, 323–330.

Soponronnarit, S., Wetchacama, S., Swasdisevi, T., Poomsa-ad, N., 1999. Managing moist paddy by drying, tempering and ambient air ventilation. Drying Technology 17, 335–344.

Soponronnarit, S., Wetchacama, S., Trutassanawin, S., Jariyatontivait, W., 2001. Designing, testing and optimization of vibro-fluidised paddy dryer. Drying Technology 19, 1891–1908.

Steffe, J.F., Singh, R.P., 1980. Theoretical and practical aspects of rough rice tempering. Transactions of the American Society of Agricultural Engineering 23, 775–782.

Sutherland, J.W., Ghaly, T.F., 1990. Rapid fluid-bed drying of paddy rice in the humid tropics. In: Naewbanij, J.O. (Ed.), Proceedings of the Thirteenth ASEAN Seminar on Grain Post Harvest Technology, Bandar Seri Begawan, Brunei Darussalam. ASEAN Grain Postharvest Programme, Bangkok, Thailand, pp. 168–180.

Taweerattanapanish, A., Soponronnarit, S., Wetchakama, S., Kongseri, N., Wongpiyachon, S., 1999. Effects of drying in head rice yield using fluidization technique. Drying Technology 17, 345–353.

Tolaba, P., Aguerre, R.J., Suárez, C., 1999. Drying simulation of corn with tempering. Drying Technology 17, 1081–1093.

Wiset, L., Srzednicki, G., Driscoll, R., Nimmuntavin, C., Siwapornrak, P., 2000. Effects of high temperature on rice quality. Proceedings of the XIV Memorial Commission Internationale du Génie Rural World Congress, 28 November–1 December 2000, Tsukuba, Japan, pp. 794–799.

Yap, A.B., Juliano, B.O., Perez, C.M., 1988. Artificial yellowing of rice at 60 °C. In: Naewbanij, J.O. (Ed.), Proceedings of the Eleventh ASEAN Technical Seminar on Grain Postharvest Technology, 23–26 August, 1988 Kuala Lumpur, Malaysia. ASEAN Grain Postharvest Programme, Bangkok, Thailand, pp. 3–20.

Zhang, Q., Litchfield, J.B., 1991. An optimization of intermittent corn drying in laboratory scale thin layer dryer. Drying Technology 9, 233–244.

Drying Kinetics and Inversion Temperature in a Low-Pressure Superheated Steam-Drying System

P. Suvarnakuta,† S. Devahastin,*,† S. Soponronnarit,‡ and A. S. Mujumdar§

Department of Food Engineering and School of Energy and Materials, King Mongkut's University of Technology Thonburi, Bangkok 10140, Thailand, and Department of Mechanical Engineering, National University of Singapore, Singapore 117576, Singapore

The present study aimed at investigating the drying rates and inversion temperatures of model porous particles undergoing low-pressure superheated steam and vacuum drying. Molecular sieve beads, which were used as the model material in this work, were dried as a single layer in a low-pressure superheated steam dryer. The effects of steam temperature and pressure on the drying rates of these particles were determined. The same dryer was also operated in a vacuum mode to determine the effects of the above-mentioned operating parameters as well as the variation of the inversion temperature of the processes with the operating pressure. The differences between the values of the inversion temperature calculated only from the rates of drying in the constant rate period and those calculated from the whole drying period are pointed out and discussed. Page's equations and a single-term exponential equation were found to satisfactorily describe the kinetics of low-pressure superheated steam- and vacuum-drying systems, respectively.

Introduction

Despite the many advantages of near-atmospheric pressure superheated steam drying, there still exist some limitations, especially when applying it to drying of heat-sensitive materials, e.g., foods and bioproducts.[1] Because most foods or other heat-sensitive products melt, undergo glass transition, or are damaged at the temperature of superheated steam corresponding to the atmospheric or higher pressures, one possible way to alleviate the above-mentioned problems is to operate the dryer at reduced pressure.[1–3] In addition to being able to preserve the quality of heat-sensitive products, lowering the operating pressure may enhance the drying rates as well.[1,4,5–8]

Some investigators have recently applied the concept of low-pressure (or subatmospheric pressure) superheated steam drying (LPSSD) to various heat-sensitive materials. Elustondo et al.[3] studied subatmospheric-pressure superheated steam drying of wood slabs and shrimp, banana, apple, pear, potato, and cassava slices both experimentally and theoretically. A semiempirical model was developed assuming that water removal was accomplished by evaporation in a moving boundary, allowing the vapor to flow through the dry layer built up as drying proceeds. The model proposed was found to predict the drying kinetics reasonably well. More recently, Devahastin et al.[9] studied experimentally drying of carrot cubes in both low-pressure superheated steam and vacuum dryers. They observed that the differences between the two sets of drying rate data (low-pressure superheated steam and vacuum drying) were smaller at higher drying temperatures. This suggested that raising the drying temperature further would eventually lead to equal rates of drying at the so-called inversion temperature[1,10] because of the increased temperature difference between the steam and product as well as a reduction in the initial steam condensation[11] that occurs as the wet material enters the drying chamber at a temperature lower than the saturation temperature of steam at prevailing pressure. Such information on the inversion temperature for the LPSSD system and the effect of vacuum pressure on this temperature is still missing, however. Shibata et al. (respectively in refs 4 and 12) have studied the steam-drying mechanisms of sintered spheres of glass beads under atmospheric pressure and vacuum. They reported that the drying mechanisms of the two processes were different and that superheated steam drying under vacuum gave lower critical moisture contents as well as higher drying rates in the falling rate period (FRP) than those in air drying under vacuum. However, they have not reported any information about the inversion temperature of the systems.

The present work, therefore, aimed at investigating the effect of vacuum pressure on the value of the inversion temperature by comparing the single-layer drying rates obtained in LPSSD and in vacuum drying of model porous particles, viz., molecular sieve beads. In addition, the values of the inversion temperature calculated only from the rates of drying in the constant rate period (CRP) were compared with those calculated from the whole drying period (CRPs and FRPs) in order to point out the fundamental differences between the two sets of temperatures, obtained from two different sets of drying rate information, beyond which drying rates in LPSSD are higher than those in vacuum drying. Three simple mathematical models that enable prediction of the drying behavior of molecular sieves undergoing LPSSD and vacuum drying were also proposed and compared.

* To whom correspondence should addressed. Tel.: +662 470 9246. Fax: +662 470 9240. E-mail: sakamon.dev@kmutt.ac.th.

† Department of Food Engineering, King Mongkut's University of Technology.

‡ School of Energy and Materials, King Mongkut's University of Technology.

§ National University of Singapore.

10.1021/ie049675r CCC: $30.25
Published on Web 02/10/2005

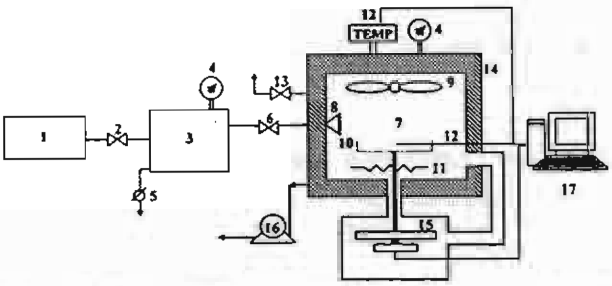

Figure 1. Schematic diagram of the low-pressure, superheated steam dryer and associated units: 1, boiler; 2, steam valve; 3, steam reservoir; 4, pressure gauge; 5, steam trap; 6, steam regulator; 7, drying chamber; 8, steam inlet and distributor; 9, electric fan; 10, sample holder; 11, electric heater; 12, online temperature sensor and logger; 13, vacuum breakup valve; 14, insulator; 15, online weight indicator and logger; 16, vacuum pump; 17, PC with installed data acquisition card.

Experimental Setup, Material, and Methods

Experimental Setup. A schematic diagram of the low-pressure superheated steam dryer and its accessories is shown in Figure 1. The dryer consists of a stainless steel drying chamber, insulated carefully with rock wool, with inner dimensions of $45 \times 45 \times 45$ cm^3; a steam reservoir, which received steam from the boiler and maintained its pressure at around 200 kPa (gauge); and a liquid ring vacuum pump (model ET32030, Nash, Trumbull, CT), which was used to maintain a vacuum in the drying chamber. A steam trap was installed to reduce excess steam condensation in the reservoir. An electric heater, rated at 1.5 kW, controlled by a proportional–integral–derivative controller (model E5CN, Omron, Tokyo, Japan), was installed in the drying chamber to control the steam temperature and to minimize condensation of steam in the drying chamber during start-up; with the use of a heater, the initial steam condensation during the start-up period was reduced considerably. A variable-speed electric fan was used to disperse steam throughout the drying chamber. The steam inlet was made into a conical shape and was covered with a screen to help in the distribution of the steam in the chamber. The sample holder was made of a stainless steel screen with dimensions of 12×12 cm^2. The change of the mass of the sample was detected continuously (at 1 min intervals) using a load cell (model Ucg-3kg, Minebea, Nagano, Japan), which was installed in a smaller chamber connected to the drying chamber by a flexible hose (in order to maintain the same vacuum pressure as that in the drying chamber) and also to an indicator and recorder (model AD 4329, A&D Co., Tokyo, Japan). The temperature of the steam was also measured continuously using type K thermocouples, which were connected to an expansion board (model no. EXP-32, Omega Engineering, Stamford, CT). Thermocouple signals were then multiplexed to a data acquisition card (model no. CIO-DAS16Jr., Omega Engineering, Stamford, CT) installed in a PC. LABTECH NOTEBOOK software (version 12.1, Laboratory Technologies Corp.) was used to read and record the temperature data.

Material and Methods

Molecular sieve beads (no. 69837, Fluka, Buchs, Switzerland) that have a pore size of 0.4 nm and an average diameter of 3.02 mm with a standard deviation of 0.34 mm and a particle density of 750 kg/m^3 were used as the test material in this work. Prior to the start of each experiment, distilled water (6.7 g) was slowly sprayed onto the beads (22 g) to make the initial moisture content of the beads around 0.3 kg/kg (db), which was roughly the maximum moisture-holding capacity of the beads. The particles were then left in a tightly closed box at room temperature for about 6 h to allow them to equilibrate. The drying experiment was performed by placing roughly 28.7 g of water-saturated particles (about 1000 beads) on the sample holder as a single layer. The drying chamber was then sealed tightly, and valve 2 was opened to allow the steam from the boiler to flow into the reservoir; the steam pressure was maintained at about 200 kPa (gauge) in the reservoir. A vacuum pump was then switched on to evacuate the drying chamber to the desired operating pressure, and the steam regulator was opened to slowly flash the steam into the drying chamber. Because of the low-pressure environment in the chamber, the steam became superheated. An electric heater was used to maintain the steam temperature at the desired drying temperature. Although the ratio of the steam pressure in the steam reservoir to that in the drying chamber was rather high, the effect of the adiabatic expansion of steam introduced into the drying chamber on the steam temperature was rather small. This is because

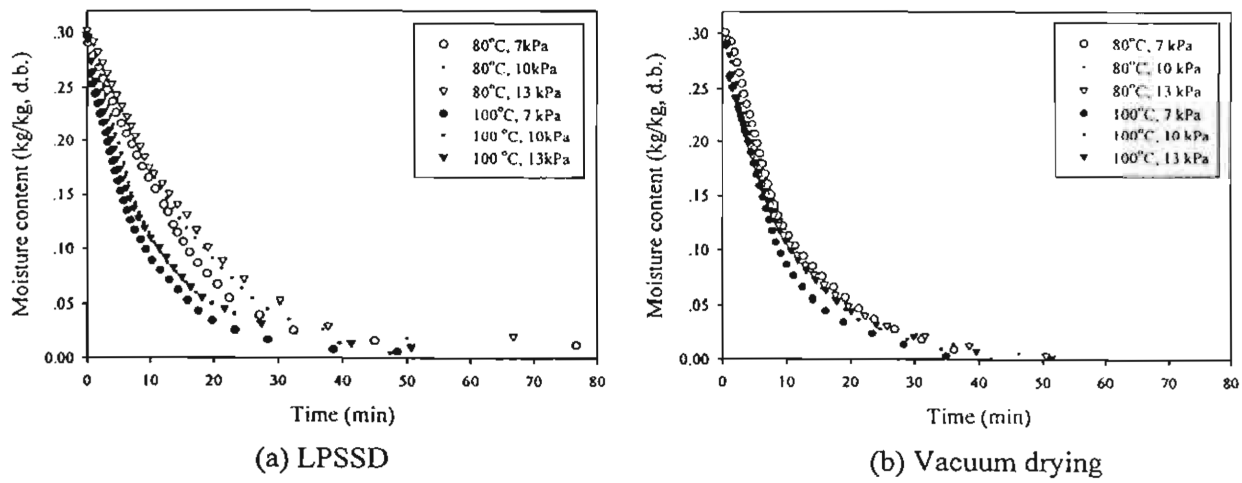

Figure 2. Drying curves of molecular sieve particles.

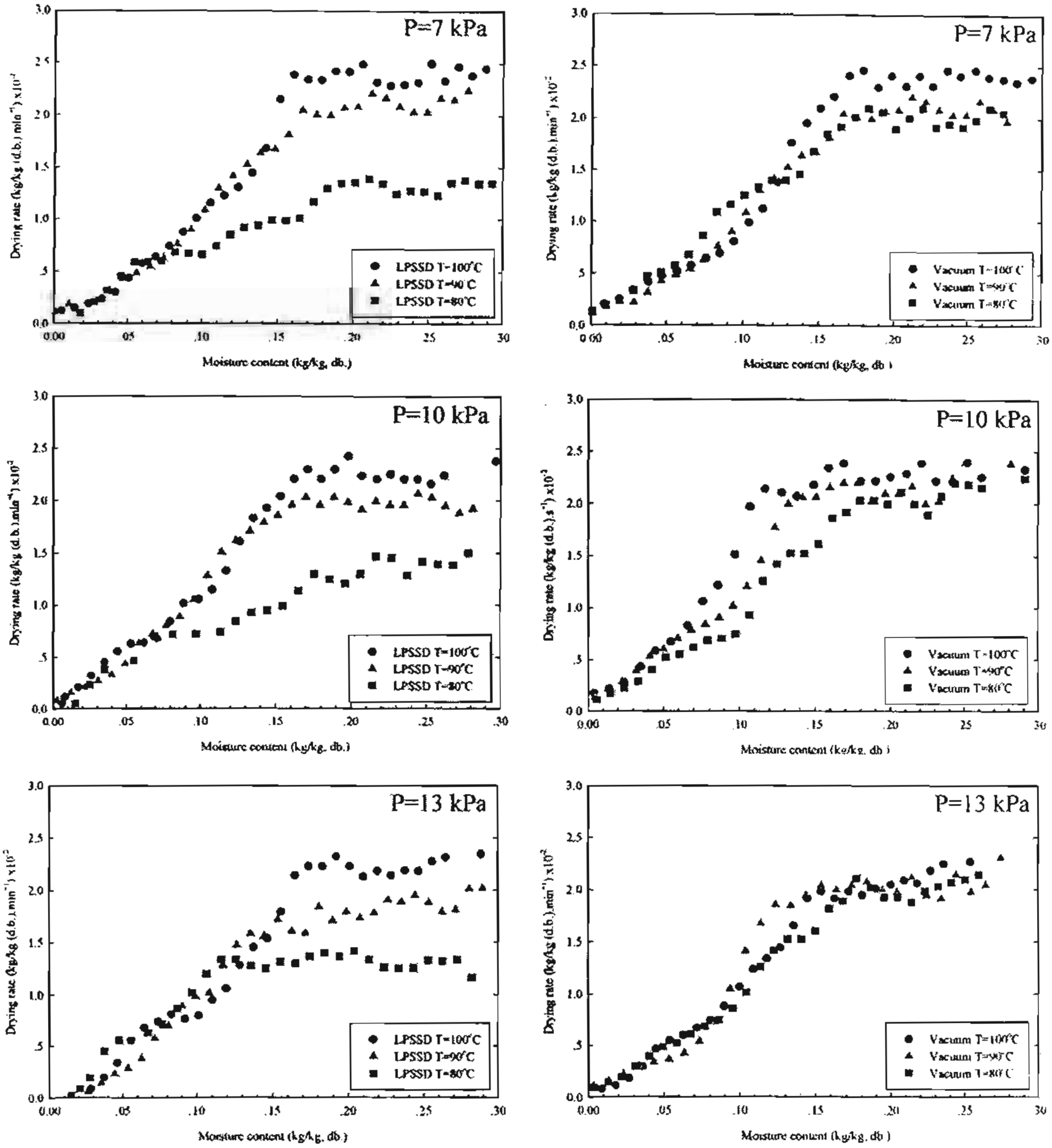

Figure 3. Drying rate curves of molecular sieve beads undergoing LPSSD and vacuum drying at various operating pressures.

an electric heater was installed in the drying chamber to help in the stabilization of the steam temperature. In addition, the temperature measurement was done carefully to ensure that the variation of the steam temperature within the drying chamber was negligible. At the end of drying, the breakup valve was opened to allow air into the drying chamber before opening up the chamber door and loading off the sample.

The experiments were performed under the following conditions: steam absolute pressures of 7, 10, and 13 kPa; steam temperatures of 80, 90, and 100 °C. The flow rate of steam into the drying chamber was maintained at about 26 kg/h, and the speed of the fan was fixed at around 2100 rpm. All experiments were performed in duplicate.

For vacuum-drying experiments, the same experimental setup was used but without the application of steam to the drying chamber. The same operating conditions as those used for LPSSD were therefore achievable.

Results and Discussion

Drying Rates of Porous Particles. Molecular sieve beads, which were saturated with water [the initial moisture content was about 0.3 kg/kg (db) or 23% (wb)], were dried to their equilibrium moisture content at each operating condition in the dryer using both low-pressure superheated steam and vacuum conditions. During each experiment, the drying rates were calculated from the recorded weight changes, during both the CRPs and FRPs. Because, strictly speaking, the inversion temperature is defined only for surface moisture evaporation and not for internal moisture removal, the drying rates in the CRP are reported first. The overall average drying rates, based on the rates in both the CRPs and FRPs, are then calculated and compared with the rates in the CRP to point out the fundamental differences between the values of the inversion temperatures calculated using only the rates in the CRP and those obtained using the overall average drying rates in both drying periods.

First, the drying curves for the single layer of particles undergoing LPSSD and vacuum drying at some selected conditions are shown in Figure 2. While the drying curves for LPSSD at different conditions are quite different and the effect of the temperature on the drying curves is greater than the effect of the pressure, the drying curves for vacuum drying at different operating conditions are rather similar. It is seen that the drying times of LPSSD at an operating temperature of 80 °C were longer than those of vacuum drying for all operating pressures tested. However, the drying times for both processes operated at 100 °C were quite similar. This is due to the fact that an increased drying temperature led to higher drying rates, resulting from sharply increased temperature differences or gradients between the samples and the ambient steam in the case of superheated steam drying. However, the differences between the air temperature and the particle surface temperature in vacuum drying increased only slightly as the drying temperature increased. In addition, it can be observed that the equilibrium moisture contents of the beads undergoing LPSSD were much higher than those undergoing vacuum drying. For example, the equilibrium moisture contents of particles dried at 80, 90, and 100 °C using LPSSD at an operating pressure of 7 kPa were 1.5, 0.9, and 0.2% (db), respectively, while the equilibrium moisture contents of particles were 0.09, 0.05, and 0.02% (db), respectively, in the case of vacuum drying at the same pressure. This is due to a higher humidity condition in the drying chamber of LPSSD and, hence, a reduced vapor pressure gradient, which is the driving force of the drying process. Therefore, the drying times of most LPSSD were longer than those of vacuum drying.

Figure 3 shows a comparison of the observed drying rate curves in superheated steam drying with those in vacuum drying at different operating conditions. For all conditions, the drying rates fluctuated marginally but remained nearly constant as the moisture content decreased until the critical moisture content for each condition was reached. The drying rates then decreased continuously in the FRP. It can be seen from this figure that the critical moisture content was different for different conditions in the case of superheated steam drying [the critical moisture contents of particles dried, for example, at 80, 90, and 100 °C were 20, 17, and 15% (db), respectively, at an operating pressure of 7 kPa] but were quite similar in the case of vacuum drying [17% (db) over the temperature range of 80−100 °C at an operating pressure of 7 kPa]. It was also observed that the lower-pressure and higher-temperature superheated steam led to larger amounts of water evaporation and also to higher critical moisture contents.

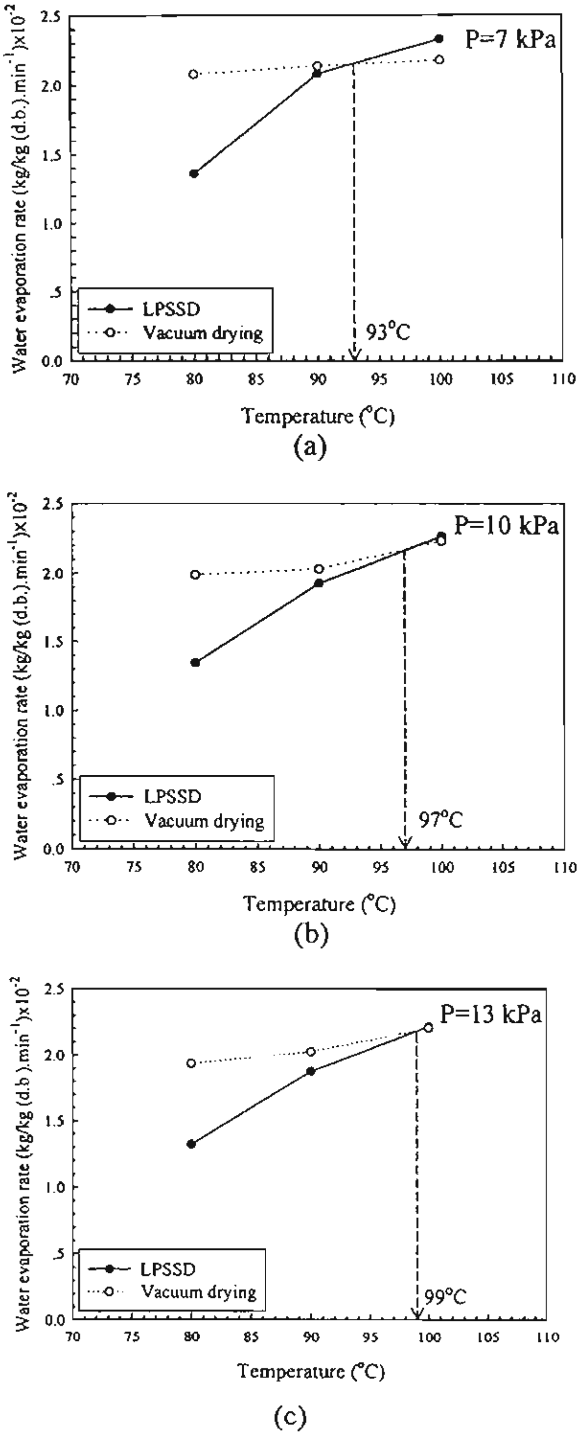

Figure 4. CRP evaporation rates of moisture from molecular sieve beads at various operating pressures.

Figure 4 gives the rates of water evaporation during the CRP at various operating temperatures and pressures. It was found, as expected, that raising the drying temperature led to higher CRP drying rates because of an increased temperature difference between the steam (or air) and the samples as well as a reduction of the initial steam condensation in the case of superheated steam drying. In the case of LPSSD, the temperature

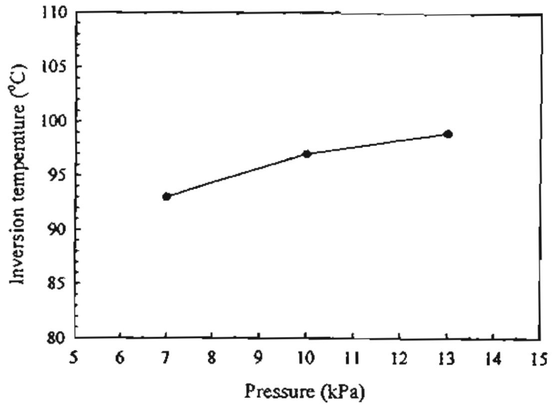

Figure 5. Effect of the operating pressure on the inversion temperature (based on CRP drying rates) of molecular sieve beads.

difference is the difference between the superheated steam temperature and the saturation temperature at the corresponding operating pressure, while for vacuum drying, the difference is between the air temperature and a temperature between the wet-bulb temperature and the saturation temperature (not saturation temperature because, in this case, the level of vacuum was not so high that the effect of convection by the fan could be negligible). While the temperature differences (or driving forces for heat transfer) in vacuum drying were higher at lower operating temperatures than those observed in LPSSD, the values of the heat-transfer coefficient of the medium in the case of vacuum drying were lower because of the inferior thermal properties of air. Raising the drying temperature, however, led to higher temperature differences and, hence, higher CRP drying rates. The counteracting effects of the heat-transfer coefficient and the temperature difference led to the inversion phenomenon, as is evident in Figure 4, where the CRP drying rates of vacuum drying and LPSSD are seen to be equal. Beyond the inversion temperature, the CRP drying rates of steam drying were higher than those of vacuum drying because of both the increased temperature difference and the higher heat-transfer coefficient.

When the operating pressure was increased (at the same operating temperature), it can be seen that the drying rate was lower. This was due to the fact that the boiling temperature of water at higher pressure is higher; this leads to a decreased temperature difference and, hence, a lower drying rate.

As mentioned earlier, the CRP drying rates depend on the rate of heat transfer and, hence, the difference between the surface temperature of the sample and the drying medium temperature. For this reason, the drying temperature had only a small effect on the rates of vacuum drying as compared with the case of LPSSD because the particle surface temperature in the case of vacuum drying (which relates somehow to the wet-bulb temperature) changes only slightly with an increased drying temperature compared with the change of the boiling temperature, especially at lower operating pressures.

Inversion Temperature. Figure 5 shows the effect of the operating pressure on the inversion temperature, which was calculated from the CRP rates (Figure 4). The inversion temperature at each operating pressure was obtained from the plots of the drying rates at the point where the rates of vacuum drying and LPSSD were equal.

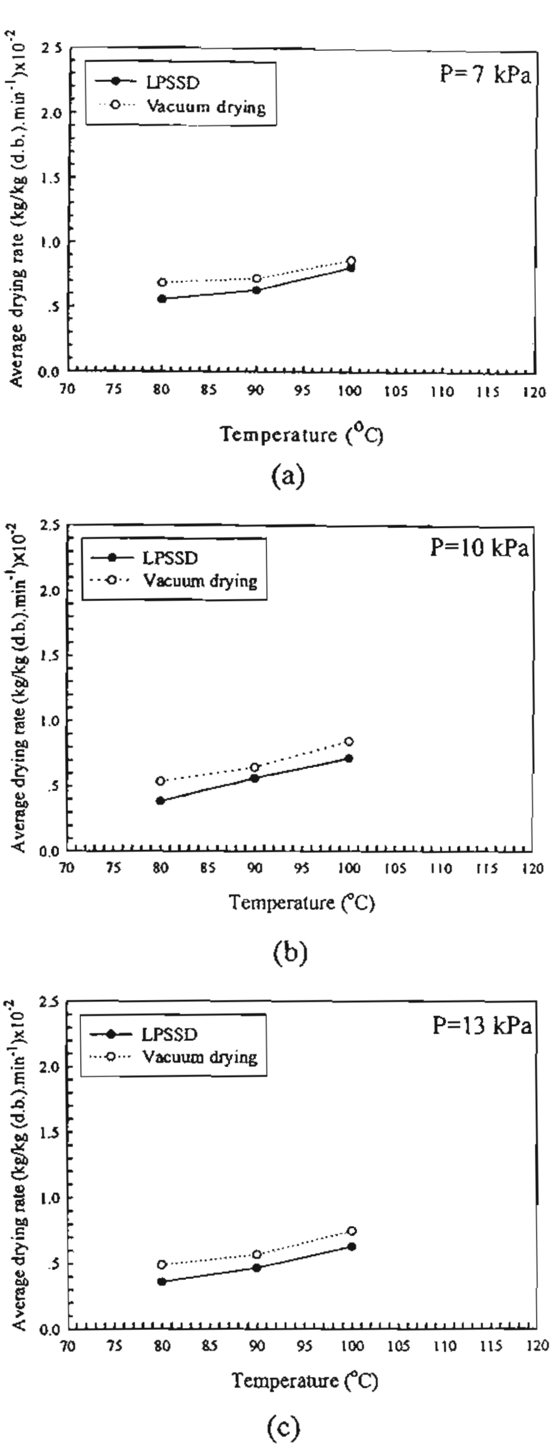

Figure 6. Average rate (CRP + FRP) of moisture removal from molecular sieve beads at various operating pressures.

Figure 6 shows the overall average drying rates calculated from combined CRP and FRP drying rates at various operating pressures. As mentioned earlier, the CRP drying rates depend only on the external heat- and mass-transfer conditions because free water is always available for evaporation at the surface of the sample. However, in the FRP, the rates depend not only on the rate of external heat transfer but more on

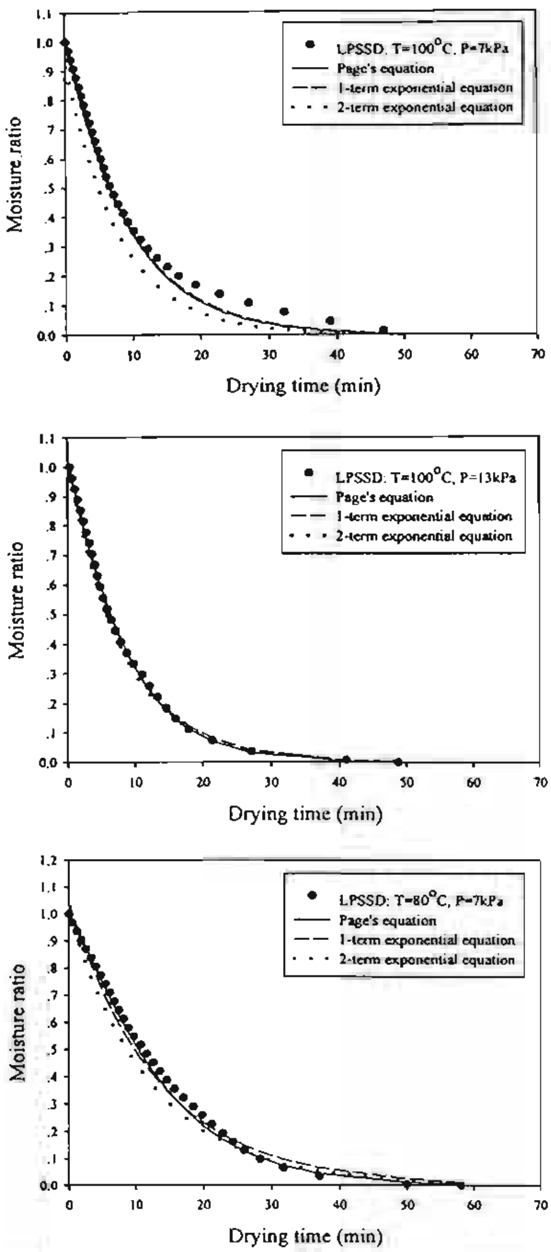

Figure 7. Comparison of fitted models with the experimental data in the case of LPSSD.

internal resistances to heat and mass transfer, which are somewhat material-dependent. Therefore, the average drying rates calculated from combined CRP and FRP rates were not the same as the CRP drying rates. It can be seen from Figures 4 and 6 that the differences between vacuum- and steam-drying CRP rates are greater than those between vacuum and steam drying calculated from combined CRP and FRP rates. This is due to the fact that in FRP the resistances to heat and mass transfer of superheated steam drying are lower than those of vacuum drying because the drying medium of steam drying is water vapor and, hence, there is no diffusional resistance of water from the sample into the drying medium. These effects of the FRP drying rates, therefore, increase the values of the combined (or overall) drying rates of superheated steam drying and, hence, lead to smaller differences between the overall drying rates of vacuum and steam drying. No inversion temperature was observed from the plots of the overall drying rates as well.

Mathematical Modeling. Simple mathematical models that enable prediction of the drying curves of molecular sieves undergoing LPSSD and vacuum drying were developed based on the well-known Page's equation,[13] single-term exponential equation, and two-term exponential equation (Arrhenius-type model). Exponential equations were listed, and their prediction abilities were compared with that of a simpler Page's equation with no real physical basis but just to illustrate that different sets of equations are suitable for different drying techniques.

Page's Equation.

$$\mathrm{MR} = \frac{X_t - X_{eq}}{X_i - X_{eq}} = \exp(-kt^n) \tag{1}$$

The parameters k and n in the equation were determined from the experimental data and were correlated as follows:

For LPSSD

$$k = -2.39 \times 10^{-1} + 2.86 \times 10^{-3}T - 7.13 \times 10^{-3}P - 3.83 \times 10^{-6}TP + 5.42 \times 10^{-2} \ln P \qquad R^2 = 0.95$$

$$n = (1.87\text{–}3.91) \times 10^{-3}T + 1.11 \times 10^{-1}P - 5.44 \times 10^{-4}TP - 4.35 \times 10^{-1} \ln P \qquad R^2 = 0.86$$

For vacuum drying

$$k = -7.42 \times 10^{-2} - 7.07 \times 10^{-5}T - 1.01 \times 10^{-2}P + 1.22 \times 10^{-5}TP + 1.12 \times 10^{-1} \ln P \qquad R^2 = 0.96$$

$$n = (1.12\text{–}2.40) \times 10^{-3}T - 7.88 \times 10^{-2}P + 4.92 \times 10^{-4}TP + 2.21 \times 10^{-1} \ln P \qquad R^2 = 0.73$$

Single-Term Exponential Equation.

$$\mathrm{MR} = \frac{X_t - X_{eq}}{X_i - X_{eq}} = a \exp(-bt) \tag{2}$$

For LPSSD

$$a = (1.12\text{–}1.41) \times 10^{-3}T + 4.53 \times 10^{-3}P - 6.87 \times 10^{-6}TP + 6.53 \times 10^{-3} \ln P \qquad R^2 = 0.75$$

$$b = -6.15 \times 10^{-2} + 1.12 \times 10^{-3}T - 9.75 \times 10^{-3}P + 7.56 \times 10^{-5}TP + 3.77 \times 10^{-2} \ln P \qquad R^2 = 0.91$$

For vacuum drying

$$a = 9.68 \times 10^{-1} + 1.22 \times 10^{-3}T + 1.59 \times 10^{-4}P - 2.73 \times 10^{-5}TP - 1.12 \times 10^{-1} \ln P \qquad R^2 = 0.94$$

$$b = 1.97 \times 10^{-2} - 3.74 \times 10^{-4}T - 2.13 \times 10^{-2}P + 1.08 \times 10^{-4}TP + 1.03 \times 10^{-1} \ln P \qquad R^2 = 0.70$$

Two-Term Exponential Equation.

$$\mathrm{MR} = \frac{X_t - X_{eq}}{X_i - X_{eq}} = a_1 \exp(-b_1 t) + c_1 \exp(-d_1 t) \tag{3}$$

For LPSSD

$$a_1 = (0.699P^{-0.051}) \exp(-51.312/T_{abs}) \qquad R^2 = 0.62$$

$$b_1 = (354.576P^{-0.0267}) \exp(-2958/T_{abs}) \qquad R^2 = 0.95$$

$$c_1 = (5.63 \times 10^{-3}P^{0.408}) \exp(-1269.76/T_{abs}) \qquad R^2 = 0.59$$

$$d_1 = (827.98P^{-0.132}) \exp(-3175.72/T_{abs}) \qquad R^2 = 0.93$$

For vacuum drying

$$a_1 = (3.709P^{0.554}) \exp(-1056.055/T_{abs}) \qquad R^2 = 0.53$$

$$b_1 = (0.164P^{0.059}) \exp(-185.677/T_{abs}) \qquad R^2 = 0.49$$

$$c_1 = (1.63 \times 10^{-3}P^{-1.082}) \exp(2773.12/T_{abs}) \qquad R^2 = 0.75$$

$$d_1 = (4.73 \times 10^{-2}P^{-0.903}) \exp(871.105/T_{abs}) \qquad R^2 = 0.95$$

The equations were fitted with the experimental data; the fitted equations were evaluated based on their R^2 and standard error of estimation. When the three drying models are compared, the results show that Page's equation fits the experimental data better than the single-term exponential equation and the two-term exponential equation in the case of LPSSD, while the single-term exponential equation fits the experimental data well in the case of vacuum drying at operating temperatures in the range of 80−100 °C and pressures of 7−13 kPa as exemplified in Figures 7 and 8. The minimum R^2 of Page's equation was 0.997 and its maximum standard error of estimation was 0.0181 in the case of LPSSD, while the minimum R^2 of the single-term exponential equation was 0.998 and its maximum standard error was 0.0233 in the case of vacuum drying. Drying constants of Page's equation (k and n) and of the single-term exponential equation (a and b) are found to depend on the operating temperature as well as pressure.

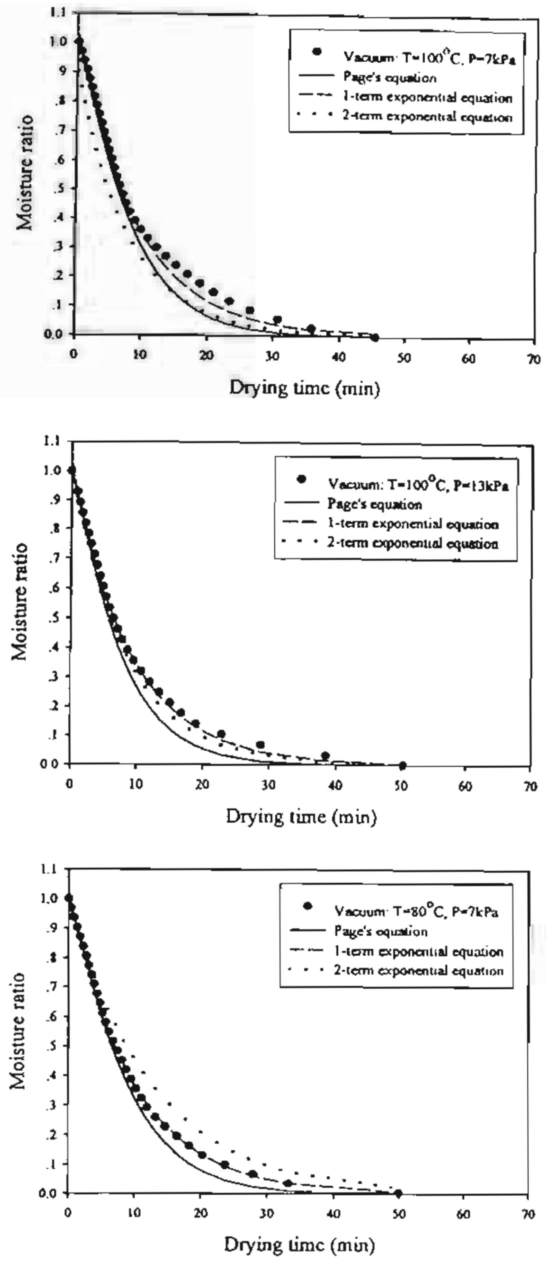

Figure 8. Comparison of fitted models with the experimental data in the case of vacuum drying.

Concluding Remarks

The effects of operating parameters, i.e., drying temperature and pressure, on the rates of vacuum drying and LPSSD of model porous particles were investigated experimentally. In addition, the values of the inversion temperature calculated only from the rates of drying in the CRP were compared with those calculated from the whole drying period (CRP and FRP) in order to point out the fundamental differences between the two sets of temperatures beyond which the drying rates in LPSSD were higher than those in vacuum drying. It was found that the inversion temperatures calculated from combined CRP and FRP rates were not the same as the inversion temperatures calculated from only CRP rates; in the former case, no inversion temperature was indeed observed within the ranges of study. Empirical models that describe the experimental drying curves are also proposed. It is found that Page's equation and the single-term exponential equation can fit well the experimental data for LPSSD and vacuum drying, respectively, over the ranges of operating temperature of 80−100 °C and pressure of 7−10 kPa.

Acknowledgment

The authors express their sincere appreciation to the Thailand Research Fund (TRF), National Science and Technology Development Agency (NSTDA), and the International Foundation for Science (Sweden) for supporting this study financially.

Nomenclature

a = constant of the single-term exponential model
a_1 = constant of the two-term exponential model
b = constant of the single-term exponential model
b_1 = constant of the two-term exponential model

c_1 = constant of the two-term exponential model
d_1 = constant of the two-term exponential model
k = constant of Page's equation
MR = moisture ratio
n = constant of Page's equation
P = absolute pressure, kPa
t = drying time, min
T = temperature of the drying medium, °C
T_{abs} = temperature of the drying medium, K
X_{eq} = equilibrium moisture content, kg/kg (db)
X_i = initial moisture content, kg/kg (db)
X_t = moisture content at any time, kg/kg (db)

Literature Cited

(1) Mujumdar, A. S. Superheated steam drying—Technology of the future. In *Mujumdar's Practical Guide to Industrial Drying*; Devahastin, S., Ed.; Exergex: Brossard, Canada, 2000; pp 115–138.

(2) Kumar, P.; Mujumdar, A. S. Superheated-steam drying: A bibliography. *Drying Technol.* **1990**, *8*, 195.

(3) Elustondo, D.; Elustondo, M. P.; Urbicain, M. J. Mathematical modeling of moisture evaporation from foodstuffs exposed to subatmospheric pressure superheated steam. *J. Food Eng.* **2001**, *49*, 15.

(4) Shibata, H.; Mada, J.; Shinohara, H. Drying mechanism of sintered spheres of glass beads in superheated steam. *Ind. Eng. Chem. Res.* **1988**, *27*, 2353.

(5) Shibata, H.; Mada, J.; Funatsu, K. Prediction of drying curves on sintered spheres of glass beads in superheated steam under vacuum. *Ind. Eng. Chem. Res.* **1990**, *29*, 614.

(6) Senda, Y.; Bando, Y.; Yasuda, K.; Nakamura, M.; Sugimura, Y.; Shibata M. Development of superheated steam dryer at reduced pressure. *Proceedings of the 1st Asia–Pacific Drying Conference*, Bali, Indonesia, 2001; p 247.

(7) Elustondo, D. M.; Mujumdar, A. S.; Urbicain, M. J. Optimum operating conditions in drying foodstuffs with superheated steam. *Drying Technol.* **2002**, *20*, 381.

(8) Elustondo, D.; Elustondo, M. P.; Urbicain, M. J. Drying with superheated steam: Maximum drying rate as a linear function of pressure. *Chem. Eng. J.* **2002**, *86*, 69.

(9) Devahastin, S.; Suvarnakuta, P.; Soponronnarit, S.; Mujumdar, A. S. A comparative study of low-pressure superheated steam and vacuum drying of a heat-sensitive material. *Drying Technol.* **2004**, *22*, 1845.

(10) Iyota, H.; Nishimura, N.; Onuma, T.; Nomura, T. Drying of sliced raw potatoes in superheated steam and hot air. *Drying Technol.* **2001**, *19*, 1411.

(11) Iyota, H.; Nishimura, N.; Onuma, T.; Nomura, T. Simulation of superheated steam drying considering initial steam condensation. *Drying Technol.* **2001**, *19*, 1425.

(12) Shibata, H.; Mada, J.; Shinohara, H. Steam drying of sintered glass bead spheres under vacuum. *Ind. Eng. Chem. Res.* **1988**, *27*, 2385.

(13) Page, G. Factors influencing the maximum rates of air drying shelled corn in thin layers. Master's Thesis, Purdue University, West Lafayette, IN, 1949.

Received for review April 21, 2004
Revised manuscript received November 10, 2004
Accepted January 5, 2005

IE049675R

Available online at www.sciencedirect.com
SCIENCE DIRECT
ELSEVIER
Journal of Stored Products Research 41 (2005) 387–400
Journal of STORED PRODUCTS RESEARCH
www.elsevier.com/locate/jspr

Investigations on head-rice yield and operating time in the fluidised-bed drying process: experiment and simulation

Nattapol Poomsa-ad[a], Apichit Terdyothin[b], Somkiat Prachayawarakorn[c,*], Somchart Soponronnarit[b]

[a]*Faculty of Engineering and Computer Science, Mahasarakham University, Mahasarakham 44150, Thailand*
[b]*School of Energy and Materials, King Mongkut's University of Technology Thonburi, Suksawat 48 Road, Bangkok 10140, Thailand*
[c]*Faculty of Engineering, King Mongkut's University of Technology Thonburi, Suksawat 48 Road Tongkru, Bangkok 10140, Thailand*

Accepted 7 June 2004

Abstract

This analysis of the drying process is based on experiments and simulations of the influence of temperature in the fluidised-bed dryer, moisture content and tempering period on head-rice yield, and operating time. A mathematical model incorporating the head-rice yield equation for predictions of the moisture content and the grain temperature in each drying stage and the final head-rice yield, is in good agreement with experimental data. The moisture content after first-stage drying and tempering have a dominant effect on head-rice yield and operating time in reducing high-moisture contents to a safe level. The simulation results recommend that the allowable temperature should be not higher than 150 °C for the first stage and the moisture content after first-stage drying should be not lower than 22.5% dry basis, with subsequent tempering for at least 25 min.

Keywords: Dehydration; Head rice; Fluidised bed; Grain; Modelling

*Corresponding author. Tel.: +662-4270-9221; fax: +662-428-3534.
E-mail address: somkiat.pra@kmutt.ac.th (S. Prachayawarakorn).

0022-474X/$ - see front matter
doi:10.1016/j.jspr.2004.06.002

Nomenclature

C_a	specific heat of dry air, kJ/kg °C
C_v	specific heat of water vapour, kJ/kg °C
C_{pw}	specific heat of moist paddy, kJ/kg °C
D	effective diffusivity, m^2/s
h_{fg}	latent heat of water, kJ/kg
I_c	tempering index, decimal
M	moisture content, decimal or per cent dry basis
M_{eq}	equilibrium moisture content, decimal dry basis
M_{av}	average inlet moisture content at time t, decimal dry basis
M_f	average moisture content at time $= t + \Delta t$, decimal dry basis
M_i	average moisture content at time $= t$, decimal dry basis
M_{in}	initial moisture content, decimal dry basis
$M_{s,t}$	surface moisture content at time t, decimal dry basis
$\dot{m}_a$	mass flow rate of dry fresh air, kg/s
m_p	mass of dry matter, kg
l	half height of cylinder axis, m
R	ratio of dry mass of grain to mass of air, kg dry matter /kg dry air
RHY	relative head-rice yield
r	co-ordinate along the radius of cylinder, m
r_o	radius of paddy, m
T_{abs}	absolute temperature, K
T_f	exhaust-air temperature, °C
T_{in}	inlet-air temperature, °C
t	drying time or tempering time, minute or s
V_p	particle volume, m^3
W_f	exhaust-humidity ratio of air, kg water/kg dry air
W_{in}	inlet-humidity ratio of air, kg water/kg dry air
z	length of cylinder, m
θ	grain temperature, °C
θ_{in}	inlet-grain temperature, °C

1. Introduction

High-moisture paddy grains must be dried rapidly to prevent deterioration, and in this study the fluidised-bed drying system is considered. The paddy drying process is traditionally divided into three steps in order to reduce the moisture content to a safe level of 16.5% dry basis. Paddy is first dried for a few minutes at a temperature above 130 °C, then the grain is tempered for a certain period and, as the last step, the tempered paddy is dried again with ambient air or slightly heated air until its moisture content reaches the safe storage level.

The tempering period is the stage in which paddy is kept in a closed bin without airflow. After a sufficiently long period of tempering, the moisture profile throughout the paddy becomes uniform. This uniformity provides a decrease of tensile stress occurring inside the grains from the first drying stage, thus maintaining high head-rice yield after subsequent drying (Steffe et al., 1979; Zhang and Litchfield, 1991; Li et al., 1999; Soponronnarit et al., 1999). In addition, tempering also reduces the drying time in the final stage, resulting in more effective energy utilisation. The parameters determining head-rice yield are tempering period, moisture contents at the start and at the end of the first stage, and grain temperature after the first stage (tempering temperature). The tempering temperature is related to drying-air temperature and drying time. In practice, these parameters vary widely across the industry, depending upon the owners' experiences. Hence, operating times longer than necessary for obtaining optimum grain quality may be used. A thorough investigation of these factors in paddy processing is needed.

Therefore, the objectives of the present work were: (1) to study the effect of initial moisture content, inlet-air temperature and tempering period on head-rice yield, and to establish a head-rice yield equation: (2) to determine suitable operating conditions which provide a superior quality head-rice yield and optimum operating time. To achieve the second objective, a mathematical model has been formulated that is capable of predicting moisture content, grain temperature and relative head-rice yield (RHY).

2. Mathematical model of drying system

The paddy drying process consists of a drying unit, a tempering unit and an ambient-air ventilation unit (Fig. 1). A mathematical model for each stage was developed.

The formulation of the mathematical model was based on the following assumptions:

- The paddy kernel were of uniform size and a finite cylindrical shape.
- The grains in the bed were perfectly mixed such that every individual grain had the same moisture content at any drying time.
- Internal diffusion was the dominant mechanism for moisture transport in the grains.
- The drying air was in thermal equilibrium with the exiting grain kernels, so that the grain temperature was equivalent to the exhaust air temperature.
- The temperature gradient inside the kernels and grain shrinkage were negligible.

The model of a drying process with the above assumptions must comprise three governing equations, mass balance, energy balance between air and grain bed, and the drying-rate equation.

2.1. Heat and mass balances

In a small interval of time Δt, a certain amount of moisture evaporates from the grain bed into the air, resulting in a change in the humidity ratio. This moisture balance can be written as

$$W_f = R(M_i - M_f) + W_{in}, \qquad (1)$$

where W_f is the exhaust-humidity ratio of air (kg water/kg dry air), W_{in} the inlet-humidity ratio of air(kg water/kg dry air), M_i the average moisture content at time $= t$, decimal dry basis, M_f the average moisture content at time $= t+\Delta t$, decimal dry basis and R the ratio of dry mass of grain to mass of air $(m_p/(\dot{m}_a \times \Delta t))$, decimal.

The exhaust-air temperature from the fluidised-bed dryer can be determined by Eq. (2),

$$T_f = (C_a T_{in} + W_{in}(h_{fg} + C_v T_{in}) - W_i h_{fg} + RC_{pw}\theta_{in})/(C_a + W_f C_v + RC_{pw}), \quad (2)$$

where T_f is the exhaust-air temperature (°C), T_{in} the inlet-air temperature (°C), θ_{in} the inlet-grain temperature (°C), C_a the specific heat of dry air (kJ/kg °C), C_v the specific heat of water vapour (kJ/kg °C), C_{pw} the specific heat of moist grain (kJ/kg °C), and h_{fg} the latent heat of moisture evaporation (kJ/kg).

At the inlet, the grain temperature is equal to the ambient air temperature.

2.2. Drying kinetics for a single kernel

Moisture migration within a kernel is described by mass diffusion during the drying and tempering stages. For a finite cylinder, the partial differential equation for moisture diffusion in a single paddy kernel can be written as

$$\frac{\partial M}{\partial t} = D\left[\frac{\partial^2 M}{\partial r^2} + \left(\frac{1}{r}\right)\frac{\partial M}{\partial r} + \frac{\partial^2 M}{\partial z^2}\right], \quad (3)$$

where D is the effective moisture diffusion (m^2/s), M the moisture content, decimal dry basis, r the co-ordinate along the radius of cylinder (m), t the time (min or s), and z the length of cylinder (m).

The expression for D obtained by Poomsa-ad et al. (2002) is given by

$$D = 5.41141 \times 10^{-6} \exp\left(-\frac{28436.4}{T_{abs}}\right), \quad (4)$$

where T_{abs} is the absolute air temperature (K). Eq. (4) is valid over the temperature range from 373.15 to 443.15 K. The average air temperature between the inlet and exhaust conditions was used to calculate the effective diffusion coefficient.

2.3. Initial and boundary conditions

Moisture content within the grain at the inlet can be assumed to be spatially uniform and the gas-film resistance around the grain surface is presumed negligible, allowing the moisture content at the surface to equilibrate with the drying air

$$\begin{array}{ll} t = 0, \quad 0 \leqslant r \leqslant r_o, & M = M_{in}, \\ -l \leqslant z \leqslant +l, & M = M_{in}, \\ t > 0, \quad r = r_o, & M = M_{eq}, \\ z = \pm l, & M = M_{eq}, \\ t > 0, \quad r = 0, & \frac{\partial M}{\partial r} = 0, \end{array}$$

where M_{in} is the initial moisture content, decimal dry basis, M_{eq} the moisture content at the equilibrium, decimal dry basis, and l the half height of cylinder representing grain (m).

The moisture equilibrium equation of Laithong (1987) used in the present study is given by

$$1 - \Phi = \exp\{(-4.584 \times 10^{-6})T_{abs}(100M_{eq})^{2.397}\}. \tag{5}$$

The solution of Eq. (3) can be found by the finite difference method. In calculation, the grain shape was divided into 80 nodes in length and 10 nodes in radius. The average moisture content for a single kernel can be determined by

$$M_{av} = \frac{1}{V_p}\iint 2\pi M(r,z,t)\,\mathrm{d}r\,\mathrm{d}z, \tag{6}$$

where M_{av} is the average moisture content at time t, decimal dry basis, and V_p the volume of a single kernel (m^3).

Eqs. (1)–(4) can be solved by iteration. Assuming the exhaust air temperature, the amount of water evaporation from the grains into the air can be determined by Eqs. (3)–(6). The value of W_f from Eq. (1) allows recalculation of T_f by Eq. (2). Iteration leads to final values of M_f and T_f at time t.

2.4. Initial and boundary conditions for tempering stage

During this period, moisture inside a paddy kernel moves to the exterior surface, but does not evaporate to the environment due to the limited volume in tempering storage and consequent lack of air movement. The validity of this behaviour has been noted by Sabbath (1970) and Steffe (1979). The boundary and initial conditions for the tempering period are as follows:

$$\begin{array}{lll} t = 0, & & M = M(r,z), \\ t > 0, & r = r_o, & \frac{\partial M}{\partial r} = 0, \\ z = \pm l, & & \frac{\partial M}{\partial z} = 0, \\ t > 0, & r = 0, & \frac{\partial M}{\partial r} = 0. \end{array}$$

2.5. Head-rice yield

RHY can be written in the general function as

$$RHY = f(\theta, M, t), \tag{7}$$

where RHY is the RHY yield, M the preset moisture content, per cent dry basis, t the tempering time (min), and θ the grain temperature (°C).

RHY is defined as the ratio of head rice obtained from the drying process to that from ambient-air drying. Details of this equation will be discussed in the section on results and discussion. After determining the required tempering time, head rice can then be calculated. In calculating moisture content, we assume that drying at the second stage using ambient air does not affect the quality due to the low drying rate.

2.6. Ambient-air ventilation

The analogous equations of heat and mass balances throughout the thin bed as previously represented are used again for the ventilation stage by replacing θ_{in} in Eq. (2) by the tempering temperature or grain temperature after the first stage, and then solving for moisture content with Eq. (3). At this stage, the grain temperature is much higher than the ambient air temperature so the grain temperature is used as an input parameter in calculating the effective diffusion coefficient. The grain temperature and the inlet-air humidity are used to calculate the equilibrium moisture content with Eq. (5). Initial and boundary conditions for the single grain kernel during this step are given by

$$\begin{aligned}
&t = 0, && M = M(r, z),\\
&t > 0, \quad r = r_o, && M = M_{eq},\\
&z = \pm l, && M = M_{eq},\\
&t > 0, \quad r = 0, && \frac{\partial M}{\partial r} = 0.
\end{aligned}$$

3. Materials and methods

The freshly harvested paddy was rewetted, mixed and kept in cool storage at 3–5 °C for 5–7 days. Before starting the experiment, the cooled paddy was kept in ambient air until the grain temperature was close to ambient temperature. A schematic drying system is shown in Fig. 1. The drying system comprised a cylinder-shaped drying chamber of 20 cm diameter and 140 cm height, a 12 kW electrical heater and a backward curved-blade centrifugal fan driven by a 1.5 kW motor. Drying-air temperature was controlled by a proportional integral derivative controller with an accuracy of ± 1 °C. A mechanical variable speed unit regulated airflow rate. Moist paddy was dried initially by a batch-type fluidised-bed dryer. After the moisture content of the paddy was reduced to a preset value, the paddy was collected in a glass bottle with a diameter of 12 cm and a height of 10 cm and kept in an oven at a temperature equal to the grain temperature after drying. Finally, it was ventilated immediately by an ambient airflow until its moisture content was close to 16.5% dry basis. A 300 g sample was kept in a sealed plastic bag for 2 weeks before testing the head-rice yield.

Paddy prepared at three moisture levels, 35%, 30% and 25% dry basis, was dried at drying-air temperatures of 110, 130, 150 and 170 °C and drying times of 1, 2, 3 and 4 min. Such conditions were performed at a fixed-bed air velocity of 2.2 m/s and a bed thickness of 10 cm. Tempering times studied in the present work were 0, 15, 30 and 45 min. Temperatures at different positions were measured with an accuracy of ± 1 °C by K-type thermocouples connected to a data logger. The moisture content of the paddy was determined in an air oven at a temperature of 103 °C for 72 h. For head-rice yield, a 125 g paddy sample was dehusked with a two-rubber roller machine and the bran removed with a SATAKE milling machine. Head rice was separated from the broken rice by a sieving screen. Head rice is defined in this study as the ratio of the head-rice mass to the original paddy mass.

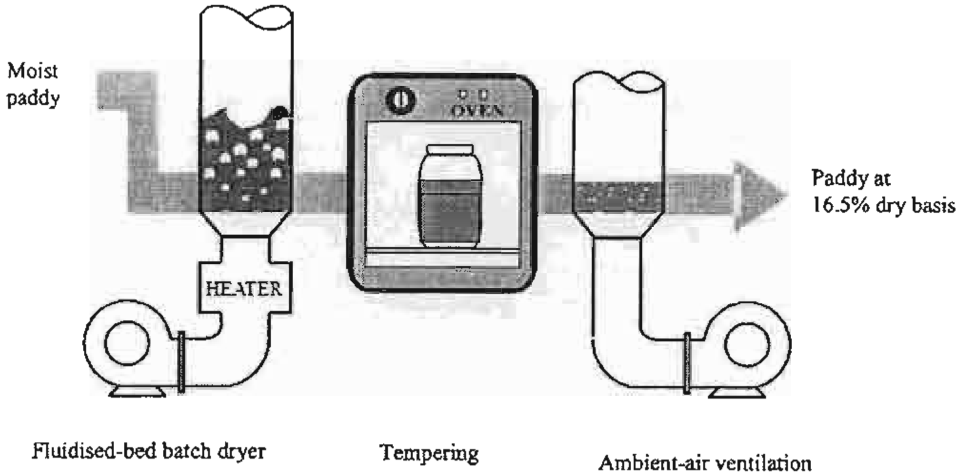

Fig. 1. Schematic diagram of a paddy drying system.

4. Results and discussion

4.1. Effect of drying conditions on RHY without tempering

Fig. 2 shows the effect of final moisture content and grain temperature on RHY at different initial moisture contents. Both final moisture content and grain temperature showed a strong influence on head-rice yield reduction. Most of the data show the RHYs lower than 40% if there was no tempering treatment between stages. Corresponding grain temperatures varied widely between 80 and 115 °C depending upon initial moisture content, inlet-air temperature and drying time.

High values of RHY (>90%) can be obtained for the initial moisture contents of 30 and 35% dry basis when final moisture content after the first stage is higher than 25% dry basis, corresponding to grain temperatures between 60 and 95 °C. For an initial moisture content of 25% dry basis, however, moisture content should not be reduced below 20% dry basis.

Broken rice exists after milling as a result of the steep moisture gradient in the grain produced by the rapid drying (Kunze, 1996). This causes the development of compressive stresses at the grain surface and tensile stresses at the centre. When the compressive stresses exceed the tensile stresses of grain at its centre, grain cracking develops, leading to less mechanical resistance during milling.

4.2. Effect of tempering time on RHY

The RHY from a set of tempering times is shown in Fig. 3. The percentage of RHY became higher with increased tempering time. The head-rice yield showed a small improvement with the 15-min tempering time as represented in Fig. 3a and increased to a moderate level with a longer tempering time. The improved quality was mainly in paddy dried to moisture contents lower than 24% dry basis at the first stage, which previously represented poor head-rice yield as shown

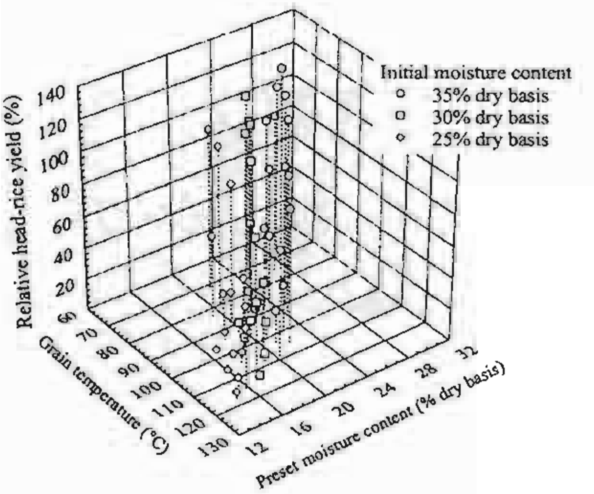

Fig. 2. Effects of preset moisture content and grain temperature after fluidised-bed drying on RHY (without tempering).

in Fig. 2. Values of RHY were now greater than 60% for a 30-min tempering time, as presented in Fig. 3b, with a few results at lower levels. For the case of 45 min as shown in Fig. 3c, results showed a similar trend to that in Fig. 3b. The better quality of the head-rice yield may be due to the combined effects of partially gelatinised grain and relaxing of the moisture gradient inside the grains.

4.3. The prediction equation for RHY

Multiple-linear regression was used to fit experimental data to a polynomial equation. The form of the prediction equation for RHY chosen was

$$RHY = A + Bt + Ct_,^2 \quad R^2 = 0.82, \tag{8}$$

where

$$A = -39.232 + 8.4227\,M - 0.34060\,T - 0.029105\,TM,$$
$$B = 25.945 - 1.1878\,M - 0.24443\,T + 0.012302\,TM,$$
$$C = -0.33610 + 0.015028\,M + 0.0032590\,T - 0.00015762\,TM,$$

t, M and T were tempering time in minutes, moisture content in per cent dry basis and tempering temperature in °C, respectively. The correlation coefficient between model and data was 0.82. This equation was valid in the following range:

15.5% dry basis $< M < 30\%$ dry basis,

$65\,°C < T < 115\,°C$,

$0\,min < t < 60\,min$.

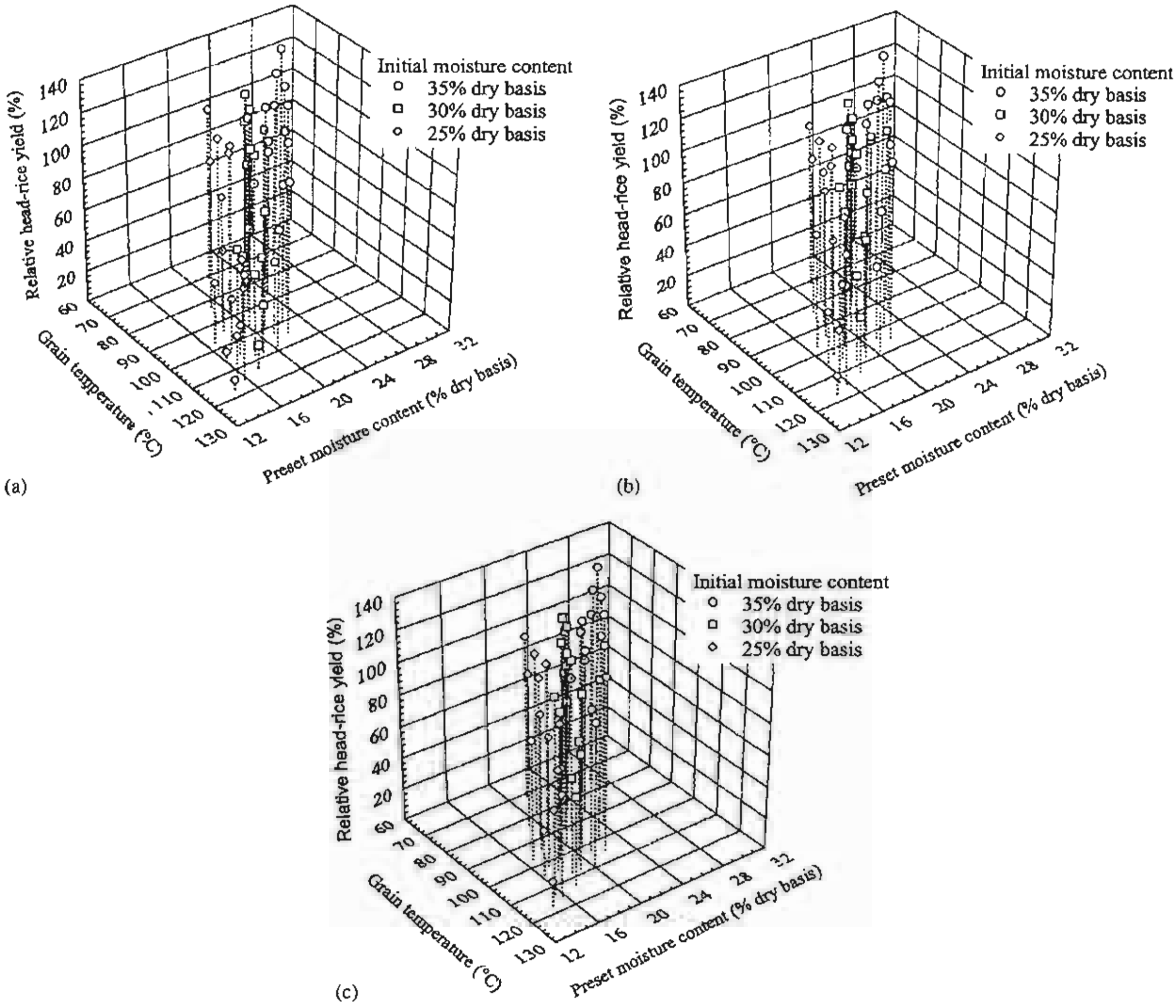

Fig. 3. Effects of preset moisture content and grain temperature after fluidised-bed drying (tempering temperature) on RHY at different tempering times. (a) Tempering time of 15 min, (b) tempering time of 30 min, and (c) tempering time of 45 min.

4.4. Mathematical model validation

Experimental data for grain temperature and moisture content obtained from Soponronnarit et al. (1999) were used in comparison with the model. Fig. 4 shows moisture content, grain temperature and head-rice yield during the drying, tempering and ambient air ventilation stages obtained from the experiments and the predictions, indicating that the predictions are in agreement with the experimental results. As seen in Fig. 4b, the temperature dropped steeply during the small interval of ventilation, thus causing great reduction of head-rice yield if the grain was not passed through the tempering section first even though the outlet moisture content of paddy was not too low at the first stage. This effect can be seen clearly in Fig. 4c for the case (B) where the initial moisture content of paddy was 30% dry basis. However, such an effect is unimportant for case (A) where the initial moisture content was relatively higher than in case (B). This might be because the high moisture content, along with the high temperature, encouraged the development of a polymeric network of starch in the paddy structure, thus making the kernel more strengthened.

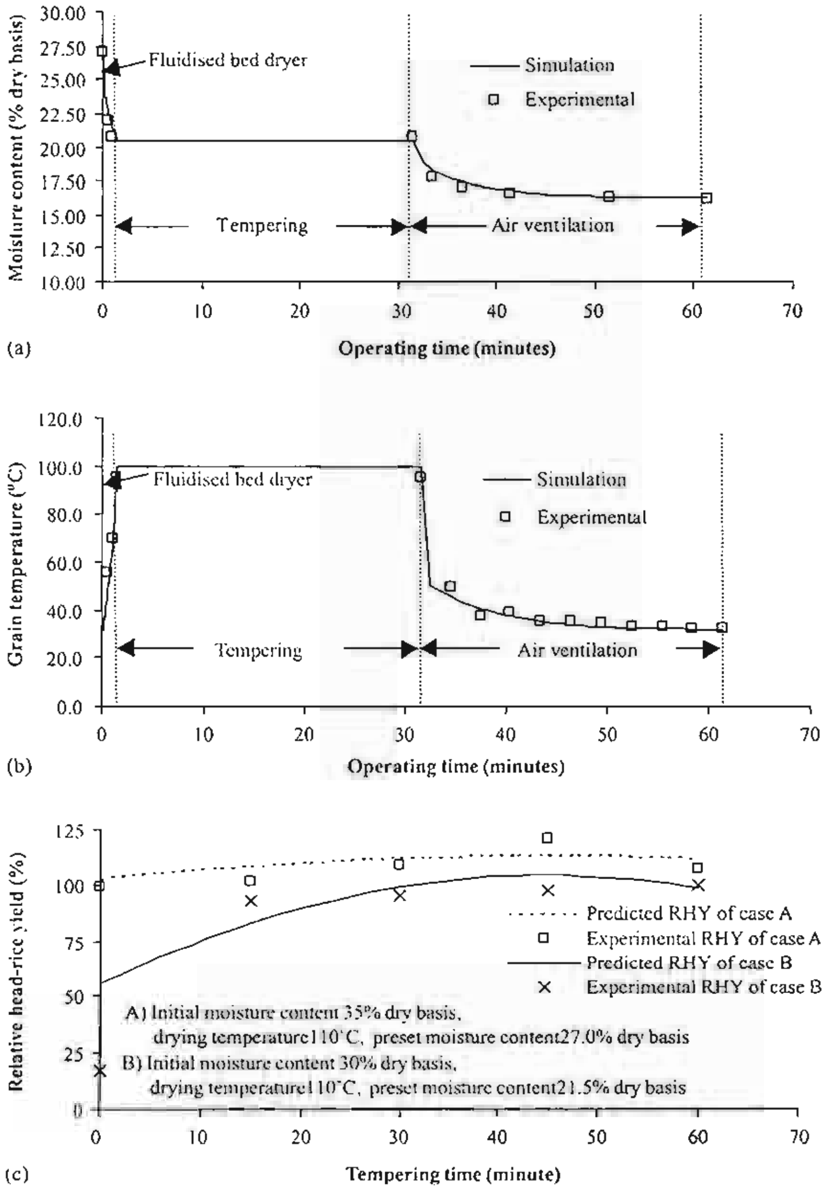

Fig. 4. Comparison of moisture content, grain temperature and RHY between experiments and simulations. (a) Moisture content, (b) grain temperature, and (c) RHY.

The results for head-rice yield indicate that the change in head-rice yield is rather complicated and depends on a number of parameters i.e. moisture content, tempering time and grain temperature. Such parameters ultimately relate to drying temperature. To obtain the appropriate drying conditions, that provide least drying time and maximise drying capacity and head-rice yield, the equations for heat and mass with incorporation of the head-rice equation need to be solved together.

4.5. *Effects of operating parameters on the operating time and the head-rice yield*

Even though drying time in the fluidised-bed dryer was only a small fraction of total operating time, it strongly affected the time required for the subsequent processes, i.e., tempering and ventilation, and head-rice yield. Thus, moisture content after first-stage drying, initial moisture content and drying temperature must be considered in this study.

The developed mathematical model was employed to determine the total operating time to achieve both a final moisture content of 16.5% dry basis and a grain temperature of 35 °C. Criteria for these simulations were as follows: (1) the fluidised-bed dryer was operated at a superficial air velocity of 2.2 m/s and a static bed thickness of 10 cm; (2) the ambient air was ventilated through a thin layer bed of 3 cm with a superficial air velocity of 0.075 m/s; (3) ambient conditions were 30 °C and 60% relative humidity, a normal range for tropical countries.

Tempering index is an important guideline to indicate how far the moisture content at the surface deviates from the equilibrium value at a finite time in the tempering stage. Several researchers (Steffe and Singh, 1980; Zhang and Litchfield, 1991; Tolaba et al., 1999) defined this index as

$$I_c = \frac{(M_{s,t} - M_{s,t=0})}{(M_{s,t=\infty} - M_{s,t=0})}, \tag{9}$$

where I_c is the tempering index and $M_{s,t}$ refers to the moisture content at the kernel surface at time t. Average moisture content of the kernel surface can be determined by the following equation:

$$M_{s,av} = \frac{\sum M_i V_i + \sum M_j V_j}{\sum V_i + \sum V_j}, \tag{10}$$

where i, j and V refer to the curved surface, the plane surfaces and the volume of the cylinder, respectively. Complete tempering (tempering index = 1.0) results in the most efficient drying performance when compared with the case of incomplete tempering (tempering index < 1.0). The required time for this is infinite. Steffe and Singh (1980) and Zhang and Litchfield (1991) found that a tempering index of 0.95 is an appropriate value which provides local moisture contents inside the grain similar to those obtained from the complete tempering. This value was thus used as a base line throughout these simulations.

The effects of preset moisture content and initial moisture content on RHY and operating time are shown in Figs. 5 and 6, respectively. Operating time increased linearly with increase in the preset moisture content but was independent of the initial moisture content. The increase in operating time resulted from the last stage requiring prolonged ventilation time. In considering the quality of paddy, it indicates that high RHY may be achieved when the preset moisture content of paddy is not too low.

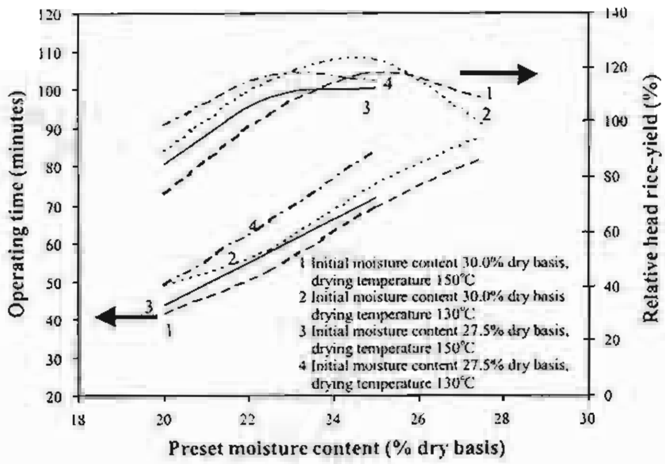

Fig. 5. Effect of preset moisture contents on total process time and RHY.

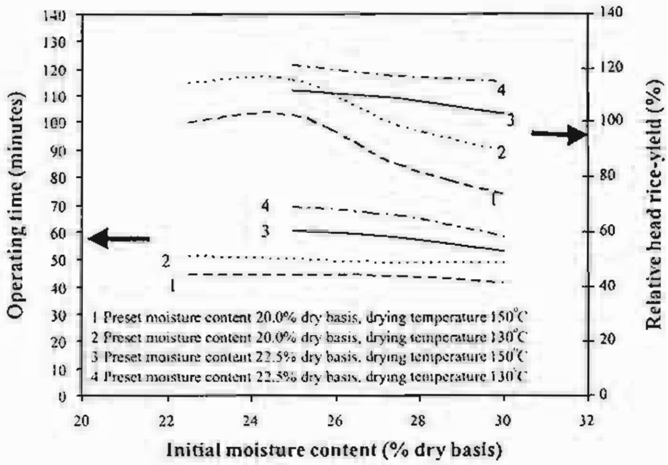

Fig. 6. Effect of initial moisture contents on total process time and RHY.

Some of the conditions which provided superior quality (as shown in Figs. 5 and 6) were selected to determine the effect of temperature on operating time and head-rice yield. In these simulations, we limited preset moisture contents at first-stage exit to 20 and 22.5% dry basis. The results demonstrate in Fig. 7 that operating time decreased moderately with increased temperature, as expected. RHY increased slightly with temperature until 130 °C and then decreased. These results suggest that inlet temperature should not be higher than 150 °C and preset moisture content should not be lower than 22.5% dry basis for high-temperature fluidised-bed drying.

Plots of tempering time versus RHY and operating time for drying temperatures of 130 and 150 °C are shown in Fig. 8. This figure shows that air ventilation through the paddy bed immediately after drying gave a very low quality of head rice in spite of relatively high values of

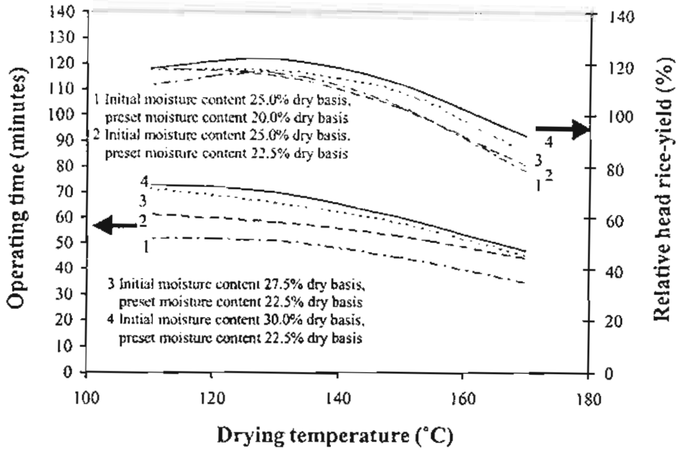

Fig. 7. Effect of drying temperatures on total process time and RHY.

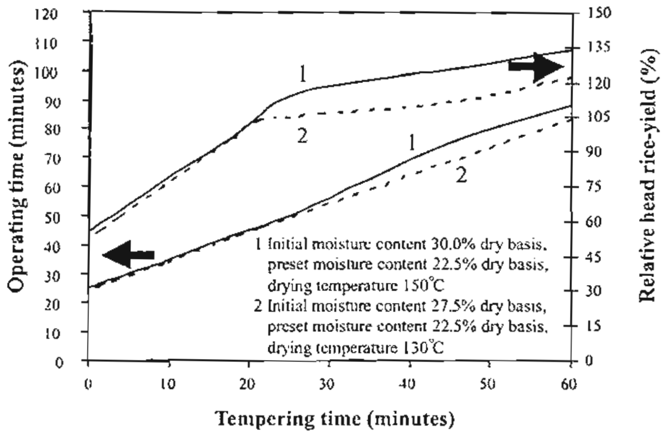

Fig. 8. Effect of tempering times on total process time and RHY.

preset moisture contents. Head-rice yield increased rapidly with tempering time. But after 25 min, the head-rice yield appeared to reach a limit, beyond which improvement was insignificant. Under such conditions, the colour of white rice is still acceptable as reported by Soponronnarit et al. (1999).

5. Conclusions

The experimental and simulation results for drying using the fluidised-bed dryer, tempering and ambient air ventilation can be summarised as follows:

1. A drying process with no tempering between stages causes low head-rice yield. The reduction in head-rice yield can be improved by the tempering technique.

2. A second-order polynomial equation can be fitted to experimental values of head-rice yield with the tempering time in which their coefficients are related to preset moisture content and grain temperature.
3. As a compromise between operating time and high head-rice yield, the maximum temperature to be used for the first-stage is 150 °C and the moisture content at any level should not be reduced to lower than 22.5% dry basis in the fluidized bed. The tempering time for such conditions must be at least 25 min.

Acknowledgements

The authors would like to express their sincere thanks to the Thailand Research Fund for financial support and The Division of Agricultural Engineering, Department of Agriculture, Thailand, for milling tests.

References

Kunze, O.R., 1996. Effect of drying on grain quality. In: Champ, B.R., Highley, E., Johnson, G.I. (Eds.), Grain Drying in Asia. Proceedings of an International Conference held at the FAO Regional Office for Asia and the Pacific, Bangkok, Thailand, 17–20 October 1995, ACIAR Proceedings No. 71, pp. 178–185.

Laithong, C., 1987. Study of thermo-physical properties of rough rice. Master's Thesis, King Mongkut's Institute of Technology Thonburi, Bangkok.

Li, Y.B., Cao, C.W., Yu, Q.L., Zhong, Q.X., 1999. Study on rough rice fissuring during intermittent drying. Drying Technology 7, 1779–1793.

Poomsa-ad, N., Soponronnarit, S., Prachayawarakorn, S., Terdyothin, A., 2002. Effect of tempering on subsequent drying of paddy using fluidisation technique. Drying Technology 20, 195–210.

Sabbath, M.A., 1970. Convective heat transfer coefficient and tempering effects on cooling rate of shelled corn. Ph.D. Thesis, Purdue University, Lafayette, IN.

Soponronnarit, S., Wetchacama, S., Swasdisevi, T., Poomsa-ad, N., 1999. Managing moist paddy by drying, tempering and ambient-air ventilation. Drying Technology 17, 335–344.

Steffe, J.F., 1979. Moisture diffusion and tempering in the drying of rough rice. Ph.D.Thesis, Department of Agricultural Engineering, University of California, Davis. Unpublished.

Steffe, J.F., Singh, R.P., 1980. Theoretical and practical aspects of rough rice tempering. Transactions of the American Society of Agricultural Engineering 23, 775–782.

Steffe, J.F., Singh, R.P., Bakshi, A.S., 1979. Influence of tempering time and cooling on rice milling yields and moisture removal. Transactions of the American Society of Agricultural Engineering 22, 1214–1218 1224.

Tolaba, P., Aguerre, R.J., Suárez, C., 1999. Drying simulation of corn with tempering. Drying Technology 17, 1081–1093.

Zhang, Q., Litchfield, J.B., 1991. An optimization of intermittent corn drying in a laboratory scale thin layer dryer Drying Technology 9, 233–244.

Drying Technology, 23: 205–223, 2005

ISSN: 0737-3937 print/1532-2300 online
DOI: 10.1081/DRT-200047892

Taylor & Francis
Taylor & Francis Group

Simultaneous Momentum, Heat, and Mass Transfer with Color Change during Paddy Storage in Silo

Somkiat Prachayawarakorn*
Faculty of Engineering, King Mongkut's University of Technology Thonburi, Bangkok, Thailand

Chate Choteboon and Somchart Soponronnarit
School of Energy and Materials, King Mongkut's University of Technology Thonburi, Bangkok, Thailand

Abstract: A theoretical model has been developed to describe heat, mass, and momentum phenomena in cylinder-shaped silos where paddy is stored. Calculation based on the model predicts local temperature and moisture within the silo as a function of time and space. This information is then coupled with known kinetics of color change to predict yellowness or whiteness generated during storage. The model is evaluated using the published data. Natural air currents and the corresponding moisture migration are small for short storage periods and more extensive for long-term storage. The calculated result shows the similar trend to the published data in that moisture migrates from the central region, where the grains experience high temperature, to the outer regions, where the grains have lower temperatures. Paddy near the wall and on the top of the silo has relatively lower whiteness than at inner areas for storing it at 15% wet basis, this low luminosity is in part motivated by relative humidity, which is relatively high at such areas. At elevated initial moisture contents, paddy at the inner areas has lower whiteness due to large accumulation of heat from grain respiration, hence, it is a predominant effect on the color change, while the humidity plays a minor role.

Keywords: Mixed convection; Paddy; Storage; Yellowness

*Correspondence: Somkiat Prachayawarakorn, Faculty of Engineering, King Mongkut's University of Technology Thonburi, Suksawat 48 Road, Bangkok 10140, Thailand; E-mail: somkiat.pra@kmutt.ac.th

INTRODUCTION

Freshly harvested paddy contains moisture content higher than 25% dry basis. At this moisture level, paddy cannot be kept for a long time. In common practice, water content inside the kernel is removed by convective dryers; i.e., mixed flow, fluidized bed, and circulating dryer. The safe moisture level is between 14 and 16% dry basis. After processing, paddy is stored in silos, at least 6 months before milling. This storage period is a typical condition used in rice industries for domestic consumption.

During storage period, heat generated from respiration of grains and insects increases the temperature in grain bulk. The gradient of temperature subsequently encourages the air currents to circulate within the bulk. The natural air currents lead to water vapor in warm regions of the grain stores escaping to cooler areas.[1,2] In the warm regions, vapor pressure in gas phase is high and moisture content in grains is loosed. As the air reaches the cooler regions, its relative humidity escalates, thereby gaining moisture content of grains. The moisture migration produces non-uniformity of moisture content of paddy. The areas where the moisture content of grains is increased may lead to deterioration of their qualities, i.e., grain agglomeration and loss of native color and head-rice yield. The grain agglomeration is found near the walls of silos where the vapor pressure is low and the temperature gradient is relatively large,[3] and the discoloration is found inside of the bulk where temperature is high.

Another factor affecting the natural convection in silos is the solar radiation. The amount of heat absorbed by silos due to radiation mode is difficult to predict due to many factors, including silo position, geographical area, absorptivity/reflectivity properties of material, and cloudiness.[2] However, the radiative heat transfer effect is insignificant compared to the heat from the respiration. With radiation effect, temperature variation in the bulk was present only at a depth not far from the periphery.[4]

In the present work, the transport models of heat, mass, and momentum in conjunction with the kinetics of rice yellowing are developed to describe phenomenological and color changes that occur when the grains are stored under tropical weather conditions.

MATHEMATICAL MODEL

The paddy is supposed to be stored in a perfectly sealed silo that has a cylindrical geometry with a dimension of 6 m height and 3 m diameter as shown in Fig. 1. This simple geometry is rather modified to make the calculation easily. In fact, silos that are used in the rice industry have a cylindrical shape with a conical base. The conical base is designed for effectively unloading paddy from the bin, without a dead zone. In addition to the simple geometry, the moisture migration and temperature gradient presumably occur in two-dimensional systems, both radial and axial directions. However, this simplified approach can be extended to grain storages that are three-dimensional systems or that have arbitrary shapes. The method involves using a mathematical transformation of the grain storage into a computational domain that has the simple geometry of a cube.[5,6] The fundamental equations of heat, mass, and momentum, including the kinetics of rice yellowing, apply to storages, regardless of their shape, and the initial and boundary conditions must be given to solve the problems of convective flow and quality change.

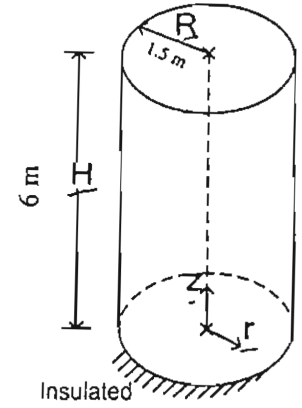

Figure 1. Idealized geometry of grain storage.

Heat Transport Model

The stored grains release the energy from their respiration, resulting in an increase of temperature in the bulk. The increased temperature produces the natural convective air flow that carries not only moisture but also heat from one region to others. To describe such change, the energy balance was made for a small element in the grain bulk and the energy equation is written as:

$$\rho_s \varepsilon_s (C_s + WC_1)\frac{\partial T}{\partial t} + \rho_a \varepsilon_a (C_a + \omega C_1)\frac{\partial T}{\partial t} + \rho_a (C_a + C_v)\left[v_r \frac{\partial T}{\partial r} + v_z \frac{\partial T}{\partial z}\right]$$
$$= k_{\text{eff}}\left[\frac{\partial^2 T}{\partial r^2} + \frac{1}{r}\frac{\partial T}{\partial r} + \frac{\partial^2 T}{\partial z^2}\right] + \rho_s \varepsilon_s (Q_r - 0.6 h_v)\dot{\mathrm{D}}\mathrm{ML} \quad (1)$$

In writing Eq. (1), the energy source from solar radiation is negligible since grain is a good insulator. The first two terms on the left-hand side of Eq. (1) account for the change of temperatures of grain and air with time, assuming temperature in phases of solid and gas to be equal.

The last term on the left-hand side of Eq. (1) represents the bulk heat flow, carried by the natural convective currents. The net change of internal energy, plus the heat flow term, is equal to the energy conducted through the grain bulk, presented by the first term on the right-hand side of Eq. (1), and the generation energy released from paddy, presented by the second term on the right-hand side of Eq. (1). The generation energy is obtained from the respiration energy minus the energy used for vaporizingthe water, which is produced from grain respiration.

The temperature distribution in the bulk can be known when the initial and boundary conditions are specified. In this work, we suppose the temperatures at the wall and on the top of silo equal to weather temperature, and average ambient temperature on the day and night times are used as boundary condition. In addition, it is usual to assume that the floor of the silo is thermally insulated. Along the periphery of grain bulk, the following boundary conditions are:

$$T(R,z,t) = T(t) \quad \text{at } r = R \quad 0 \le z \le H \text{ for } t \ge 0 \tag{2}$$

$$T(r,H,t) = T(t) \quad \text{at } z = H \quad 0 \le r \le R \text{ for } t \ge 0 \tag{3}$$

$$\frac{\partial T(r,0,t)}{\partial z} = 0 \quad \text{at } z = 0 \quad 0 \le r \le R \text{ for } t \ge 0 \tag{4}$$

The last boundary condition assumed is the maximum temperature at the center as given by

$$\frac{\partial T(0,z,t)}{\partial z} = 0 \quad \text{at } r = 0 \quad 0 \le z \le H \text{ for } t \ge 0 \tag{5}$$

Rate of dry matter loss, $\dot{\mathrm{D}}\mathrm{ML}$, can be readily determined if the moisture content of paddy is known. Respiration is the process of oxidizing carbohydrates and producing carbon dioxide and water vapor, as well as energy. Respiration therefore consumes the amount of dry matter of paddy. Teter[7] reported that the rate of dry matter loss was higher with higher moisture content. His data were statistically fitted with two empirical equations proposed in the present study, each of which is suitably described for each moisture range. A power equation was applied to low moisture content of 13 to 16% wet basis and a polynomial equation with a third degree was used for a higher range of moisture content. The empirical equations of dry matter loss for such moisture ranges are expressed by:

$$\dot{\mathrm{D}}\mathrm{ML} = 7 \times 10^{-11}(100 \times W)^{8.531} \quad 0.13 \le W \le 0.16 \text{ wet basis} \tag{6}$$

$$\begin{aligned}\dot{\mathrm{D}}\mathrm{ML} = &-0.0636(100 \times W)^3 + 4.0827(100 \times W)^2 \\ &- 80.608(100 \times W) + 505.38 \quad 0.16 \le W \le 0.28 \text{ wet basis}\end{aligned} \tag{7}$$

To obtain the temperature distribution, Eq. (1) is written as the discretized form, in which the first derivatives are written using backward differences and the second derivatives with central differences, and then solved by alternating direction implicit method.[8] This method treats the problem as being implicit in the direction of one coordinate, the r coordinate given by the present work, during the first half of a time increment and the temperatures in the z-direction are carried out explicitly. During the second half, the temperature in z component is advanced implicitly, while temperatures in the r-direction are treated explicitly. Temperature distribution in the bulk is known by simply solving a set of Eq. (1)–(7) using the tridiagonal method algorithm.[8]

Moisture Transport Model

Moisture migration in silos is caused by two possible mechanisms, natural convection and diffusive transport, with the first mechanism in the majority. The moisture movements in the bulk can accordingly be described by:

$$\rho_s \varepsilon_s \frac{\partial W}{\partial t} + \rho_a \varepsilon_a \left(v_r \frac{\partial \omega}{\partial r} + v_z \frac{\partial \omega}{\partial z} \right) = D_{\mathrm{eff}} \varepsilon_a \rho_a \left(\frac{\partial^2 \omega}{\partial r^2} + \frac{1}{r}\frac{\partial \omega}{\partial r} + \frac{\partial^2 \omega}{\partial z^2} \right) + 0.6 \rho_s \varepsilon_s \dot{\mathrm{D}}\mathrm{ML} \tag{8}$$

The first term on the left-hand side of Eq. (8) presents the moisture content of paddy that will decrease or increase depending upon the local relative humidity and temperature surrounded the existing kernels, and the second term describes the water vapor flow in bulk. On the right-hand side, the first term shows the water vapor diffusion through the void spaces of bulk grain; the last term accounts for the water vapor produced by the respiration.

In this study, we assume that the water vapor cannot diffuse through the wall of the silo and the moisture content of stored grains initially has uniform moisture content. Hence, the boundary conditions may be written as

$$\frac{\partial \omega(R,z)}{\partial r} = 0 \quad \text{at } r = R \text{ and } 0 \le z \le H \tag{9}$$

$$\frac{\partial \omega(r,H)}{\partial z} = 0 \quad \text{at } z = H \text{ and } 0 \le r \le R \tag{10}$$

$$\frac{\partial \omega(0,z)}{\partial r} = 0 \quad \text{at } r = 0 \text{ and } 0 \le z \le H \tag{11}$$

$$\frac{\partial \omega(r,0)}{\partial z} = 0 \quad \text{at } z = 0 \text{ and } 0 \le r \le R \tag{12}$$

Except for the other boundaries, the boundary in Eq. (9) implies the lowest moisture content at the central bulk. Before solving Eq. (8) to detemine the moisture content, it is essential to know the humidity ratio of air surrounding the kernels. The air humidity is calculated by using a psychometric equation given elsewhere.[3] Due to very low natural convective currents, the moisture content of the grains changes very slowly, and the explicit method is used to calculate the moisture content at the internal nodes for the advanced time step.

Momentum Model

Darcy's equation, where the pressure gradient is directly proportional to the velocity gradient and the hydrostatic head, is applied to describe the buoyancy-driven flows in silo, and is mathematically expressed as

$$\nabla p = \frac{\mu}{\kappa}\vec{v} - \rho_a g \tag{13}$$

Rearrangement of Eq. (13) and writing in terms of velocity components yields:

$$v_r = -\frac{\kappa}{\mu}\frac{\partial p}{\partial r} \tag{14}$$

$$v_z = -\frac{\kappa}{\mu}\left(\frac{\partial p}{\partial z} + \rho_a g_z\right) \tag{15}$$

Differentiation of Eq. (14) with respect to z is minus with the r derivative of velocity component in Eq. (15), giving

$$\frac{\partial v_r}{\partial z} - \frac{\partial v_z}{\partial r} = \frac{\kappa g_z}{\mu}\frac{\partial \rho_a}{\partial r} \tag{16}$$

To account for the buoyancy force effect, the air density varying with temperature is approximated by Boussinesq's equation,

$$\rho_a = (\rho_a)_o[1 - \beta(T - T_o)] \tag{17}$$

White[9] defined the velocity components in the form of stream functions as follows:

$$v_r = \frac{1}{r}\frac{\partial \psi}{\partial z} \tag{18}$$

$$v_z = -\frac{1}{r}\frac{\partial \psi}{\partial r} \tag{19}$$

Differentiation of Eqs. (17) and (19) with respect to r, and Eq. (18) with respect to z, is replaced into Eq. (16), yields the expression for behavior of stream function:

$$\frac{\partial^2 \psi}{\partial^2 z} + \frac{\partial^2 \psi}{\partial^2 r} = -\frac{r\kappa g_z(\rho_a)_o\beta}{\mu}\frac{\partial T}{\partial r} + \frac{1}{r}\frac{\partial \psi}{\partial r} \tag{20}$$

Because of the impermeable surfaces at the wall, bottom, and top, the following boundary conditions on stream function are

$$\psi(R,z) = 0 \quad \text{at } r = R \quad 0 \le z \le H \tag{21}$$

$$\psi(r,H) = 0 \quad \text{at } z = H \quad 0 \le r \le R \tag{22}$$

$$\psi(r,0) = 0 \quad \text{at } z = 0 \quad 0 \le r \le R \tag{23}$$

In addition to the impermeable boundaries, the necessary boundary condition for central region of the bulk, which presents no flow across the line of symmetry, is

$$\psi(0,z) = 0 \quad \text{at } r = 0 \quad 0 \le z \le H \tag{24}$$

The stream function expression, along with the boundary conditions, was solved explicitly using temperature field calculated from Eq. (1). The calculation procedure was repeated until the temperature difference between two subsequent calculations was less than 10^{-3}.

Kinetics of Rice Yellowing

During grain storage, the environmental conditions in the bulk, i.e., relative humidity and temperature, stimulate the color of paddy to be changed from white to yellow. The color change, measured by the b-value, was explained accordingly by zero-order reaction:[10]

$$\frac{db}{dt} = k \tag{25}$$

where

$$k = \exp\left(71.87 - 25.32\mathrm{RH} - \frac{25{,}919.3}{T + 273.15} + \frac{10{,}712.78\mathrm{RH}}{T + 273.15}\right) \tag{26}$$

The relationship between the whiteness and b-value was given by[11],

$$W = 85.1 - 3.36b \tag{27}$$

Table 1. Some physical and thermal properties used in the model

Specific heat $C_s = 1.292 + 4.2\,W$*
Effective thermal conductivity $k_{eff} = 0.319 + 0.479\dfrac{W}{1+W}$*
Permeability of grain bulk $\kappa = 9.27 \times 10^{-9}$**
Porosity $\varepsilon_s = 0.623 - 0.25\,W$*
Bulk density $\rho_s = 552 + 282\,W$*

*See Soponronnarit[16] and **Thorpe.[3]

RESULTS AND DISCUSSION

The result from calculation should be independent of the grid sizes and the time steps. In general, as the grid sizes and time steps are made smaller, the errors resulting from the discretization of the governing equations become smaller. In the present study, many grid sizes, together with the time steps, were tried and it was found that a grid size of 16 points in the radial direction and 61 points in the axial direction, and a time step of 50 seconds, were fine enough to represent the simultaneous transport of heat, mass, and momentum. Some physical and thermal properties used in the model are presented in Table 1. Figure 2 illustrates the cyclic change of ambient air temperature during storage and it is used as boundary condition in Eqs. (2) and (3) for solving the thermal transport equation.

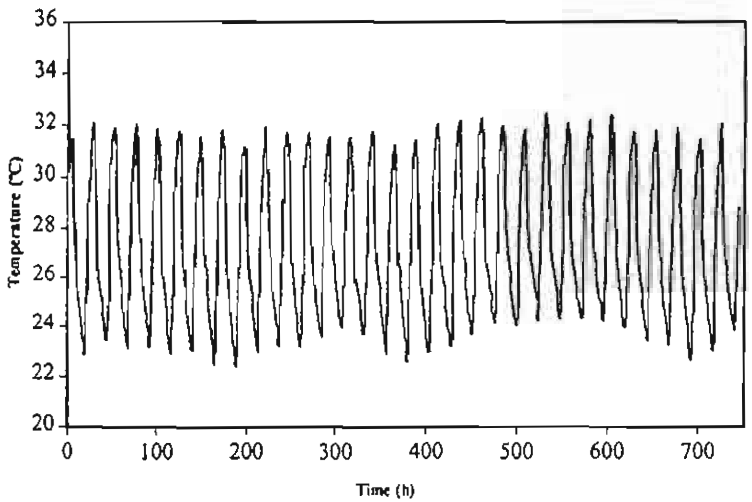

Figure 2. Illustration of ambient air temperature during storage.

The mathematical model was validated with the experimental data as reported by Naupanich et al.[12] In their work, paddy with an initial moisture content of 14 to 15% wet basis was stored in steel silos, with a dimension of 6 m height and 3 m diameter for which a 20-ton paddy was kept. Paddy was collected in two silos, one with the inside wall layered with bamboo sheet and another silo without bamboo sheet. The grain temperature at the beginning was 30°C. The experiments were started in March and finished in October, covering the critical period when paddy is easily deteriorated.

Validation of the Model

Figure 3 shows the change of temperature in the bulk when paddy was stored in the silos with the inside wall covered with bamboo sheet and without bamboo sheet. The temperature difference for both silos throughout the storage period is very small, presenting the grains acting as a good insulator so that a bamboo sheet lining does not assist heat prevention from the outside. The average temperatures within bulk for both silos are increased by approximately 2°C for 4-month storage and 5°C for 7-month storage. A comparison between experimental and predicted results is also shown in Fig. 3. Both experiment and calculation show the same tendency, with temperature being highest at the middle and declining toward the exterior surface. The variation in temperature of the paddy bulk is probably due to the combined effect of natural air flow and respiration reaction that is usually higher with higher moisture content.

Figure 4 illustrates the experimental and calculated moisture profiles of paddy in silo the period of 6-month storage. After long-term storage, moisture content of paddy stored in the silo changes such that the moisture content of paddy at the inner positions of bulk is lower than at the outer positions, with the highest moisture content near the silo wall. For the 6-month storage, the moisture content of paddy, measured at 3 m height from the silo base, was 13.5% w.b. at the center and 15.8% w.b. near the wall. This change, which is opposite to the result of measured temperature, confirms that moisture migrates from warm regions to cooler regions. The moisture migration is due to the combined effects of water vapor diffusion, which transports through interglanular spaces, as a result of vapor pressure difference and convective airflow as a result of temperature difference.

Temperature Distribution

Figure 5 shows the simulation results of temperature distribution in the bulk at different storage periods. In calculation, we supposed that paddy

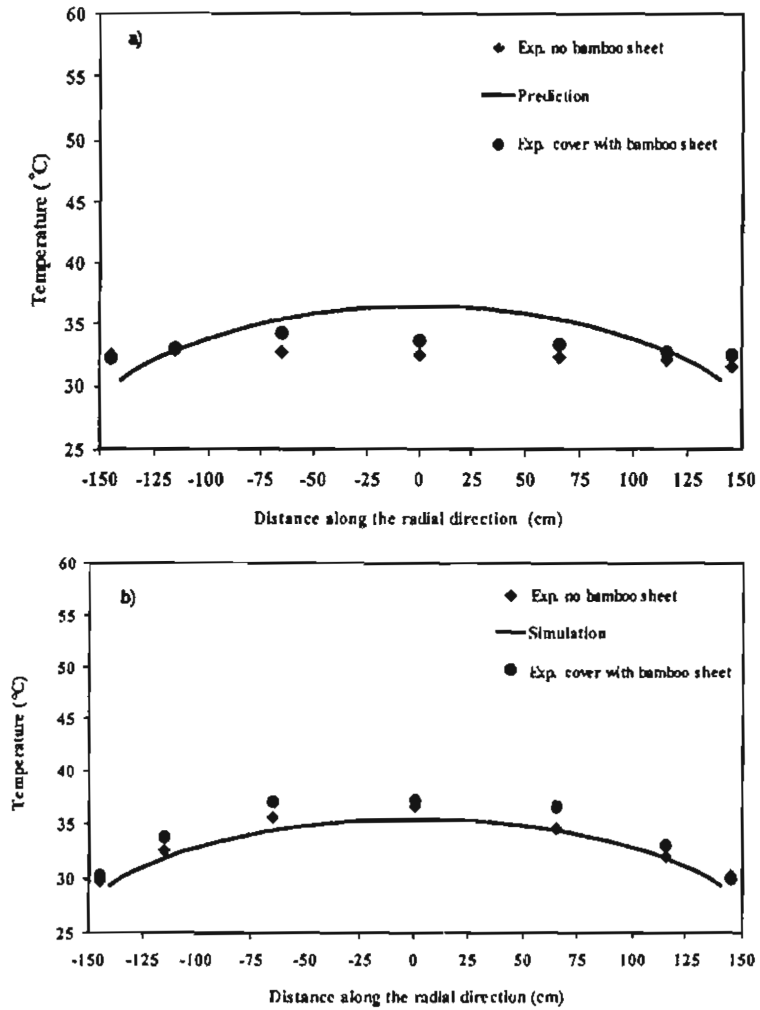

Figure 3. Temperature distribution in steel silos covered with and without bamboo sheet and prediction from the model (at positions of 3 m height from base): a) 4 months storage, and b) 7 months storage.

kept in the silo had an initial moisture content of 15% wet basis. After one month, a small creation of temperature gradient is obvious, as indicated by a small number of isothermal lines, and when the grains are stored for longer than 4 months a larger temperature gradient is evident. Note that at 8-months storage, temperatures inside the bulk are reduced

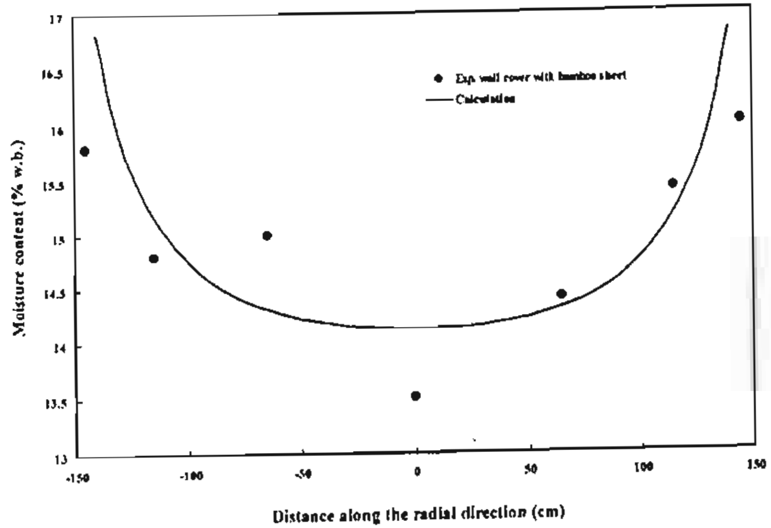

Figure 4. Moisture profile in silo at the period of 6 months storage and prediction from the model (measured at 3 m height from base).

to be relatively lower than that at 4-months storage (average ambient air temperature of 32°C at 4th month storage). This result is affected by the change of weather condition: the ambient temperature at 8-months storage was relatively cooler (average ambient air temperature of 29°C), resulting in more heat transferring from paddy bulk to the environment.

From this figure it also can be seen that the high temperature zone is moved to the upper level. If the storage period is extended further, we expect the higher temperature to be taken place above the middle region of the grain bulk. This part is reflected by the high-temperature air currents that move up to the higher level.

Streamlines and Velocity Components

Figure 6 presents the stream lines at different storage periods. The buoyancy-driven air flow transports within the grain bulk in a way that it moves vertically up to the top part at the center region and then moves down near the inside wall. The natural convection flows that occur are very low for short storage periods and become higher for a longer period, similar to the behavior of temperature distribution. The stream lines presented in Fig. 6 were used to calculate the velocity components of radial and axial directions by Eqs. (18) and (19), respectively, and the calculated results are shown in Fig. 7. It is clear that the radial velocity is very high

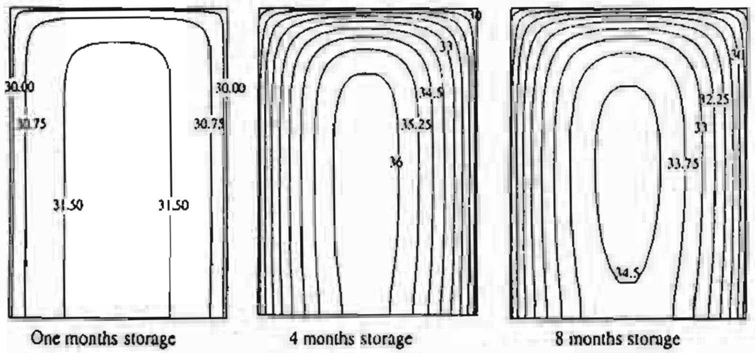

Figure 5. Temperature distribution in grain bulk.

at the bottom and on the top of the grain bulk and almost zero for the region far from the edges, indicating that any flow within the bulk exists only in the axial direction as shown in Fig. 7b. The radial velocity on the top moves in the direction from the inside to the outside, whereas it moves in the opposite direction for the bottom region, as indicated by the arrow.

Moisture Distribution

Figure 8 shows the moisture migration in silo where it is absent at the 1 month storage, although there is a small temperature gradient and

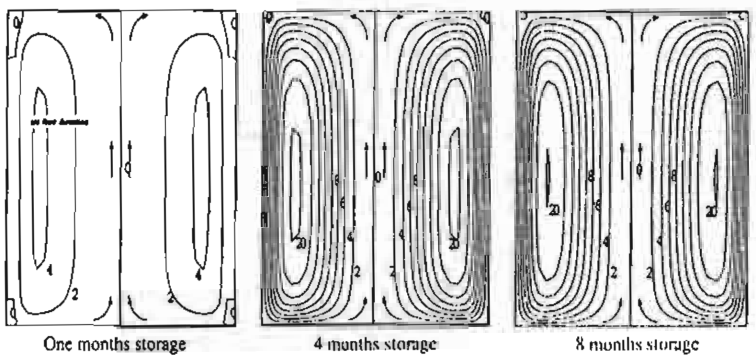

Figure 6. Stream lines at different periods of storage ($\times 10^{-6}$ m^3/s).

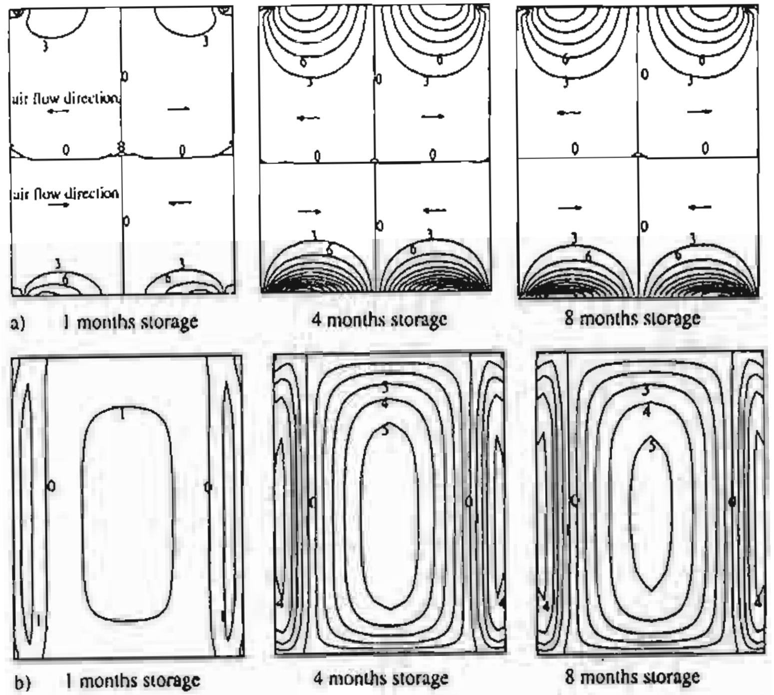

Figure 7. Change of velocity components at different storage periods ($\times 10^{-6}$ m/s): a) velocity component in radial direction, and b) velocity component in axial direction.

natural convective air flow. As the storage period is longer than 4 months, the moisture movement is shown up near the inside of the wall and at the top of silo where the moisture content of paddy increases to 15.6% wet basis. This reflects the effects of the temperature field and the flow field where the air rises from the warm central region to the upper surfaces. At 8 months storage, the moisture content of paddy changes to 16.1% wet basis at the periphery, whereas the moisture content of paddy at the central region becomes lower than the initial value. This moisture content is highest compared to that at the other regions, and it corresponds to the region where the vertically downward velocities are high, as evidence of many stream lines close together. The calculated results agree with several findings,[1,3] in which the grains near the wall and at the top of the bin gained in moisture content, resulting in the agglomeration of grains.

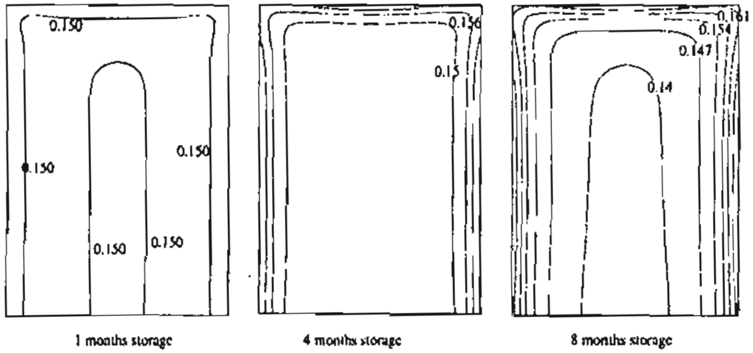

Figure 8. Moisture distribution in silo at different storage periods (decimal wet basis).

Whiteness Distribution

Color of product reflects a sensation to human eye and the visual examination is common method of evaluating product quality. In view of commercial, the white color for paddy is favorably preferred and is accepted for premium price. The change of color, due to browning reactions, is caused by the reactive components in paddy activated under suitable storage condition.

As reported by several researchers for agricultural materials, the maximum browning rate occurs under the range of relative humidity of 70 to 80%.[13,14] In simulation, we assumed that the color of stored paddy had an initial b-value of 11.5, corresponding to value of rice whiteness of 46.4. The combined effects of natural convective flow and temperature gradient produce the color change, from white to yellow color, and its change is relatively more complicated than the moisture migration behavior since the development of yellow pigment is stimulated by the temperature and relative humidity, the first being the most important factor. The natural air currents carrying the water vapor evaporated from the grains generate the different levels of relative humidity at the positions within the bulk. The complex behavior is elucidated in Fig. 9. The value of whiteness is inversely related with b-value, according to Eq. (27). In general, higher temperature and relative humidity result in lower whiteness. At the first month storage, the value of whiteness around the exterior surface of the grain bulk is slightly lower than that at the interior, indicating the dominant effect of relative humidity on lowering of whiteness value, while the temperature effect is insignificant because the temperature difference between inner and outer is small, as previously shown in Fig. 4.

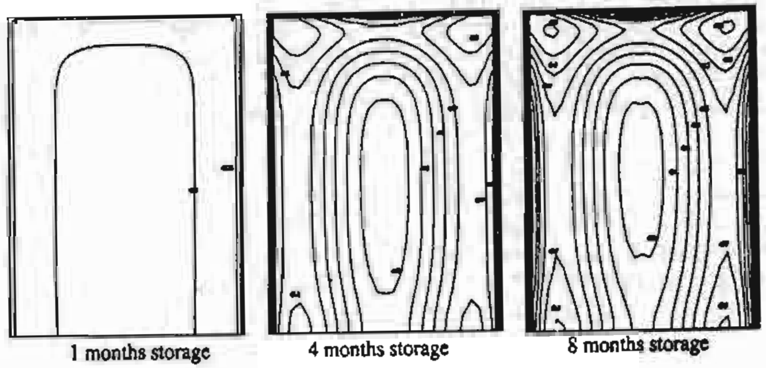

Figure 9. Whiteness distribution in the bulk during storage (initial moisture content of 15% wet basis).

When the difference of temperature is larger for a longer period, i.e., 3 months storage, the change of whiteness within the bulk is, in turn, different from that found for shorter storage periods. In this case, the values of whiteness at the inner part of the grain bulk are almost lower than at the outer part, except for the color of paddy near the wall and on the top of silo, which shows a value of 43.5. The lower whiteness at the inner areas, compared to the outer areas, is caused by the higher temperature within bulk, which plays an important role in forming yellow pigment.

In contrast, for the paddy near the wall and on the top of the bulk where the radial and axial velocities are very high, the temperature is less influential to the color development compared with the relative humidity effect. The prevalent contribution of relative humidity stimulates the reactive components existing inside the kernel and thus leads to relatively lower value of rice whiteness at such areas than at the inner part. The similar result is also found in 8 months storage.

Effect of Initial Moisture Content

This section draws attention to the applicable developed models to explore how long the moist paddy can be kept, without deterioration of color, when the paddy at different initial moisture contents is stored. This information is very useful for related industries to ensure that the paddy is still safe. In harvesting season a large amount of paddy is directly transported to the industries and it may not be dried immediately due to limitation of drying equipment, so that the remaining portion in

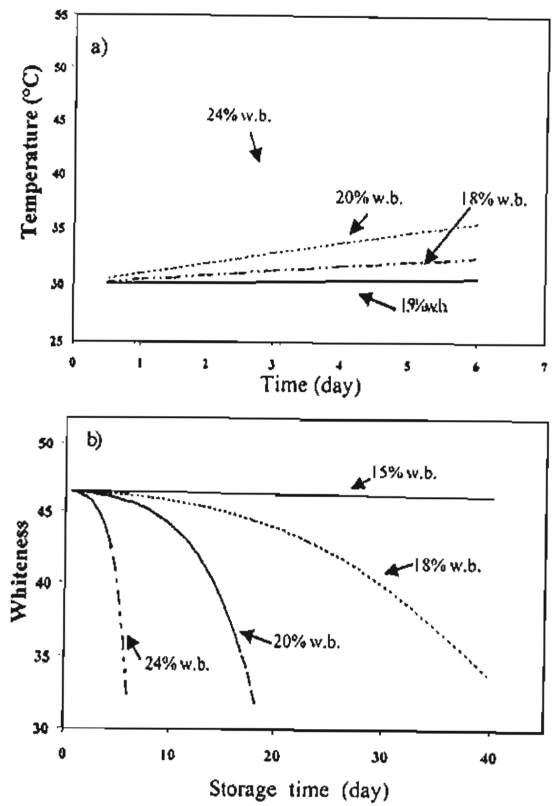

Figure 10. Changes of temperature and color of paddy with storage time at different initial moisture contents: a) average temperature, and b) whiteness.

practice is placed on a concrete pad under shade. In the simulation, we supposed that paddy was kept in a silo.

The simulated results shown in Fig. 10 are presented in a form of the average value. The average values of temperature and whiteness are respectively calculated by:

$$\overline{T} = \frac{\iint T(r,z)2\pi r dr dz}{\iint 2\pi r dr dz} \tag{28}$$

$$\overline{W} = \frac{\iint W(r,z)2\pi r dr dz}{\iint 2\pi r dr dz} \tag{29}$$

The increase in temperature in the bulk strongly depends on initial moisture content and the storage period. The rapid rise in temperature, due to high respiration rate of paddy, is obvious with high initial moisture content. This is clearly illustrated in Figure 9a by the case of initial moisture content of 24% wet basis at which temperature linearly strikes from 30°C at the beginning to 45°C on the fourth day of storage. As the initial moisture content becomes lower, the increasing rate of temperature is obviously lower. Similarly, Raj and Singaravadivel[15] reported that a temperature rise of 2, 6, and 19°C over the ambient temperature was observed in moisture contents of 17.9%, 22.8%, and 25.7% wet basis, respectively, after seven days for storing paddy without drying.

According to the result of temperature change, the limitation of storage period for storing paddy at high moisture level, i.e., 18, 20, and 24% wet basis, is governed only by the temperature, since the high temperature promotes the components inside the kernel to be more reactive. In this circumstance, the whiteness of paddy goes from highest value at the periphery of silo to the lowest value at the center. However, the relative humidity is somewhat more important for the paddy at low moisture content, due to low respiration rate, and this effect is shown in Fig. 9.

As shown in Fig. 10b, the drop of whiteness value is very fast for initial moisture content of 24% wet basis and the yellowing rate declines with lowering of initial moisture content. To obtain the acceptable white color, the paddy at initial moisture contents of 24, 20, and 18% wet basis should not be kept longer than 4, 9, and 18 days, respectively; otherwise, the color of paddy in some places within bulk becomes lower than 35, which is not acceptable for producing white rice.

CONCLUSIONS

The temperature gradient is a main cause of the natural convective air currents and the corresponding moisture migration in the paddy bulk. Mathematical models for the heat, mass, and momentum transfers, with incorporation of yellowing kinetics, are used to describe their changing behaviors in the cylinder-shaped silo and the computational results reasonably agree with the published data. The amount of air currents and water migration is very small for short storage periods and becomes larger for a longer period, thereby gaining in moisture content of paddy at the outer region of the bulk. In contrast to water movement behavior, the paddy located at the inner part of the bulk has a relatively lower whiteness than at the outer part, except for the sample near the wall and at the top of the bulk where the whiteness is lowest. The simulation has been made further to investigate the initial moisture content effect and the results show a shorter storage period with higher initial moisture content if the color of paddy is to be maintained as an acceptable white color.

NOMENCLATURE

C	specific heat, kJ/kg°C
D_{eff}	effective diffusivity of water vapor through grains, m^2/s
DML	rate of dry matter loss, kg/s
g	gravity vector, m^2/s
H	height of silo, m
h_v	heat of vaporisation, J/kg
k_{eff}	effective thermal conductivity of paddy, W/m^2°C
Q_r	heat from respiration, J/kg of dry matter
P	pressure, Pa
R	radius of silo, m
RH	relative humidity of air, decimal
r	distance in radial direction, m
T	temperature, °C
t	time, s
v	velocity vector, m/s
W	moisture content of paddy, decimal dry basis, or whiteness
z	distance in axial direction, m
ψ	stream function, m^3/s
ε	porosity
ρ	density, kg/m^3
ω	humidity ratio, kg water/kg dry air
κ	permeability of grain bulk, m
μ	viscosity of air, Pa s/m
β	volume expansivity of air, 1/K

Subscripts

a	dry air
l	water
O	reference state
r	radial direction
s	dry matter of paddy
v	water vapour
z	axial direction

ACKNOWLEDGEMENT

The authors thank the Thailand Research Fund for supporting this work.

REFERENCES

1. Griffith, H.J. Bulk storage of grain: a summary of factors governing control of deterioration. Melbourne, Australia, CSIRO Division of Mechanical Engineering, Report ED8, 1964.
2. Freer, M.W.; Siebenmorgen, T.J.; Couvillion, R.J.; Loewer, O.J. Modeling temperature and moisture content changes in bunker-stored rice. American Society of Agricultural Engineers **1990**, *33*, 211–220.
3. Thorpe, G.R. Modelling moisture migration in stored grains. In *Grain Drying in Asia: Proceedings of an International Conference*, Bangkok: Thailand, October 17–20, 1995; Champ, B.R., Highly, E., Johnson, G.I., Eds.; 1995; 99–122.
4. Babbit, J.D. Thermal properties of wheat in bulk. Canadian Journal Res. **1945**, *23*, 388–401.
5. Singh, A.K.; Thorpe, G.R. A solution procedure for three-dimensional free convective flow in peaked bulks of grain. Journal of Stored Products Research 1993, *29*, 221–235.
6. Shih, T.I.P.; Bailey, R.T.; Nguyen, H.L.; Roelke, R.J. Algebraic grid generation for complex geometries. International Journal of Mechanical Fluids 1991, *13*, 1–31.
7. Teter, N.C. *Grain Storage*. Published by SouthEast Asia Post-Harvest Research and Development Programme, Searca College: Philippines, 1981, 1–86.
8. Hoffman, J.D. *Numerical Methods for Engineers and Scientists*, McGraw-Hill, Inc. 1992, 42–50.
9. White, F.M. *Fluid Mechanics*, 3rd Ed.; McGraw-Hill, Inc. 1994.
10. Soponronnarit, S.; Srisubati, S.; Yoovidhya, T. Effect of temperature and relative humidity on yellowing rate of paddy. Journal of Stored Products Research **1998**, *34*, 323–330.
11. Tirawanichakul, Y.; Prachayawarakorn, S.; Tungtrakul, P.; Chaiwatpongskorn, W.; Soponronnarit, S. Experiments on in-store paddy drying under tropical climate: Simulation and product quality. Drying Technology **2003**, *21*, 1049–1064.
12. Naupanich, M.; Tapan, V.; Tungpinijkul, V.; Wuthisin, P.; Songsermpong, S.; Noosawad, S. Report on development of steel silo for stored paddy. Department of Agricultural Farm Machinery, 1993, 1–20.
13. Prachayawarakorn, S.; Sawangduanpen, S.; Saynampheung, S.; Poolpatarachewin, T.; Soponronnarit, S.; Nathakarakule, A. Kinetics of colour change during storage of garlic slices as affected by relative humidity and temperature. Journal of Food Engineering **2004**, *62*, 1–7.
14. Rapusas, R.S.; Driscoll, R.H. Kinetics of non-enzymatic browning in onion slices during isothermal heating. Journal of Food Engineering **1995**, *24*, 417–429.
15. Raj, S.A.; Singaravadivel, K. Biodeterioration in rice (*Oryza sativa* L.) due to low, medium and high moisture. International Biodeterioration **1990**, *27*, 237–248.
16. Soponronnarit, S. (in Thai) Grain drying, 7th Ed., King Mongkut's University of Technology Thonburi: Bangkok Thailand, 1997.

Drying Technology, 23: 225–248, 2005

ISSN: 0737-3937 print/1532-2300 online
DOI: 10.1081/DRT-200047883

Taylor & Francis
Taylor & Francis Group

Simulation of a Mixed Air and Superheated Steam Drying System

Yuvanaree Namsanguan*, Sumran Tichangtong, Warunee Tia, and Somchart Soponronnarit
School of Energy and Materials, King Mongkut's University of Technology, Bangkok, Thailand

Sakamon Devahastin
Department of Food Engineering, King Mongkut's University of Technology, Bangkok, Thailand

Abstract: Numerical simulation of a cabinet-type superheated steam drying system was conducted and validated experimentally using shrimp as the test material. The experimental and simulated drying temperatures used were in the range of 140–160°C while the volume flow rate of steam of $1.04\,m^3/s$ was used throughout. The initial masses of the drying product were 50.7 and 31.2 kg, with initial moisture contents of 4.0 kg/kg and 3.61 kg/kg dry basis, respectively; the final moisture content of the dried product was 0.25 kg/kg dry basis. The simulated moisture content of shrimp, the drying medium temperature at the outlet of the dryer, and the performance of the dryer in terms of drying time, drying rate, specific energy consumption, and drying efficiency, were verified using available experimental data. The results showed that the simulated results agreed well with the experimental results. Based on the present study, the desirable operating conditions were also evaluated for the dryer for shrimp by considering the optimized performance and good product quality.

Keywords: Dryer performance; Drying efficiency; Drying rate; Shrimp drying; Specific energy consumption

*Correspondence: Yuvanaree Namsanguan, School of Energy Materials, King Mongkut's University of Technology Thonburi, 91 Pracha U-tid Road, Bangkok 10140, Thailand. Tel.: 662-470-8663; Fax: 662-470-8663; E-mail: yuvanaree@yahoo.com

INTRODUCTION

In the superheated steam drying (SSD) process superheated steam acts both as the heat source and as the drying medium to take away the evaporated water from the drying product. Since SSD necessarily produces steam (albeit at lower specific enthalpy) equal in amount to the water evaporated from the product, it would be possible to recover all of the latent heat supplied to the SSD by condensing the exhaust steam or by mechanical or thermal compression for re-use in the dryer or elsewhere.[1-3] Energy recovery, which leads to the lower net energy consumption of the dryer, is therefore possible. The closed steam drying process is clean (better pollution control), absent of the risk of explosion and burning, and also able to enhance the drying rate due to high heat transfer coefficient.[4-7]

Superheated steam drying has recently received considerable attention for drying food and other heat-sensitive products due to its several advantages; e.g., absence of oxidative reactions due to lack of oxygen and its ability to yield products that have lower degree of shrinkage and good color;[8-11] a number of food products have recently been dried successfully in SSD of various designs.[12-15] For shrimp, SSD has been found to be an attractive drying process. Prachayawarakorn et al.[16] investigated the drying of shrimp using superheated steam and found that the use of SSD was very beneficial, since boiling and drying, which are the two main steps of the production of dried shrimp, can be performed in a single step with superheated steam as the drying medium. The color and shrinkage of the dried product were also found to be better than shrimp dried in a conventional hot air dryer. However, the system used was relatively inefficient and had large footprint and included several such units as a steam generator, a steam superheater, a drying chamber, and a blower to deliver the steam to the drying chamber. This bulkiness also resulted in excessive energy usage. For the successful development of the commercial scale dryer, the system should be more compact, available at lower cost, and able to save more energy.

Soponronnarit et al.[17] designed and constructed the prototype of a superheated steam cabinet dryer, which used steam evaporating from the drying product as the drying medium. As reported by several investigators, when superheated steam drying is performed in a closed system, the vapor evaporating from the drying material itself can be utilized as the drying medium;[18,19] when a dryer is operated in a completely closed circuit, air inside the dryer changed to humid air, then highly humid air (or an air–steam mixture), and superheated steam would almost completely replace the air. Similarly, for this dryer, during the first period of drying, the drying medium was treated as the mixture of air and superheated steam. As drying proceeded, the amount of steam evaporated from the product gradually increased while the air was released from the dryer through a small venting hole. The ratio of superheated steam to air increased until the mixture became mostly superheated steam. Steam was forced to flow parallel to a series of wire screens where the samples sat upon in the dryer. Due to the use of vapor evaporated from the drying product as the drying medium, energy consumption was minimized.

Another notable advantage of this dryer prototype is that it can be operated without a steam generator; steam is recirculated and reheated by a burner. To make the energy recovery more efficient, the exhaust gas from the combustion chamber is used to supply heat to the steam at the heat exchanger before being released to the environment. This process saves a significant amount of capital and operating cost of the dryer. However, one of the most important problems experienced in this dryer is the nonuniformity of the flow of drying medium in the dryer, especially at the entrance of the drying chamber. This causes variation of the product's final moisture content. As recommended by Nijdam and Keey[20] and Kiranoudis and Markatos,[21] a uniform flow distribution can be attained by using flow guides or baffles in the drying chamber entrance. Three guide vanes were then installed at appropriate locations in the dryer to help distributing the steam.

Although there are numerous works, both experimental and numerical, that reported results on superheated steam drying of various products, no published work is available on modeling of a complete drying system including the dryer, burner, heat exchanger, and blower, especially for a system similar to that studied in the present work. Such information is necessary if the system is to be used successfully in industry. The objective of this study was therefore to simulate a cabinet-type superheated steam drying system using shrimp as the drying material; the simulation was validated with available experimental results. Variables considered in the model were the drying temperature, the amount of the wet product, and the initial moisture content of the product; the volume flow rate of the drying medium was fixed in this work. Criteria for validation of the model were the moisture content of shrimp, the drying medium temperature at the outlet of the dryer and the dryer performance. In addition, the suitable drying conditions for optimum performance of the dryer in terms of the specific energy consumption (SEC), drying efficiency (DE), and acceptable product quality were determined.

MATHEMATICAL MODEL

Figure 1 shows the drying system simulated in the present study, and a diagram of the drying system is shown in Fig. 2. The system is very

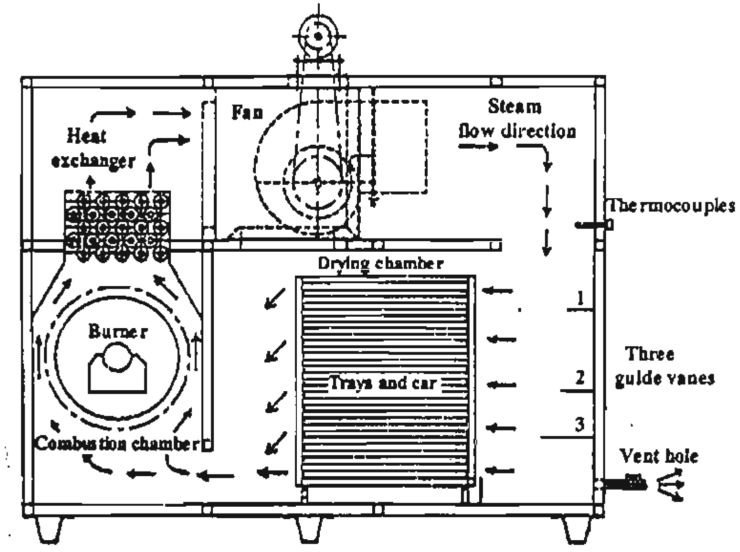

Figure 1. Simulated drying system.

compact, *viz.* $1.27 \times 2.24 \times 1.675\,m^3$. The wall of the drying system is insulated with asbestos. The unit consists of a $0.95 \times 0.8 \times 0.98\,m^3$ drying chamber, an oil burner rated between 35.5 and 71 kW, a cylindrical combustion chamber of 0.4 m in diameter and 1.1 m in length with surrounding fins providing a total heat transfer area of $4.59\,m^2$, a compact heat exchanger with 24 finned tubes providing a total heat transfer area of $16.8\,m^2$, and a 0.75 kW forward-curved blade centrifugal fan, which is used to circulate the drying steam through the dryer. The dryer has a maximum capacity of 50 kg.

In this case, steam, which was generated from evaporation of water in the product, was used as the drying medium. The vapor was circulated in the drying chamber (CV.1) and reheated by a burner, which generated heat through a combustion chamber (CV.2). Before being released to the environment, the flue gas exhausting (m_g) from the combustion chamber was reused to supply heat to the drying medium (m_3) at the heat exchanger (CV.3). Drying was performed at a pressure slightly above atmospheric pressure; thus, the evaporated moisture of the product became superheated steam only after passing through the combustion chamber and heat exchanger. However, during the first period of drying, steam generated from the product was not enough to fill the whole dryer and there was still some air in the drying chamber; the dryer had a small vent

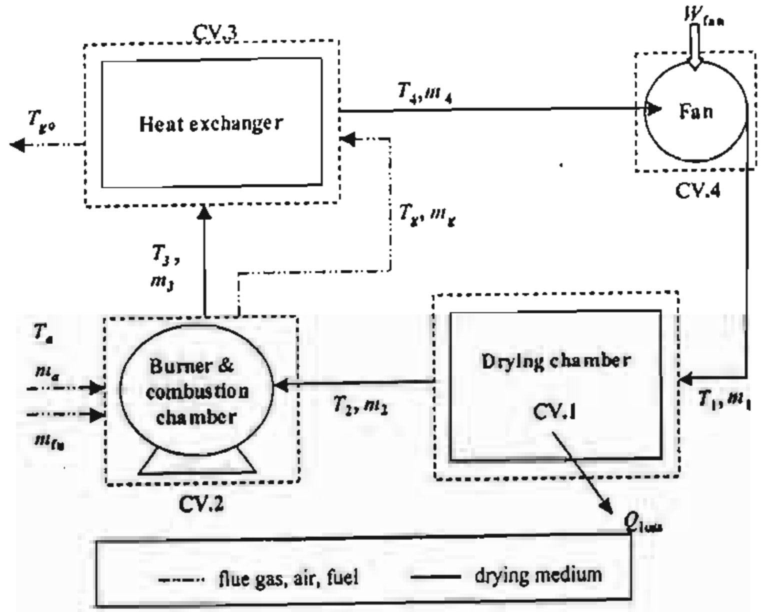

Figure 2. Diagram of the simulated drying system (CV = control volume).

hole to release air to the atmosphere until the drying medium became purely superheated steam. Unfortunately, from the experimental characteristic curve of the fan power requirement, it was found that air was still present and mixed with superheated steam for the whole drying process. Consequently, the drying medium was treated as a mixture of air and superheated steam in the model developed similarly to the studies of Costa and Silva,[22] Schwartze and Brocker,[23] and Chu et al.;[24] properties of the drying medium were calculated as properties of a fluid mixture according to the methods of Avallone and Baumeister[25] and Chow and Chung[26] by using the ratio of steam and air estimated from the experimental data of the fan power requirement versus the drying time.

The mathematical model of the drying system consists of a drying model, a burner and combustion chamber model, a heat exchanger model, and a performance model. The assumptions made in the development of these models are as follows: drying medium was a mixture of air and superheated steam, thermal equilibrium existed between the drying medium and the product, the change in internal energy of the dryer and product was negligible, and the effect of product shrinkage during drying was negligible.

Drying Model

First of all, the moisture content of the drying product (shrimp) was calculated using the analytical solution of a simple liquid diffusion equation. It was assumed that the initial moisture content of the product was uniform and the moisture content at the surface of the product was in equilibrium with the surrounding drying medium immediately after the start of the drying process. By considering shrimp as a spherical body, the diffusion equation is written as Eq. (1).[27] The choice of the spherical geometry of shrimp was due to the fact that the only correlations for the effective moisture diffusivity of shrimp available in the literature are based on a spherical geometry.[16]

$$MR = \frac{M(t) - M_{eq}}{M_{in} - M_{eq}} = \frac{6}{\pi^2}\sum_{n=1}^{\infty}\frac{1}{n^2}\exp\frac{n^2\pi^2 D_{eff} t}{a^2} \quad (1)$$

The correlations for the effective diffusion coefficients were those of Prachayawarakorn et al.[16] who dried shrimp using both superheated steam and hot air.

$$\text{Superheated steam:} \quad D_{eff} = 0.00253 \exp\left(\frac{-32,714.9}{RT_{abs}}\right) \quad (2a)$$

$$\text{Hot air:} \quad D_{eff} = 0.00034 \exp\left(\frac{-25,578.0}{RT_{abs}}\right) \quad (2b)$$

where T_{abs} is the absolute temperature of the drying medium used. The effective diffusion coefficient of shrimp dried in a mixture of air and superheated steam is weighed as follows:

$$D_{eff,m} = \frac{\sum(m_i D_{eff,i})}{m} \quad (2c)$$

where $m = m_s + m_d$ denotes the total mass of the mixture; m_s and m_d denote the masses of the constituent gases; and the subscripts $i = s$ and $i = d$ denote superheated steam and air, respectively.

The properties of the air and superheated steam mixture leaving the drying chamber were calculated by performing mass and energy balances in control volume 1 (CV.1) of Fig. 2. Both air and superheated steam were individually assumed to be an ideal gas because their Z factors are very close to unity[28] in the ranges of drying temperature and pressure used in the present study. An ideal gas behavior could be assumed in this case as the level of pressure was in an atmospheric range. The drying medium was therefore treated as an ideal gas mixture. Then, mass and energy balances in CV.1 can be written us follows:

$$\text{Mass balance:} \quad m_2 = m_1 + \Delta m \quad (3)$$

where $\Delta m = m_p(M_i - M_o)/\Delta t$

$$\text{Energy balance:} \quad (m_{d,1}c_{pa} + m_{s,1}c_{ps})T_1 = (m_{d,2}c_{pa} + m_{s,2}c_{ps})T_2 + \Delta m h_{fg} + Q_{loss} \quad (4)$$

where m_1 and m_2 are the total mass flow rates of the mixture entering and leaving the drying chamber, respectively; $m_1 = m_{d,1} + m_{s,1}$ and $m_2 = m_{d,2} + m_{s,2}$.

Burner and Combustion Chamber Model

In this system, the energy needed to heat up the drying medium to the desired temperature was supplied by a burner instead of an electric heater. Diesel oil was used as the fuel in the burner and energy was generated from the burner and transferred to the drying medium through the combustion chamber. From CV.2, two parts of mass balance, one of which belongs to the drying medium and another belongs to the fuel, are written in Eqs. (5) and (6), respectively. For combustion, 20% excess air and 14.5 air/fuel ratio (A/F) were used in the model.

$$m_3 = m_2 \quad (5)$$

$$m_g = [1 + 1.2(A/F)]m_{fu} \quad (6)$$

Energy balance equations are given in Eqs. (7), (8), and (9). For an energy balance in Eq. (9), since the flue gas temperature was high (≈1000°C) and the wall of the combustion chamber was very thin, it was assumed that the wall resistance was negligible. This implies that there was no difference in temperature between inside and outside surfaces of the combustion chamber wall. Eq. (9) can also be decomposed into Eqs. (9a) and (9b):[29]

$$m_{fu}\,\mathrm{LHV} = m_g c_{pg}(T_g - T_a) + Q_{tr} \quad (7)$$

$$Q_{tr} = (m_{d,2}c_{pa} + m_{s,2}c_{ps})(T_3 - T_2) \quad (8)$$

$$Q_{tr} = Q_{conv,i} + Q_{radia,i} = Q_{conv,o} + Q_{radia,o} \quad (9)$$

$$Q_{tr} = h_{c,i}A_i(T_g - T_w) + \sigma A_i(\varepsilon_g T_g^4 - \alpha_g T_w^4) \quad (9a)$$

$$h_{c,i}A_i(T_g - T_w) + \sigma A_i(\varepsilon_g T_g^4 - \alpha_g T_w^4) = \eta_o h_{c,o}A_o(T_w - T_{ar}) + \varepsilon_s\sigma A_o(T_w^4 - T_{ar}^4) \quad (9b)$$

where T_{av} is the average drying medium temperature passing through the combustion chamber, which is defined as $T_{av} = (T_2 + T_3)/2$.

Heat Exchanger Model

Based on CV.3, the equations for mass and energy balances can be written as follows:

$$m_4 = m_3 = m_2 \tag{10}$$

$$Q_{he} = (m_{d,2}c_{pa} + m_{s,2}c_{ps})(T_4 - T_3) = m_g c_{pg}(T_g - T_{go}) \tag{11}$$

$$Q_{he} = \varepsilon C_{min}(T_g - T_3) \tag{12}$$

where ε is the effectiveness of the heat exchanger and C_{min} is the minimum heat capacity rate corresponding to the hot fluid (flue gas).

$$\varepsilon = 1 - \exp\left((\mathrm{NTU})^{0.22}/C_r\left\{\exp\left[-Cr(\mathrm{NTU})^{0.78}\right] - 1\right\}\right) \tag{12a}$$

$$\text{and } \mathrm{NTU} = \frac{U_o A_o}{C_{min}} \tag{12b}$$

$$C_{min} = C_h = m_g c_{pg} \tag{12c}$$

$$\text{and } C_{max} = C_c = m_{d,2}c_{pa} + m_{s,2}c_{ps} \tag{12d}$$

$$C_r = C_{min}/C_{max} \tag{12e}$$

Energy Consumption of Fan

The rate of electricity consumption (W_{fan}) for driving the fan (CV.4) can be calculated by the following equation:

$$W_{fan} = \frac{Q\Delta P}{\eta_f \eta_m} \tag{13}$$

Performance Model

The performance of the dryer is defined in terms of the specific energy consumption (SEC), average drying rate (DR), and drying efficiency (DE). They can be calculated from:

$$\mathrm{SEC} = (2.6\mathrm{E} + Q_h)/[(M_{in} - M_f)m_p] \tag{14}$$

$$\mathrm{DR} = m_w/\mathrm{DT} \tag{15}$$

$$\mathrm{DE} = Q_{evap}/Q_{in} \tag{16}$$

where 2.6 is the energy conversion factor.[17]

Solution Procedure

As mentioned earlier, the simulation was performed to study the drying characteristics of shrimp as well as the performance of the mixed air and superheated steam drying system. The inputs for the model are the initial moisture content and initial mass of the product, the volume flow rate of the drying medium, the drying temperature, the fuel flow rate in the burner, and other constants listed in the previous section. The temperature of the drying medium at the entrance of the drying chamber (T_1) was set equal to the drying temperature, and the humidity ratio of air at the beginning of the process was estimated initially from the experimental fan power requirement. The ratio of air and superheated steam along the drying process was estimated from the experimental data of the fan power requirement versus the drying time as mentioned earlier; Fig. 3 presents the experimental fan power data and the fraction of steam evaluated. The temperature of the mixture leaving the combustion

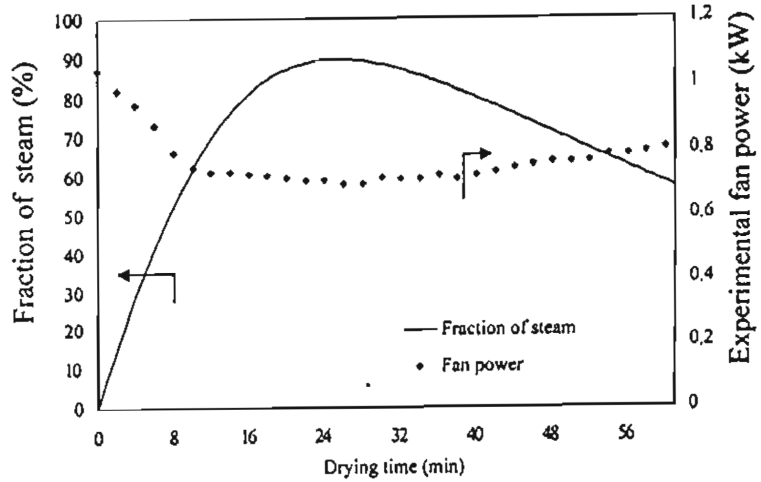

Figure 3. Evolution of fraction of steam estimated from experimental fan power requirement.

chamber (T_3), the temperature of flue gas exiting the combustion chamber (T_g), the average temperature of mixture passing through the combustion chamber (T_{av}), the temperature of the wall of the combustion chamber (T_w), the rate of heat transfer from the combustion chamber to the drying medium (Q_{tr}), and the rate of heat exchanged at the heat exchanger (Q_{he}) were initially guessed values. The steps of the simulation are as follows: the drying model, the burner and combustion chamber model, and the heat exchanger model were simulated, and the temperature of the mixture leaving the drying chamber (T_2), all other guessed values, and the final moisture content of the product were checked. The relative humidity of the mixture, however, was not checked except at the beginning of the process because the mixture of air and superheated steam behaved like moist air during the beginning of the drying process. Thus, the model also included a subroutine to check for moisture condensation (relative humidity <1) in the case when the temperature of the drying medium at the outlet of the drying chamber (T_2) was less than 100°C, which occurred only at the beginning of the drying process. Newton-Raphson technique was used for checking the guessed values and determining the acceptable ones. Next, an energy consumption of the fan and the burner were computed and then moisture content of product after drying was checked. To calculate the final moisture content of the product at each time step, Eq. (1) was differentiated with respect to time and solved numerically using fourth-order Runge-Kutta algorithm. In this case, M_{eq} was assumed to be zero.[16] Regarding the moisture content of the product after drying, if the final moisture content of the product was higher than the desired value, the moisture content of the product before drying was replaced by the moisture content after drying, and the time step was advanced. Since the moisture of the product evaporated and became superheated steam, the mass flow rate of superheated steam leaving the drying chamber during this time step would be that of superheated steam entering the drying chamber during the next time step ($m_{s,1}{}^{k+1} = m_{s,2}{}^{k}$). The calculation continued until the moisture content of the product was less than or equal to the desired value. Finally, the performance of the dryer was determined.

RESULTS AND DISCUSSION

Validation of Model

The experimental shrimp drying data that were used to verify the present model were conducted by Soponronnarit et al.[17] The experimental and simulated drying conditions were as follows: the drying temperatures in the range of 140–160°C, the volume flow rate of the drying medium of

1.04 m^3/s, the initial masses of product of 50.7 and 31.2 kg, the initial moisture contents of 4.0 kg/kg and 3.61 kg/kg dry basis (80% and 78.3% wet basis, respectively), and the final moisture content of 0.25 kg/kg dry basis (20% wet basis). Drying was performed at a pressure slightly above the atmospheric pressure.

Evolution of Product Moisture Content

The simulated moisture content of shrimp is shown in Fig. 4 where drying conditions employed were the drying temperatures of 140–160°C, the initial masses of product of 50.7 kg, and the initial moisture content of 4.0 kg/kg dry basis. The other drying conditions were fixed as described above. As the drying temperature increased, the moisture reduction rate was higher and the drying time was reduced, as expected, because a higher drying temperature led to a higher effective diffusion coefficient of shrimp; the existence of an inversion temperature of 140°C has indeed been found by Prachayawarakorn et al.[16] The experimental moisture content evolution of shrimp is not shown here since there is no such data available. However, the experimental and simulated total drying times and drying rates are compared as shown in Table 1 (Test nos. 1–6). It is seen that the drying times (DT) obtained from the model and those obtained from the experiments are relatively close. The results indicate that the drying model is able to predict the drying rate (DR) accurately.

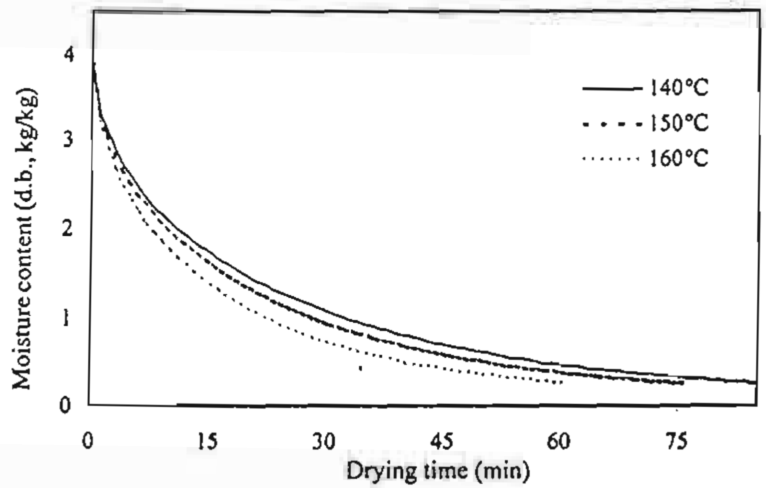

Figure 4. Evolution of simulated moisture content (Test nos. 4, 5, and 6).

Table 1. Comparison between experimental and simulated results of shrimp drying

Description	Test no. 1		2		3		4		5		6	
	Exp.	Sim.	Exp.	Sim.	Exp.	Sim.	Exp.	Sim.	Exp.	Sim.	Exp.	Sim.
Product conditions												
Initial moisture content (kg/kg d.b.)	3.61	3.61	3.61	3.61	4.0	4.0	4.0	4.0	4.0	4.0	4.0	4.0
Final moisture content (kg/kg d.b.)	0.27	0.25	0.27	0.25	0.25	0.25	0.22	0.25	0.21	0.25	0.23	0.25
Initial weight (kg)	31.2	31.2	31.2	31.2	31.2	31.2	50.7	50.7	50.7	50.7	50.7	50.7
Final weight (kg)	8.4	8.5	8.4	8.5	7.9	7.8	12.4	12.7	12.3	12.7	12.1	12.7
Drying conditions												
Drying temperature (°C)	142.7	140	150.3	150	158.3	160	142.3	140	150.4	150	159.9	160
Volume flow rate (m^3/s)	1.04	1.04	1.04	1.04	1.04	1.04	1.04	1.04	1.04	1.04	1.04	1.04
Dryer performance												
Drying time (min)	76	82	64	72	44	48	86	87	70	76.5	60	61
Drying rate (kg water evap./h)	18.1	16.6	21.4	19.0	31.8	29.2	26.7	26.2	32.9	29.8	38.6	37.4
Energy consumption												
Diesel fuel (kg)	2.8	3.04	2.9	3.26	2.8	3.06	3.25	3.29	3.9	4.26	3.55	3.61
Electricity (kW-h)	1.5	1.58	1.35	1.33	0.95	0.93	1.7	1.68	1.38	1.42	1.2	1.07
Specific primary energy consumption												
Diesel fuel (MJ/kg water evap.)	5.48	5.95	5.7	6.42	5.38	5.85	3.25	3.29	3.9	4.26	3.55	3.61
Electricity (MJ/kg water evap.)	0.61	0.65	0.55	0.548	0.38	0.37	0.42	0.41	0.34	0.35	0.29	0.26
Total (MJ/kg water evap.)	6.09	6.6	6.25	6.97	5.77	6.22	4.22	4.28	4.89	5.37	4.41	4.51
Drying efficiency (%)	42.7	39.4	41.6	37.3	45.1	41.7	61.7	60.6	53.2	48.4	58.9	57.6

The differences between the experimental and simulated results are less than 10%.

Drying Medium Temperature

The evolution of the experimental and simulated mean drying medium temperature at the inlet and outlet of the dryer (drying chamber, CV.1) are presented in Figs. 5–8 for various inlet drying temperatures (T_1), initial shrimp weights, and initial moisture contents. The results indicate that the drying model is capable of predicting the drying medium temperature evolution reasonably well. The outlet drying temperature (T_2) increased suddenly at the beginning of the process and then slowly increased and finally approached the inlet drying temperature. The simulated temperatures were generally slightly lower than the experimental ones during the first period of drying. This is possibly due to the fact that there was some amount of heat stored in the heat exchanging equipment during the warm-up period before the sample was placed in the drying chamber. During the warm-up period, the temperature at the drying chamber entrance was set at higher values than the desired drying temperature by about 20–40°C (shifting temperature) to help recover the heat loss during the loading of the sample; it was then reset down to the drying temperature and fixed at that value along the whole drying process. Thus,

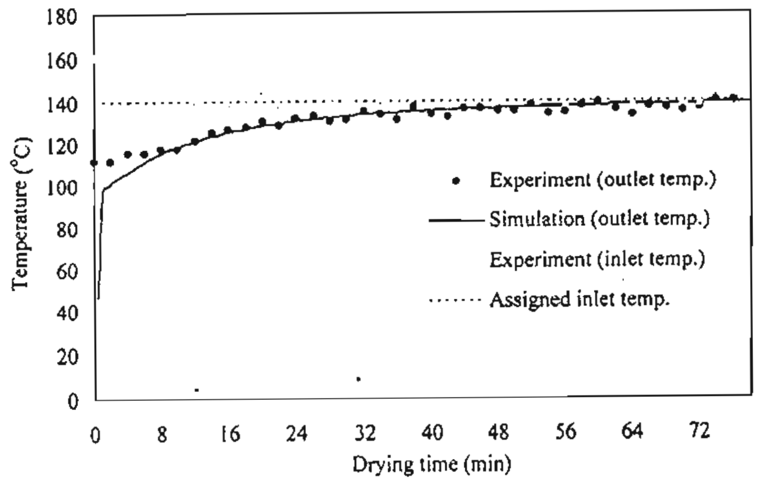

Figure 5. Evolution of simulated and experimental drying medium temperatures (Test no. 1).

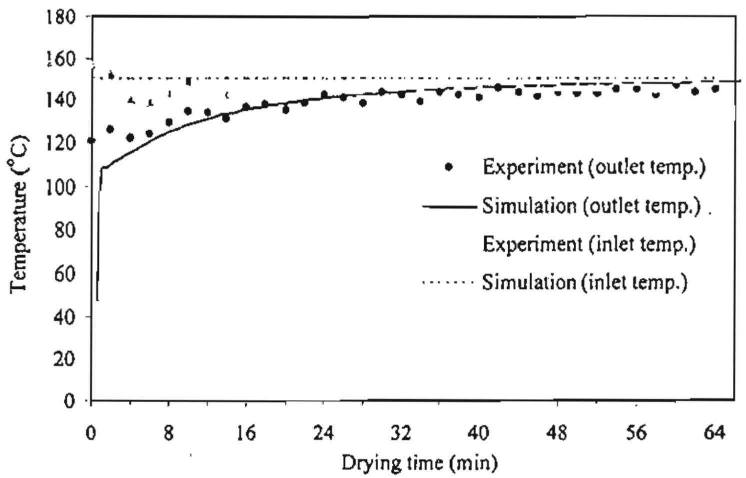

Figure 6. Evolution of simulated and experimental drying medium temperatures (Test no. 2).

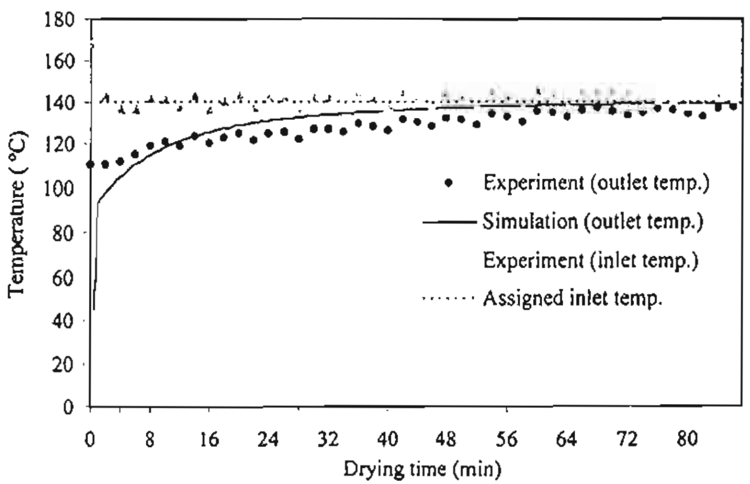

Figure 7. Evolution of simulated and experimental drying medium temperatures (Test no. 4).

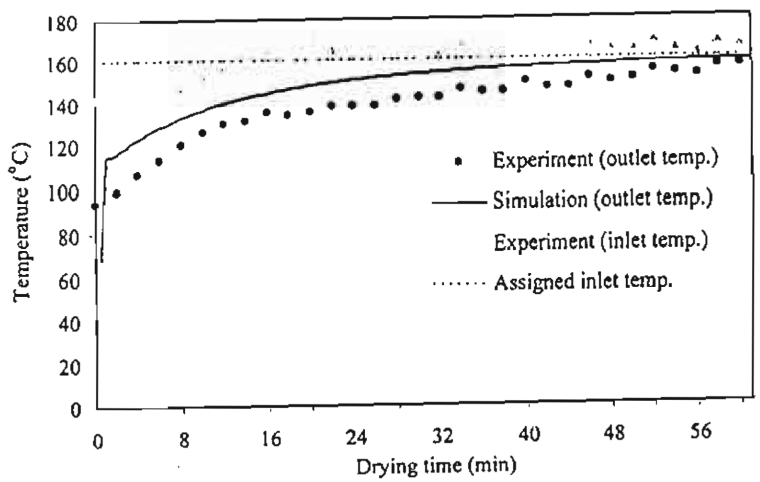

Figure 8. Evolution of simulated and experimental drying medium temperatures (Test no. 6).

the experimental outlet drying temperature was found to be slightly higher than the simulated value during the first period of drying.

Considering the drying temperature and initial mass of shrimp, it was found that the simulated results agreed very well with the experimental data when using low drying temperatures of 140–150°C and low initial shrimp weight of 31.2 kg. The difference between the experimental data and simulated results at higher drying temperatures was due to the fact that the change of the internal energy of the dryer and the product was assumed to be negligible in this study. However, it is known that the higher the drying temperature and the larger the initial weight of the product, the more change of internal energy of the dryer and the product would be observed. This is why the experimental and simulated results only agreed well when the drying medium temperature and the initial weight of the product were reduced. In addition, poorer agreements at higher drying medium temperatures also may be due to physical or chemical changes, e.g., shrinkage; the effect of product shrinkage during drying was not considered in this study.

However, as illustrated in Fig. 8, the experimental and simulated results for the case where the drying conditions were the drying temperature of 160°C and the initial weight of product of 50.7 kg (Test no. 6) seemed to be more deviated from each other than for other cases. In this test, the inlet drying temperature dropped significantly at the beginning of the drying process because of the smaller shifting temperature during the warm-up period (only 20°C above the inlet drying temperature) than in the case of other experiments. Therefore, it took a longer time for the temperature to reach the desired value during the first period of drying.

Energy Consumption And Dryer Performance

The experimental shrimp drying results that were used to verify the model and the simulated results are shown in Table 1. Specific energy consumption, drying time, drying rate, and drying efficiency were used for the verification of the mathematical model. It can be seen in this table that the simulated results agreed well with the experimental data; the differences were less than 10%. Furthermore, for clearer understanding of the data, the results of the energy consumption and the dryer performance are presented in Figs. 9–12.

The relationship between the energy consumption and the drying time is demonstrated in Fig. 9. It can be observed that the specific energy consumption increased with drying time. At low moisture content, the rate of moisture diffusion was low resulting in slow drying and high energy consumption. Since the energy consumption included two main types of energy mode, the fuel energy consumption, which was around 90–93%, and electricity consumption, which was another 7–10% of the total energy consumption, the former was the main part of the energy

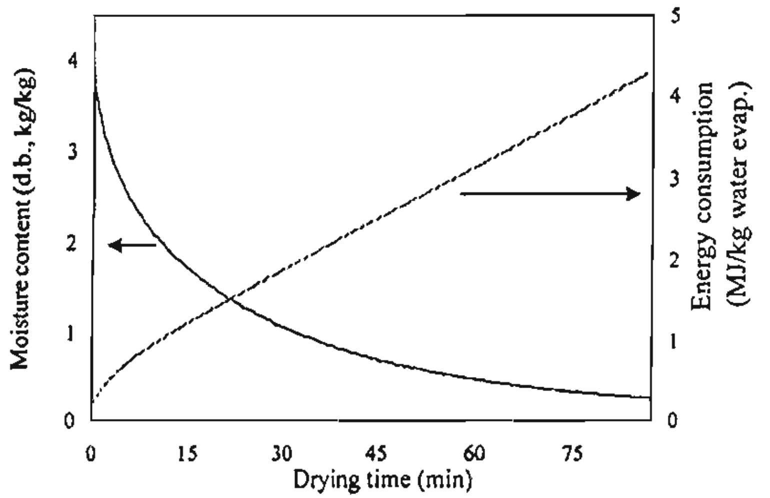

Figure 9. Evolution of simulated moisture content and specific energy consumption.

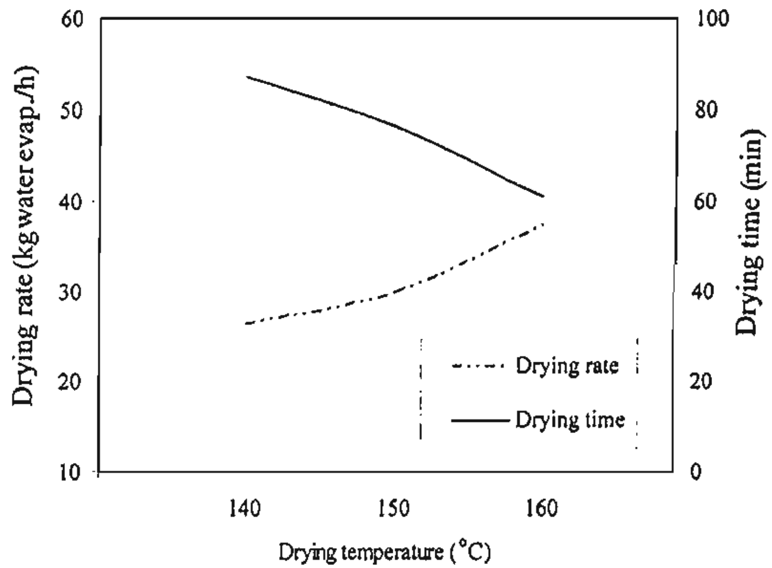

Figure 10. Evolution of simulated drying rate and drying time.

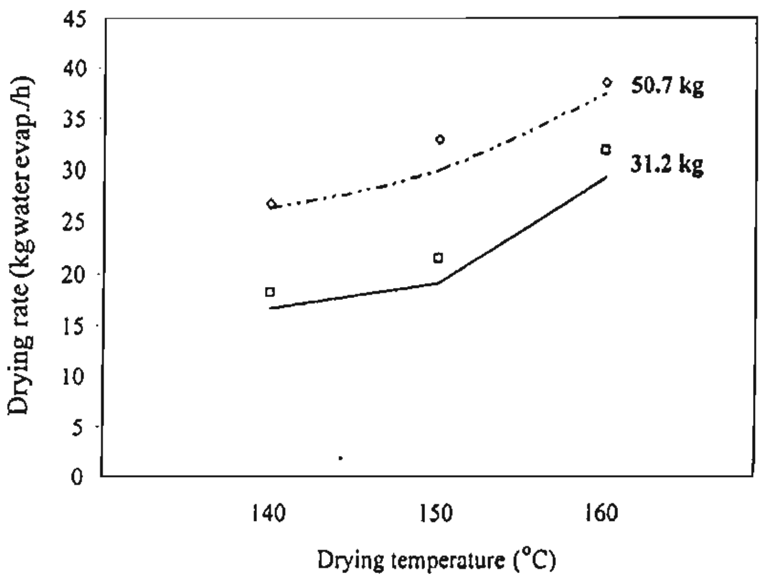

Figure 11. Evolution of simulated and experimental drying rates at different initial weights of product.

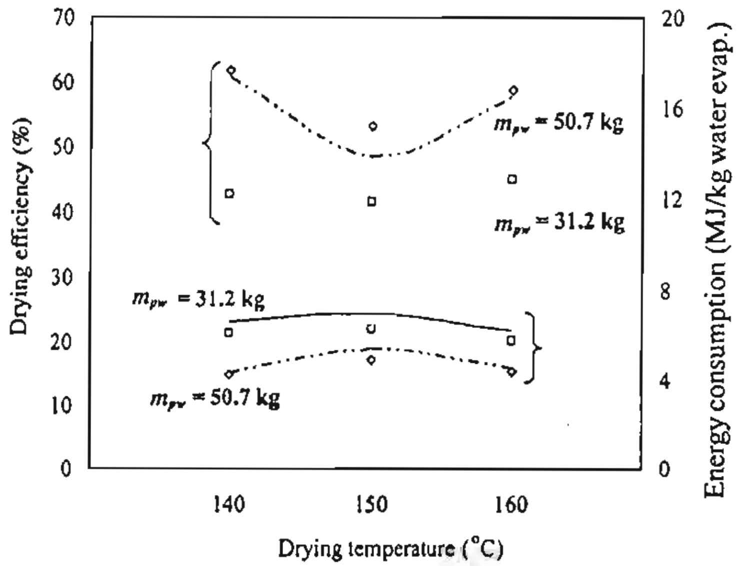

Figure 12. Evolution of simulated and experimental drying efficiencies and specific energy consumption.

usage for this dryer. It can be seen that the overall energy consumption of the system was very low compared to a conventional hot air dryer. Furthermore, using fuel as a source of energy was more economical than using an electric heater.

Figure 10 shows the evolution of the simulated drying rate and drying time when the initial weight of the product was 50.7 kg and the initial moisture content was 4.0 kg/kg dry basis. From simulation results the total drying time (DT) decreased and drying rate (DR) increased with increasing drying medium temperature. This is consistent with the fundamental drying theory since the heat transfer from the drying medium to the product increases with increased medium temperature. These trends were also similar for the case of decreasing initial weight and initial moisture content of the drying product.

Figure 11 shows the effect of drying temperature on the drying rate (DR) at different initial weights of the product. The agreement between the simulated drying rates and the experimental results is observed. It was found that the drying temperature had a significant effect on the drying rate. By considering the initial weight of the product, it was found that a lower initial weight of the product led to a slower drying rate since using a lower initial weight provided the less amount of water evaporated

from the product (m_w). As shown in Eq. (15), the drying rate is the function of the water evaporated from the product (m_w) and the drying time (DT); the simulated drying time was slightly different at the same initial weight of the product. In the case where the initial weights of the product were 50.7 kg and 31.2 kg, an increase in the drying temperature from 140 to 160°C caused the drying rate to increase from 26.2 to 37.4 kg water evap./h and from 16.6 to 29.2 kg water evap./h (simulation result), respectively.

Figure 12 shows the effect of drying temperature on the drying efficiency (DE) and the specific energy consumption (SEC). It was observed that the drying temperature affected SEC; SEC increased with increased drying temperature to the maximum point, and then decreased. This is due to the fact that drying at a higher temperature requires a higher capacity of the burner to combust the fuel (main energy part), resulting in a higher energy consumption rate than drying at a lower temperature. However, drying at this higher temperature resulted in a shorter drying time, as expected. Since the energy consumption is the product of the energy consumption rate and drying time, there possibly existed a maximum value of SEC in this range of drying temperature. An inverse relationship was also found between DE and SEC. Finally, as a result of the high initial shrimp weight, SEC could be reduced and this resulted in a higher DE since higher initial weight of the product yielded a higher drying rate. Consequently, specific energy consumption was lower when using higher initial weight of the product.

Based on the assumptions and results of this study, a maximum capacity of the raw product of 50 kg and drying temperatures between 140 and 160°C are recommended for the operation of the dryer. The drying temperature should not exceed 160°C due to the limitation of product quality (very poor color, high degree of shrinkage, and the difficulty of removing the shell from the shrimp body) as suggested by Prachayawarakorn et al.[16] From the experiments, it was also found that the desired red-orange color of dried shrimp was obtained at the drying temperature of 140°C.[8] It is possible to scale up the dryer by dividing the drying chamber into several thin sections, assuming the plug flow of the drying medium, and assuming that the temperature gradient exists only in the direction of the flow of the drying medium in the model.

CONCLUSION

Numerical simulation of a mixed air and superheated steam cabinet drying system was conducted and validated with experimental shrimp drying results. The model was found to predict the moisture reduction rates of shrimp as well as the outlet drying medium temperature relatively well.

It was also found that the simulated results agreed well with the experimental data in terms of the drying time, drying rate, energy consumption, and dryer performance. The drying temperature and the initial load of the raw product were found to affect the specific energy consumption (SEC) and the drying efficiency (DE) of the dryer; SEC decreased with an increase in the initial load of the raw product, while it increased with an increase of the drying temperature to the maximum point, and then decreased again in the range of drying temperature studied. Based on the present study, it was found that the desirable operating conditions for the dryer for shrimp would be as follows: the drying temperature of 140°C and the initial shrimp weight of 50.7 kg (for optimized performance and good product quality).

NOMENCLATURE

A_i	internal area of combustion chamber or heat exchanger (m^2)
A_o	external area of combustion chamber or heat exchanger (m^2)
A/F	air/fuel ratio (kg of air/kg of fuel)
a	particle radius (m)
C_c	cold fluid heat capacity rate (kW/K)
C_h	hot fluid heat capacity rate (kW/K)
C_{max}	maximum heat capacity rate corresponding to the cold fluid (kW/K)
C_{min}	minimum heat capacity rate corresponding to the hot fluid (kW/K)
C_r	heat capacity ratio (decimal)
c_{pa}	specific heat capacity of dry air (kJ/kg K)
c_{pg}	specific heat capacity of flue gas (kJ/kg K)
c_{ps}	specific heat capacity of superheated steam (kJ/kg K)
D_{eff}	effective diffusion coefficient (m^2/min)
DE	drying efficiency (%)
DR	drying rate (kg water evap./h)
DT	drying time (min)
E	electricity consumption (kJ)
h	convective heat transfer coefficient (W/m^{2}K)
h_{fg}	heat of evaporation (kJ/kg)
LHV	lower heating value (kJ/kg)
M	moisture content (decimal, dry-basis)
MR	moisture ratio, dimensionless
M_i	moisture content before drying at each time step (decimal, dry-basis)
M_o	moisture content after drying at each time step (decimal, dry-basis)
m	total mass flow rate or total mass (kg/s or kg)
m_{pw}	initial mass of wet product (kg)
m_w	water evaporated from product (kg)
Δm	rate of water evaporated from product (kg/s)

NTU	number of transfer units
ΔP	pressure drop (kPa)
Q	volume flow rate of drying medium (m^3/s)
$Q_{conv,i}$	convective heat transfer rate inside the wall of combustion chamber (kW)
$Q_{conv,o}$	convective heat transfer rate outside the wall of combustion chamber (kW)
$Q_{evap.}$	energy used for water evaporation of product (kJ)
Q_h	energy consumption provided by fuel (kJ)
Q_{he}	rate of heat exchanged at the heat exchanger (kW)
Q_{in}	energy input to system (kJ)
Q_{loss}	heat loss from control volume to surroundings (kW)
$Q_{radia,i}$	radiation heat transfer rate inside the wall of combustion chamber (kW)
$Q_{radia,o}$	radiation heat transfer rate outside the wall of combustion chamber (kW)
Q_{tr}	rate of heat transfer from the combustion chamber to the drying medium (kW)
R	universal gas constant (8.314 kJ/mole-K)
SEC	specific energy consumption (MJ/kg water evap.)
T	temperature (°C or K)
t	drying time (min)
Δt	time step (min)
U_o	overall heat transfer coefficient (W/m^{2}K)
W_{fan}	power of fan (kW)

Greek Letters

α_g	absorptivity of flue gas at the inside surface of combustion chamber (0.1695 decimal)
ε	effectiveness of heat exchanger (decimal)
ε_g	emissivity of flue gas at the inside surface of combustion chamber (0.1126 decimal)
ε_x	emissivity of mixture at the outside surface of combustion chamber (0.56 decimal)
η_f	efficiency of fan (0.575 decimal)
η_m	efficiency of motor (0.5 decimal)
η_o	overall surface efficiency of finned combustion chamber surface (0.94 decimal)
σ	Stefan–Boltzmann constant (5.669 10^{-8} W/m^{2}K^4)

Subscripts

a	air
abs	absolute
av	average
d	dry air
c,i	inner combustion chamber surface

c,o	outer combustion chamber surface
eq	equilibrium
f	final
fu	fuel
g	flue gas
go	exhaust gas
in	initial
m	mixture
p	dry product
s	superheated steam
w	wall of combustion chamber
1	entering the drying chamber
2	leaving the drying chamber
3	leaving the combustion chamber
4	leaving the heat exchanger

ACKNOWLEDGEMENTS

The authors express their sincere appreciation to the Thailand Research Fund (TRF) for supporting this study financially.

REFERENCES

1. Kudra, T.; Mujumdar, A.S. *Advanced Drying Technologies;* Marcel Dekker: New York, 2002.
2. Mujumdar, A.S. Superheated steam drying. *Handbook of Industrial Drying*, 2nd Ed., Marcel Dekker: New York, 1995; 1071–1086.
3. Shibata, H.; Mujumdar, A.S. Steam drying technologies: Japanese R&D. Drying Technology **1994**, *12*, 1485–1524.
4. Pronyk, C.; Cenkowski, S.; Muir, W.E. Drying foodstuffs with superheated steam. Drying Technology **2004**, *22* (5), 899-916.
5. Elustondo, D. Drying foodstuff with superheated steam. Drying Technology **2002**, *20* (1), 235–237.
6. van Deventer, H.C.; Hejimans, R.M.H. Drying with superheated steam. Drying Technology **2001**, *19* (8), 2003–2045.
7. Mujumdar, A.S. Superheated steam drying—Technology of the future. In *Mujumdar's Practical Guide to Industrial Drying;* Devahastin, S. Ed.; Exergex: Brossard, Canada, 2000; 115–138.
8. Namsanguan, Y.; Tia, W.; Devahastin, S.; Soponronnarit, S. Drying kinetics and quality of shrimp undergoing different two-stage drying processes. Drying Technology **2004**, *22* (4), 759–778.
9. Uengkimbuan, N.; Soponronnarit, S.; Prachayawarakorn, S.; Nathakaranakule, A. *Comparative study of pork dried using superheated steam and hot air.* In *Proceedings of the 3rd Asia-Pacific Drying Conference (ADC'03)*, Bangkok, Thailand, September 1–3, 2003; 679–691, 2003.

10. Tang, Z.; Cenkowski, S. Equilibrium moisture content of spent grains in superheated steam under atmospheric pressure. Transactions of the ASAE 2001, *44*, 1261–1264.
11. Chen, S.-R.; Chen, J.-Y.; Mujumdar, A.S. A preliminary study of steam drying of silkworm cocoons. Drying Technology **1992**, *10* (1), 251–260.
12. Elustondo, D.; Mujumdar, A.S.; Urbicain, M.J. Optimum operating conditions in drying foodstuffs with superheated steam. Drying Technology **2002**, *20* (2), 381–402.
13. Iyota, H.; Nishimura, N.; Onuma, T.; Nomura, T. Drying of sliced raw potatoes in superheated steam and hot air. Drying Technology **2001**, *19* (7), 1411–1424.
14. Moreira, R.G. Impingement drying of foods using hot air and superheated steam. Journal of Food Engineering **2001**, *49*, 291–295.
15. Li, Y.B.; Seyed-Yagoobi, J.; Moreira, R.G.; Yamsaengsung, R. Superheated steam impingement drying of tortilla chips. Drying Technology **1999**, *17* (1–2), 191–213.
16. Prachayawarakorn, S.; Soponronnarit, S.; Wetchacama, S.; Jaisut, D. Desorption isotherms and drying characteristics of shrimp in superheated steam and hot air. Drying Technology **2002**, *20* (3), 669–684.
17. Soponronnarit, S.; Tichangtong, S.; Prachayawarakorn, S. Prototype of superheated-steam cabinet dryer. The Journal of the Royal Institute of Thailand **2002**, *27* (4), 1079–1090.
18. Tatemoto, Y.; Bando, Y.; Oyama, K.; Yasuda, K.; Nakamura, M; Sugimura, Y.; Shibata, M. Effects of operational conditions on drying characteristics in closed superheated steam drying. Drying Technology **2001**, *19* (7), 1287–1303.
19. Yoshida, T.; Hyodo, T. Evaporation of water in air, humid air and superheated steam. Industrial and Engineering Chemistry, Process Design and Development **1970**, *9* (2), 207–214.
20. Nijdam, J.J.; Keey, R.B. Airflow behavior in timber (lumber) kilns. Drying Technology **1999**, *17* (7–8), 1511–1522.
21. Kiranoudis, C.T.; Markatos, N.C. Computer analysis of industrial batch dryer aerodynamics. Drying Technology **1998**, *16* (7), 1283–1303.
22. Costa, V.A.F, da Silva, F.N. On the rate of evaporation of water into a stream of dry air, humidified air and superheated steam, and the inversion temperature. International Journal of Heat and Mass Transfer **2003**, *46*, 3717–3726.
23. Schwartze, J.P.; Brocker, S. The evaporation of water into air of different humidities and the inversion temperature phenomenon. International Journal of Heat and Mass Transfer **2000**, *43*, 1791–1800.
24. Chu, J.C.; Finelt, S.; Hoerrner, W; Lin, M.S. Drying with superheated steam-air mixtures. Industrial and Engineering Chemistry **1959**, *51* (3), 275–280.
25. Avallone, E.A.; Baumeister, T, III. Ideal gas mixtures. In *Handbook for Mechanical Engineers*, 10th Ed.; McGraw-Hill: New York, 1997; 4–8.
26. Chow, L.C.; Chung, J.N. Evaporation of water into a laminar stream of air and superheated steam. International Journal of Heat and Mass Transfer **1983**, *26* (3), 373–383.

27. Crank, J. Diffusion in sphere. In *The Mathematics of Diffusion*, 2nd Ed.; Oxford University Press: England, 1975; 89–103.
28. Wark, K. Jr. Equations of state. In *Advanced Thermodynamics for Engineers*., McGraw-Hill: New York, 1995; 159–188.
29. Incropera, F.P.; Dewitt, D.P. *Introduction to Heat Transfer;* 3rd Ed.; John Wiley & Sons: New York, 1996.

Drying Technology, 23: 473–495, 2005

ISSN: 0737-3937 print/1532-2300 online
DOI: 10.1080/DRT-200054121

Taylor & Francis
Taylor & Francis Group

High Temperature Spouted Bed Paddy Drying with Varied Downcomer Air Flows and Moisture Contents: Effects on Drying Kinetics, Critical Moisture Content, and Milling Quality

Thanid Madhiyanon*
Department of Mechanical Engineering, Mahanakorn University of Technology, Nong Chok, Bangkok, Thailand

Somchart Soponronnarit
School of Energy and Materials, King Mongkut's University of Technology, Thonburi, Bangkok, Thailand

Abstract: This research is an experimental study on paddy drying conducted in a two-dimensional spouted bed batch dryer to investigate the effects of downcomer airflow, drying temperature, and initial moisture content on drying kinetics, milling quality, and thermal energy consumption. The system of spouted bed drying and a comparison of spouted bed drying in the present study, and fluidized bed drying in the related literature, are also discussed. Downcomer air flows of 0, 20, and 30% ([defined as mass flow rate of downcomer air/total mass flow rate of air] × 100%), inlet air temperatures of 110, 130, and 150°C, and initial moisture contents of 18–35% d.b. were used. It was found that moisture transfer did not only occur in the spout region but also took place in the downcomer region. The moisture content and temperature of the paddy dropped as grain moved downward in the downcomer, which resulted from the presence of an evaporative cooling phenomenon. The characterization of drying curves regardless of any drying condition could be described by nearly linear relationships between moisture content and time. Although high downcomer air flow and drying temperature could enhance effective moisture reduction, they caused an adverse decrease in critical moisture content and HRY (head rice yield). Critical moisture content and HRY could also increase with an increase in initial moisture content. The difference in moisture content between the initial and critical moisture contents varied between 4.5 and 8.0%d.b., depending upon drying conditions. No significant

*Correspondence: Thanid Madhiyanon, Ph.D., Department of Mechanical Engineering, Mahanakorn University of Technology, 51 Cheum-Sampan Rd., Nong Chok, Bangkok 10350, Thailand. E-mail: thanid_m@yahoo.com, thanid_m@mut.ac.th

effect on color was evident. From the point of view of HRY, the correct management of a two-stage spouted bed drying system could be a suitable and attractive alternative for rice mills. Finally, a comparison between the spouted bed drying and fluidized bed drying showed that the spouted bed had advantages over the fluidized bed in terms of product quality. The specific drying rates (kg water evaporated $h^{-1}m^{-3}$) of both techniques were comparable. With respect to energy consumption, spouted bed drying was not as efficient as fluidized bed drying for intermediate initial moisture content, but a contrary result was obtained for low initial moisture content.

Keywords: Dehydration; Dryer; Fluidized bed; Head rice yield; Product quality; Rice mill; Rough rice; Spouting; Thermal energy consumption; Whiteness

INTRODUCTION

The combination of two hydrodynamic features, i.e., pneumatic transport, which is accompanied by intensive heat and mass transfers, and moving bed transport, which gives a chance for moisture relaxation as a tempering process, is a major feature of the spouted bed technique. The spouted bed technique was reviewed by Pallai et al.[1] The design principle was proposed by Passos et al.[2] A two-dimensional spouted bed dryer was first proposed by Mujumdar[3] in order to overcome the scaling-up limitations of the conventional cylindrical-conical spouted bed. Kalwar et al.[4] and Kalwar and Raghavan[5,6] later modified it with draft plates to study the drying of soybean, wheat, corn, and shelled corn. They found that the drying kinetics of these cereal grains during the constant drying rate period did not clearly exist. But the phenomenon could be represented by Page's equation. On the contrary, the experimental results found by Wetchakama et al.,[7] Nguyen,[8] Nguyen et al.,[9] and the recent work of Wiriyaumpaiwong et al.[10] showed nearly linear moisture and time relationships. A similar result was confirmed by a mathematical simulation performed by Madhiyanon et al.[11] Tulasidas et al.[12] found that effective moisture diffusion coefficient and drying rate increased as bed height decreased. This resulted from the shorter cycle time, which increased the intensive heat transfer period in the spout region. Drying characteristics were reported elsewhere in the literature.[13–18] However, the product quality after drying has received less attention in the literature, although it is very important and usually employed in appraising the success or failure of a grain drying system.

Recently, there was an attempt to introduce the two-dimensional spouted bed drying technique into a rice mill (Madhiyanon et al.[19]). The prototype displayed a maximum capacity of $3550\,kg\,h^{-1}$ and a thermal energy consumption of 3.5–7.0 MJ (kg water evaporated)$^{-1}$, using 140–160°C drying temperatures and 0.6–0.7 fraction of air recycled. No serious loss in milling quality was observed. However, the prototype had limited success in moisture reduction due to insufficient dryer length. Madhiyanon et al.[20] developed a mathematical model for the prototype of continuous spouted bed dryer and found very good agreement between the simulated and experimental results.

However, after evaluating the experimental results of Madhiyanon et al.[19] it was believed that the continuous spouted bed paddy dryer had not been ready for positioning itself among other conventional dryers or fluidized bed paddy dryers that are now popular in Thai rice mills. Three main questions about spouted bed paddy drying have as yet not been answered, i.e., 1) how to maximize drying capacity in terms of drying rate per unit volume of dryer and related quality in terms of head rice yield; 2) if dryer length is extended in order to increase mean residence time, which results in more moisture reduction than that achieved by the prototype, are there any adverse effects on milling quality; and, finally 3) what strategies would be suitable for managing moist paddy with a variety of moisture contents. Information on the milling quality of paddy dried by spouted bed technique was rarely found. Only Nguyen et al.[9] reported that their triangular spouted bed dryer could continuously reduce paddy moisture content to around 18%d.b. with a satisfactory head rice yield regardless of drying temperature reaching up to 160°C.

The main objectives of this study are 1) to investigate the effects of introducing air through downcomer regions on drying kinetics, which is expected to promote intensive drying without any change of dryer volume; 2) to study the impact of drying conditions, i.e., drying temperatures, downcomer air flow, and initial moisture content, on the physical properties of rice after the milling process; 3) to determine a suitable system for drying paddy by spouted bed technique through analysis of the experimental results for drying kinetics and milling quality; and, finally, 4) to compare the present work and the work involved in fluidized bed paddy drying (Tirawanichakul et al.,[21] Poomsa-ad et al.[22]). We anticipate that this research will provide valuable outcomes for the rice mill industry and lead to further development of an industrial-scale continuous spouted bed paddy dryer that is acceptable for the rice mill industry.

MATERIALS AND METHODS

Materials

This experiment with paddy drying was conducted using a two-dimensional spouted bed batch dryer, as shown in Fig. 1. The dryer included

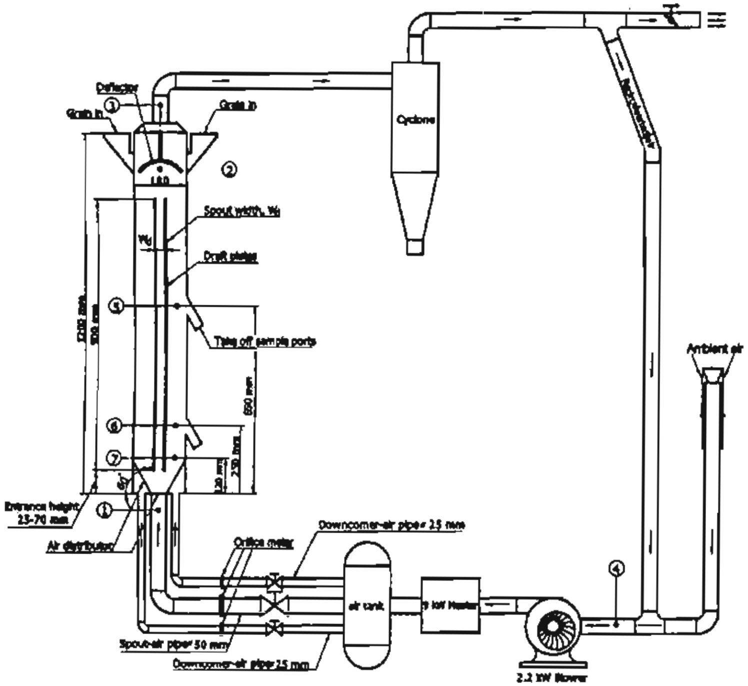

Figure 1. Schematic diagram of the two-dimensional spouted bed dryer with various downcomer air flow and temperature measurement positions.

a vertical rectangular chamber with a tempered glass window fitted to the front to permit visualization of the grain flow pattern, and a slant base chamber with an angle of 60°. Two draft plates, 90 cm in height, were installed centrally, such that each draft plate was 3.7 cm apart from the other. The overall dimensions were 80 cm in width, 8.4 cm in depth, and 120 cm in height. To investigate the drying kinetics and milling quality in terms of head rice yield and whiteness when air was introduced through the downcomer regions, hot air was distributed at the bottom of the slant base chamber through three air inlets, namely a central rectangular air inlet serving for the spout region with 3 cm in width and 8.4 cm in depth, and two round air inlets for the downcomer regions, each being 2.5 cm in diameter.

Air was heated by six electric heaters with a capacity of 1.5 kW each. The inlet air temperature was automatically controlled by a PID temperature controller with an accuracy of ±1°C. Temperatures were measured by a data logger and a temperature indicator with an accuracy

of ±1°C connected to a type K thermocouple. Air flow rates at high temperature were regulated by three orifice meters incorporating manual valves. For air recycled with temperatures under 90°C, air velocity was measured by hot wire anemometer with an accuracy of ±0.3 m/s and for temperatures of 90°C or more, a Pitot-static tube with U-tube manometer was used. A 2.2 kW variable speed drive was used to regulate blower motor speed to attain the desired air flow rate that could sustain the stability of spouting behavior, even when sharing much of the hot air for the downcomer regions. A three-phase kilowatt-hour meter was used to measure heater energy usage. One variety of long-grain rough rice, i.e., Suphanburi-1, which contains a high amylose content (27%) (Tirawanichakul et al.[21]) provided by the National Rice Research Center, Thailand, was selected as the test material.

Experiment Setup

Paddy moisture content was prepared by rewetting and keeping it in cold storage in a temperature range of 4–6°C for 7 days. During the cold storage period, paddy was mixed thoroughly once each day to ensure moisture uniformity. A preliminary study found that grain velocity was impacted upon and varied according to different fractions of downcomer air flow to total air flow, which could have either positive or negative effects on drying kinetics. Therefore, to eliminate the influence of different grain velocities accompanied by different airflows through the downcomer regions, the entrance height (see Fig. 1) was adjusted from one experiment to another to minimize any variations in grain velocity. Measurement of grain velocity was done by flow visualization and a stop watch. However, the finding in our experiments was that the maximum deviation in grain velocity did not exceed 15%. By visualizing paddy velocities, it was found that the lowest paddy velocity was 0.7 cm/s for 0% downcomer air flow, whereas it was nearly 1.0 cm/s for the remaining downcomer air flows (20 and 30%). By visualization, it could be seen that if air were allowed to flow upward through the downcomer, it would facilitate the circulation of grains at the bottom and hence grains stacked above could move downward easily to replace the ones below. In all experiments, the total mass flow rate of air was held constant at $0.053\,kg\,s^{-1}$.

The paddy samples for each set of conditions were collected at intervals of 2–3 mins for moisture content evaluation, milling quality, and energy consumption. Particularly for determining moisture variations in the downcomer region, samples were taken at distances of 23 and 63 cm above the air distributor. The total amount of sample taken from a dryer for each experiment was restricted to not more than 5% of the initial holdup (6 kg) to ensure that the process mechanism was not deviated or disturbed. Therefore, several experiments were done to complete each set of conditions and more than 280 experiments were done for this study.

Experimental Conditions

Six kilograms of paddy, which created a bed height of 72 cm, were loaded into the drying chamber for each experiment. The inlet air temperatures were set at 110, 130, and 150°C. The total air mass flow rate for all experiments was held constant at around 0.053 kg/s, and some of it was divided and sent to the downcomer regions. The percentages of downcomer air flow ([mass flow rate of downcomer air/total mass flow rate of air] × 100%) were controlled at 0 (no downcomer air), 20, and 30%, respectively. Fractions of air recycled were varied within the range 0.75 to 0.80. Besides studying the effects of downcomer air flow and drying temperature, the effect of initial moisture content on critical moisture content (considered as the lowest that moisture content could be reduced before significant grain damage) and energy consumption were also studied. Thus, paddy was rewetted until reaching desirable moisture levels in the range of 18–35%d.b.

Physical Properties

In order to determine the moisture content of the paddy, 20 g samples of paddy were weighed with an electronic balance with an accuracy of 0.0001 g and were dried in a hot air oven at 103°C for 72 h. Before determining the quality of the paddy in terms of head rice yield and whiteness, paddy samples taken at each time step were dried under room conditions for 2 weeks or until the moisture content had been reduced to around 16%d.b. Then, each 125 g paddy sample was shelled by Satake rubber roll dehusker, polished by Satake rice polisher, and graded by a Satake grader, respectively. Finally, its color was measured by a Kett digital whiteness meter, which was calibrated with a white color reference.

RESULTS AND DISCUSSION

Variation of Air and Grain Temperatures

All temperatures within the dryer were measured at the positions shown in Fig. 1. The experimental results showed that even using the varied drying temperatures with the same downcomer air flow, air and grain temperature variations showed a similar trend. The experiments carried

out at 130°C drying temperature were chosen as an example to show the influence of downcomer air flow on temperature change within the dryer, as shown in Figs. 2a–c. It was apparent that the temperature difference between the inlet and exit air temperatures (curves 1 and 3), which represented the amount of heat consumed for moisture removal, was nearly constant throughout the drying period, which did not generally occur in other batch drying techniques. This was also found in related literatures.[7–10,11] In additional, the temperature difference increased with higher downcomer air flow.

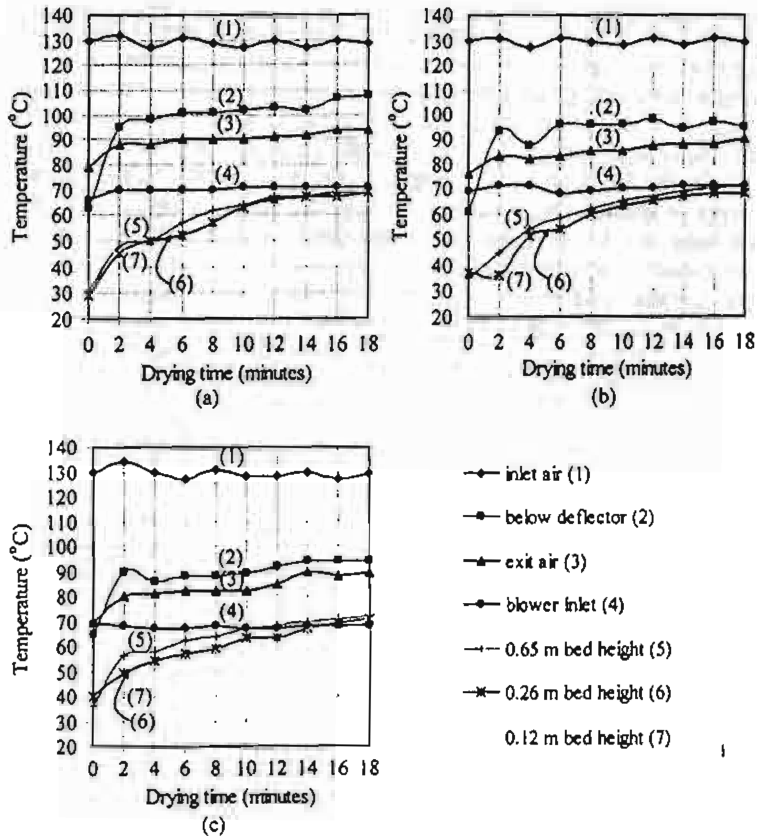

Figure 2. Variation of air and grain temperatures within the dryer according to different percentages of downcomer air flow (inlet temperature 130°C). (a) 0% Downcomer air flow. (b) 20% Downcomer air flow. (c) 30% Downcomer air flow.

According to the simulated results obtained from Madhiyanon et al.,[11] grain and air temperatures approached equilibrium within a few centimeters upstream from the air inlet. Thus, temperatures measured in the downcomer should represent the grain temperatures in the following text. Figs. 2a–c show that paddy temperatures decreased around 2–5°C during downstream movement, from 0.65 m (curve 5) to 0.12 m (curve 7). An explanatory hypothesis for this was the presence of an evaporative cooling phenomenon (instead of conventional drying process) while the paddy was traveling in the downcomer. This would be confirmed by the experimental results of moisture reduction inside the downcomer region. Finally, the effect of downcomer air flow on grain temperature was observed. When additional downcomer air flow was introduced, the paddy at the bottom had higher temperatures (curve 7) and would approximate the temperatures of the paddy in the near proximity above (curve 6). However, they were still lower than the temperatures of the paddy at the top (curve 5). Furthermore, it was also demonstrated that high grain temperature, accompanied by high downcomer air flow, was directly related to the drying rate and will be discussed later.

Moisture Reduction in the Downcomer Region

Madhiyanon et al.[11] presented simulation results that indicated that moisture reduction of grains did not only occur in the spout region, but also occurred in the downcomer region due to air leakage from the central inlet to the downcomer. This was proven experimentally by the present study. As shown in Figs. 3a–f, corresponding to experiments allowing air penetration to the downcomer (0, 20, and 30% downcomer air flow), moisture content of the paddy in the downcomer had been reduced around 0.2 to 0.7%d.b. from the moisture content at the beginning of the downcomer period for each 0.4 m trip of downstream movement (see Fig. 1 for positions of sample taking). The results also revealed that 20 and 30% downcomer air flows offered greater moisture reduction than no downcomer air flow (0%) (comparing Figs. 3a and 3f; 3b and 3d). However, in summary, it was found that operating the dryer at 20 and 30% downcomer air flows yielded no significant differences in moisture reduction. This was attributed to the moisture transfer mechanism, with internal control by moisture diffusion rather than external surface convective mass transfer. It was interesting to note that moisture reduction in the downcomer largely took place by "evaporative cooling phenomena," not conventional drying. Since the downcomer air flow had a low mass compared with that of the grain, it did not have enough energy to evaporate the moisture from the paddy. Specifically, it approached thermal equilibrium conditions with the paddy[11] and, therefore, decreased moisture in the downcomer should result from heat accumulating inside the paddy, which performed as an internal heat generator to evaporate the water at the paddy surface. Then the water was picked up by the air uniformly distributed through the downcomer, which consequently causing the paddy to cool down while moving downward in the downcomer, as previously described.

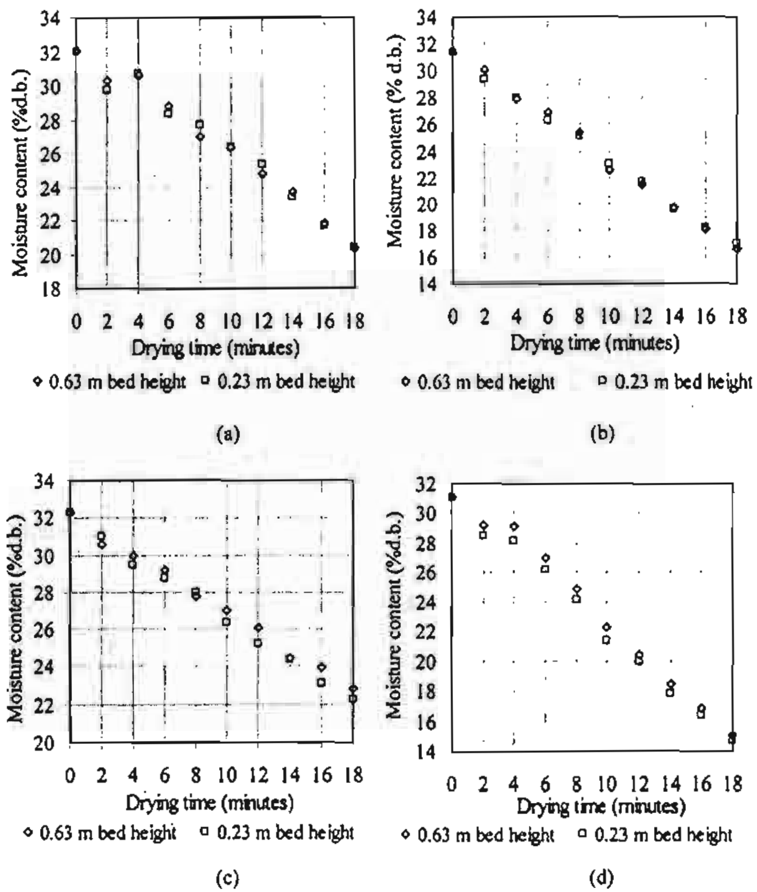

Figure 3. Moisture reduction along with the bed height in the downcomer region. (a) Inlet air temperature 130°C; 0% of downcomer air flow. (b) Inlet air temperature 150°C; 0% of downcomer air flow. (c) Inlet air temperature 110°C; 20% of downcomer air flow. (d) Inlet air temperature 150°C; 20% of downcomer air flow. (e) Inlet air temperature 110°C; 30% of downcomer air flow. (f) Inlet air temperature 130°C; 30% of downcomer air flow.

Drying Curve Characteristics and Effective Moisture Reduction

Figures 4a–c exhibits the drying characteristics and the effects of drying temperatures on effective moisture reduction, which represent a combination of moisture reduction in the spout and downcomer regions. All experiments, regardless of varieties of drying temperatures and downcomer air flow conditions, found that most of the drying curves had similar drying characteristics, in which the correlations between moisture content and time were nearly linear relationships, as can be seen in

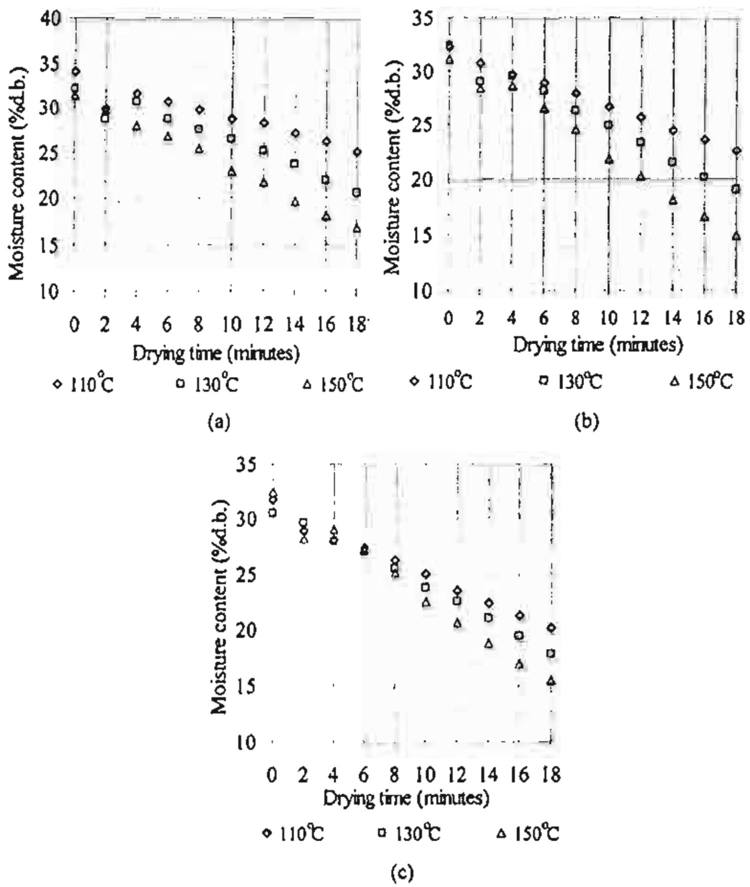

Figure 4. Nearly linear characteristic of spouted bed drying regardless of drying conditions of temperature and percentage of downcomer air flow. (a) 0% of downcomer air flow. (b) 20% of downcomer air flow.

previous studies.[7–11] This resulted from the assistance of moisture relaxation in the downcomer motion period, i.e., causing water to migrate from the inside to the outside of the grain kernel. This should facilitate water vaporization when grains transit to the spout region, where the grain is exposed to relatively high temperatures and air velocity. The drying kinetics of spouted bed are very different from the fluidized bed technique, in which the correlation between moisture content and drying time is exponential.[23,24] It was evident that the drying temperature significantly influenced the drying rate as the drying rate increased with increased drying temperature. Furthermore, in comparing Figs. 4a–c, it was clear that the drying rate was directly related to the drying temperature, since rapid decreases in moisture were achieved by applying high temperatures.

Figures 5a–c show the effect of downcomer airflow on effective moisture reduction. It was found that effective moisture reduction increased with increased downcomer airflow. However, moisture reduction in the downcomer was nearly the same, using either high or low downcomer air flow. Therefore, the difference of moisture reduction between using 0, 20, and 30% downcomer air flow should be gained from the drying mechanism in the spout region. This resulted from the grain being hotter with higher downcomer air flow, as seen in curve 7, in Figs. 2a–c.

Milling Quality

Figures 6–8 show the experimental results of milling quality, with relative head rice yield (HRY) variations with decreased moisture content at drying temperatures of 110, 130, and 150°C. At the beginning of drying, relative HRY increased and thereafter decreased along with decreasing moisture content. At the beginning, paddy drying under sufficiently high temperature and moisture content was quite suitable for initiating the gelatinization process. Therefore, the kernel became more resistant to cracking due to partial gelatinization that occurred at the surface of the rice kernel. However, as moisture was further continuously reduced, more stresses developed with a steep moisture gradient dominating the gelatinization effect, resulting in grain breakage during the milling process. In this study, initial moisture contents were classified into three levels, low (17–21%d.b.), medium (24–28%d.b.), and high (31–35%d.b.).

The Effects of Drying Temperatures, Downcomer Air Flows, and Initial Moisture Content on Critical Moisture Content

For drying paddy at a temperature of 110°C, paddy with a low initial moisture content of 21%d.b. could be safely dried to 14%d.b., which

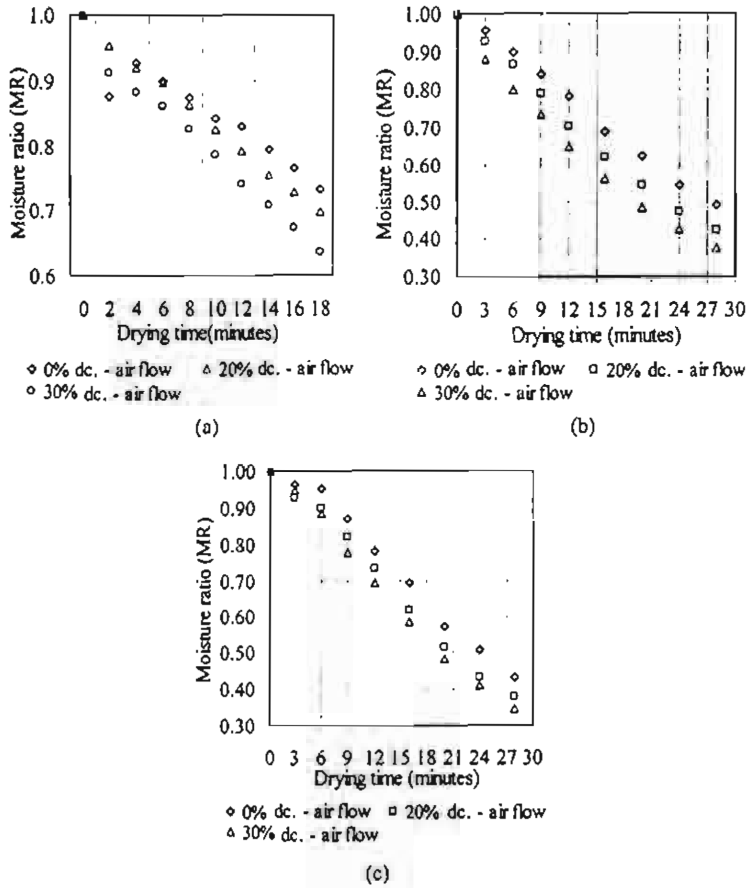

Figure 5. The effect of downcomer air flow on effective moisture reduction (dc. = downcomer). (a) Inlet air temperature 110°C. (b) Inlet air temperature 130°C.

was quite safe for storage (Fig. 6a). In the case of medium initial moisture contents of 27–28%d.b. (Fig. 6b), it was found that, in order to preserve paddy quality, paddy should not be continuously dried to a moisture level lower than the critical moisture content (defined as moisture content with 100 ± 5% relative HRY) of 21%d.b. These results are presented numerically in Table 1.

For a drying temperature of 130°C, moisture content could be reduced from 18%d.b. (low moisture content) to 13%d.b. without any

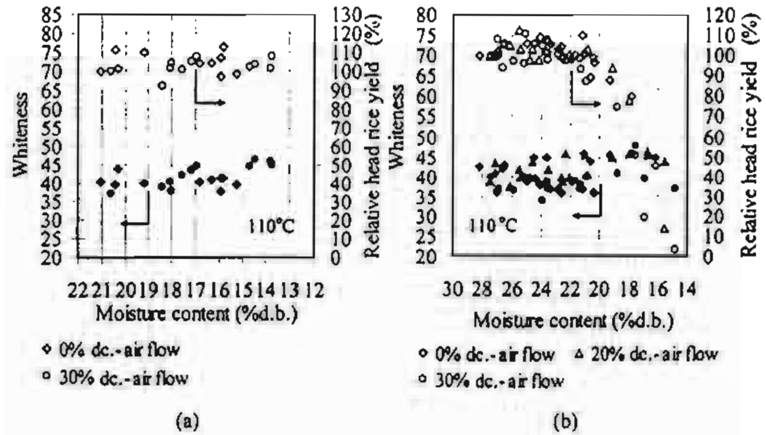

Figure 6. Variation of relative head rice yield and whiteness in relation to moisture content and initial moisture content at 110°C drying temperature (dc. = downcomer). (a) Low initial moisture content, 20.5 and 21%d.b. (whiteness reference, 37 and 40). (b) Medium initial moisture content, 27 and 28%d.b. (whiteness reference, 38 and 43).

loss of milling quality, as shown in Fig. 7a. However, as shown in Fig. 7b, paddy with a medium initial moisture content of 27–28%d.b. could not be dried below a critical moisture content of 22%d.b. in the case of 0% downcomer air flow, and the critical moisture content increased in the case of 20 and 30% downcomer air flows. In the case of a high initial moisture of 35%d.b., paddy could be dried to a critical moisture of 27–28%d.b. Table 1 gives more numeric details.

Fig. 8a shows the results of HRY under the highest drying temperature (150°C) and medium initial moisture contents of 24–25%d.b. The results show that the critical moisture content was about 19.5–20.5%d.b. and the critical moisture content for 30% downcomer air flow was less than that for 0% downcomer air flow, of around 1%d.b. For drying paddy with high initial moisture contents of 31–32%d.b., as shown in Fig. 8b, the critical moisture content was around 25–26%d.b.

In summary, a higher drying temperature was responsible for a higher critical moisture content, as seen by comparing Figs. 6b and 7b. Data in Figs. 6–8 and Table 1 show the influence of downcomer air flow on HRY, in that 0% downcomer air flow gave the best relative HRY results, while 30% downcomer air flow gave the worst. It was found that critical moisture content increased with initial moisture content. Finally, the differences between the initial and critical moisture

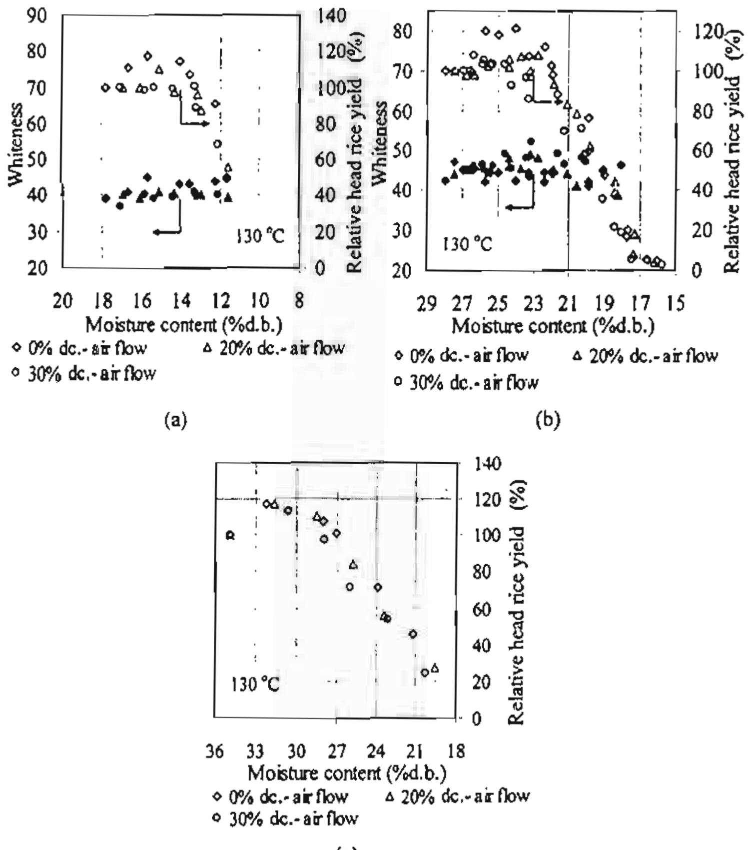

Figure 7. Variation of relative head rice yield and whiteness in relation to moisture content and initial moisture content at 130°C drying temperature (dc. = downcomer). (a) Low initial moisture content, 17%d.b. (whiteness reference, 39). (b) Medium initial moisture content, 26 and 27.5%d.b. (whiteness reference, 41 and 44. (c). High initial moisture content, 35%d.b.

contents varied between 4.5 to 8.0%d.b., depending upon the drying conditions.

Whiteness

Besides HRY, whiteness was also an important issue for judging paddy quality. The experimental results indicated no serious loss in whiteness, as shown in Figs. 6–8 and Table 1.

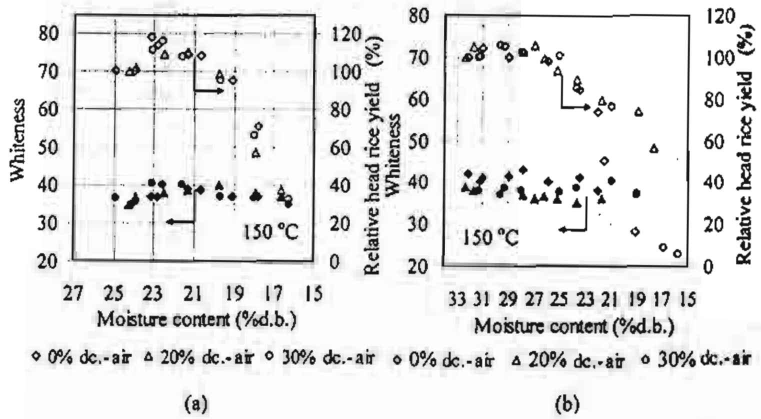

Figure 8. Variation of relative head rice yield and whiteness in relation to moisture content and initial moisture content at 150°C drying temperature (dc. = downcomer). (a) Medium initial moisture content, 24 and 25%d.b. (whiteness reference, 35 and 37). (b) High initial moisture content, 32%d.b. (whiteness reference, 38 and 42).

Thermal Energy Consumption

The experimental results (Table 2) indicated that the specific thermal energy consumption (SEC_{th}) slightly differed for any downcomer air flow and drying temperature. Using temperatures of 110, 130, and 150°C, with 75–80% recirculated air flow for drying paddy from a moisture content of 31%d.b. to approximately 15–20%d.b., consumed 5–6 MJ(kg water evaporated)$^{-1}$. These values of SEC_{th} were in line with 3.5–7.0 MJ(kg water evaporated)$^{-1}$ obtained from an industrial-scale continuous spouted bed paddy dryer prototype.[19] They were reasonable and relatively comparable with other conventional commercial dryers. Moreover, due to the almost constant drying rate characteristic of the spouted bed technique, the SEC_{th} remains almost unchanged throughout the entire drying period. Therefore, in respect to energy utilization, the spouted bed dryer would be competitive with other commercial dryers, especially for the intermediate moisture level.

Strategy for the Spouted Bed Drying Technique

The results of the paddy quality evaluation indicated that drying paddy from a high moisture content level to a level that was considered safe for storage in one stage was not recommended, and this is also true for

Table 1. Summary of the experimental results in accordance with Figures 6–8

Drying temp. (°C)	Fig. Nos.	%DC.[a] air flow (%)	Initial MC (%d.b.)	Critical MC (moisture content at 100 ± 5% relative HRY, %d.b.)	Diff.[b] (%d.b.)	Reference whiteness	Average whiteness after drying
110	Fig. 6a	0	21.0	< 15.0	5.5	41	41
		20	—	—	—	—	—
		30	21.0	< 15.0	7.0	37	43
	Fig. 6b	0	27.0–28.0	20.5–21.0	6.5–7.0	42	41
		20	27.0	20.5–21.0	6.0–6.5	41	42
		30	27.0–27.4	21.5	6.0	39	39
130	Fig. 7a	0	17.8	13.0	4.8	39	43
		20	17.0	13.0	4.0	40	40
		30	17.0	13.0	4.0	37	40
	Fig. 7b	0	27.2–28.0	22.0	5.5–6.5	45	43
		20	26.7–27.4	22.0–23.5	3.5–5.5	45	45
		30	26.4–27.0	24.0–24.5	3.0–3.5	45	47
	Fig. 7c	0	35.0	27.0	8.0	—	—
		20	35.0	27.0	8.0	—	—
		30	35.0	28.0	7.0	—	—
150	Fig. 8a	0	24.0	19.5	4.5	36	38
		20	24.2	20.0	4.2	35	38
		30	25.0	20.5	4.5	37	38
	Fig. 8b	0	32.0	25.0	7.0	42	41
		20	32.3	25.0	7.3	39	36
		30	31.3	25.0	6.3	38	38

[a]DC = downcomer.
[b]Difference in moisture content between initial and critical moisture contents.

Table 2. The specific thermal energy consumption (SEC_{th}) of the spouted bed dryer.[a]

Drying temp. (°C)	Downcomer air (%)	Initial moisture content (%d.b.)	Final moisture content (%d.b.)	SEC_{th}[b] (MJ/kg water evap.)
110	0	34.0	24.9	4.9
	20	32.3	22.5	5.7
	30	31.6	20.1	5.5
130	0	32.0	20.4	5.8
	20	32.8	20.2	5.7
	30	30.5	17.8	5.6
150	0	31.4	16.8	5.9
	20	32.2	16.6	5.2
	30	32.5	15.5	5.6

[a]Air recycled fraction ranged between 0.7 and 0.8.
[b]Using diesel oil with 97% combustion efficiency instead of electrical heaters was an assumption for these SEC_{th} calculations.

fluidized bed drying or other conventional hot air drying. Therefore, two-stage drying (coupled with an intermediate tempering process) should be quite suitable for the spouted bed paddy drying. For moist paddy with a high moisture content, such as 30%d.b., which is within the moisture content range at harvest, temperatures of 130 or 150°C without downcomer air flow can be used for first-stage drying with a consequent approximate moisture content of 24%d.b. at the end of the first stage (interpreted with the assistance of Table 1). For the second stage, a temperature of 110°C with 0–30% downcomer air flows would give a final moisture content around 17–18%d.b. which is close to safe storage level. Before storage, paddy will be cooled by ambient air and the moisture content will further drop to 16–17%d.b. Therefore, properly managed spouted bed paddy drying could be an attractive alternative for rice mills.

Comparison of Spouted Bed and Fluidized Bed Techniques

Milling Quality Comparison

Comparing the drying capacity and milling quality of the spouted bed and fluidized bed techniques should be synchronized, since high drying capacity has no meaning if the product quality after drying is unacceptable. Regarding milling quality after the drying of paddy, Poomsa-ad et al.[22] reported that while drying paddy with a high initial moisture content of 30–35%d.b. with high drying temperatures of 110, 130, 150, and 170°C in a single stage of a lab-scale fluidized bed dryer, more than 80% relative HRY, if final moisture content was above 25%d.b., could be achieved. The grain temperatures were in the range of 70–90°C. Under similar drying conditions to the present study, spouted bed dryer was able to reduce moisture content from 31 to 35%d.b. to 25 to 27%d.b. producing 100 ± 5% relative HRY (Figs. 7c, 8b, and Table 1).

For drying paddy with a medium moisture content, the study by Poomsa-ad et al.[22] found that continuous drying of paddy from 25 to 20%d.b. would have resulted in low relative HRY, which was lower than 40%, unless incorporating a subsequent tempering for 30 mins, which could raise relative HRY to more than 60%. Meanwhile, spouted bed drying could produce100 ± 5% relative HRY while reducing moisture content from 24 to 19.5%d.b. and 20 to 14%d.b. without tempering process (Figs. 6a, 8a, and Table 1). Poomsa-ad et al.[22] also noted that, to achieve high HRY under a high drying temperature in one pass of fluidized drying, corresponding to a grain temperature not above 100°C, the moisture content of paddy should not be reduced below 22.5%d.b., and a subsequent tempering for 30 mins was strongly recommended to preserve HRY.

As the above discussion has indicated, it was clear that, if starting drying with a high initial moisture content (30–35%d.b.), spouted bed drying was able to reach a lower critical moisture content compared with fluidized bed drying. In the other words, spouted bed drying could reach the same final moisture content in a single drying stage as fluidized bed drying, but achieve a higher HRY. For an initial moisture content no greater than 25%d.b., spouted bed drying offered greater moisture content decrease from the beginning, and better HRY.

Drying Capacity Comparison

The specific drying rate, defined as the drying rate per unit volume of drying chamber (kg water evaporated $h^{-1}m^{-3}$), was used as an index to measure the drying capacity of the dryer. A comparison of the specific drying rates of both techniques is shown in Table 3. The calculation of dryer volume according to spouted bed drying was based on dimensions, as shown in Fig. 1, while that of fluidized bed drying was based on the fluidized bed dryer studied by Tirawanichakul et al.[21] In that study, the dryer was of a cylindrical shape, 20 cm in diameter and 140 cm in height, and 1.9 kg of paddy corresponding to 10 cm static bed height was maintained constant. However, a drying chamber height of 100 cm, which largely matches the desired height of a fluidized bed paddy dryer was used in the present calculations. As Table 3 shows, if drying time was the only factor considered an indicator of drying capacity, it would appear that fluidized bed drying could reduce moisture substantially faster than

Table 3. Comparison of fluidized bed and spouted bed drying performance

Drying temp. (°C)	Initial moisture content (%d.b.)	Final moisture content (%d.b.)	Drying time (min)	Specific drying rate (kg water $h^{-1}m^{-3}$)
The fluidized bed drying[21]				
110	25.0	22.0	1.3	67
	28.2	21.5	2.4	78
130	28.2	22.7	1.4	110
	32.5	21.5	2.5	120
150	28.2	22.3	1.1	150
	32.5	22.0	2.0	144
The spouted bed drying (present study)				
110	21.0	14.0	15.0	80
	27.5	23.5	9.0	72
	27.5	20.9	15.0	72
130	26.9	21.2	10.0	93
	26.9	18.4	16.0	87
	35.0	27.0	12.0	103
150	25.0	18.0	10.0	116
	31.3	25.0	8.0	125
	31.3	20.9	12.0	137

spouted bed drying. However, the volume of the dryer and its holdup (capability of holding an amount of paddy for one batch of an experiment) should be taken into account for a fair comparison, and thus the specific drying rate was introduced as an indicator for this purpose.

Data in Table 3 show that the specific drying rates of spouted bed drying were comparable with those of fluidized bed drying at all drying temperatures. For fluidized bed drying, with an intermediate temperature of 110°C, the advantage of aggressive heat and mass transfer, due to the continuous contact of the grain and the air and good mixing characteristic, was counteracted by lesser driving force due to a lower temperature gradient between grain and air. Despite continuous exposure of grain to air, spouted bed drying allowed relaxation time (approximate 110 s for one cycle) in the downcomer period, which should help substantially in equalizing temperatures within the grain kernel. Thus, the surface temperature of the paddy at the end of downcomer period was not as high as when it was just emerging from the spout region, which led to enhanced heat transfer between the paddy surface and the air in the spout region.

For a high temperature of 150°C, spouted bed drying could also compete with fluidized bed drying, which could be explained by the observation that the drying characteristics of the fluidized bed were in

Arrhenius, or exponential, form, while an almost linear relationship represented the spouted bed drying characteristics. The fluidized bed conferred a steep decrease in moisture at the start of the drying process (accelerating drying speed), and thereafter moisture gradually decreased (decelerating drying speed), while a special feature of spouted bed drying was that it gave an almost constant drying rate, regardless of any moisture decrease from the initial moisture content. This made the specific drying rate of the spouted bed lag behind that of the fluidized bed at the start, while in the remaining period it could catch up with that of the fluidized bed.

Thermal Energy Consumption Comparison

Finally, the thermal energy consumption of both techniques was compared. Since experimental results of the energy consumption of a lab-scale fluidized bed were not available, records of thermal energy consumption of commercial fluidized bed dryers, as reported by Soponronnarit et al.[25] (dryers with capacities of 2.5–5 tons/h and 5–10 tons/h), were used for this comparison. That study concluded that when drying paddy with initial moisture contents between 26.0–30.6%d.b., down to 21.0–23.0%d.b., SECsth (specific thermal energy consumption) were in the range 2.5–4.0 MJ(kg water evaporated)$^{-1}$, which was quite low compared with a conventional hot air dryer. However, in the case of drying paddy with low initial moisture content, such as 22.0%d.b. down to 20.1%d.b., SECth rose steeply to 7.8 MJ(kg water evaporated)$^{-1}$. Table 2 shows that the spouted bed could dry paddy from a high initial moisture content, i.e., 31.6–32.3%d.b. down to around 20.1–22.5%d.b. with SECsth of 5.5–5.7 MJ(kg water evaporated)$^{-1}$. Moreover, due to the almost constant drying rate characteristic of the spouted bed technique, the SECth should be almost the same for any level of moisture content. Table 2 indicates that it could reduce moisture content from 30.5 to 32.5%d.b. to 15.5 to 17.8%d.b. with nearly the same SECth of 5.6 MJ(kg water evaporated)$^{-1}$. In addition, referring to the data in Table 1 and the work done by Poomsa-ad et al.[22] it was necessary to divide the drying process into two stages to reduce moisture almost to safe storage level, while simultaneously maintaining acceptable milling qualities for both drying techniques. Therefore, the fluidized bed should consume less energy than the spouted bed for first-stage drying, but the opposite result would be obtained for second-stage drying, which normally starts with moisture contents around 20.0–22.0%d.b.

CONCLUSIONS

This experimental study of paddy drying in a two-dimensional spouted bed batch dryer was conducted to investigate the effects of drying temperature, downcomer air flow, and initial moisture content on drying kinetics, critical moisture content, and product quality. A comparison of spouted bed and fluidized bed drying and an appropriate system for spouted bed paddy drying were also discussed. The conclusions of this study follow.

1. Moisture decrease in spouted bed drying was a combination of moisture reduction in both the spout and downcomer regions. The evaporative cooling phenomenon was believed to be the main cause of moisture and bed temperature reduction, along with the downward movement of the paddy within the downcomer. It was demonstrated that downcomer air flows played an important role in effective moisture reduction, in that it increased with increasing downcomer air flow.
2. Drying curves, regardless of variations in drying temperature and downcomer air flow, were characterized by almost linear relationships between moisture content and time.
3. Drying conditions, such as drying temperature, amount of downcomer air flow, and initial moisture content, also significantly influenced critical moisture content and HRY. Using a high drying temperature and introducing downcomer air flow enhanced moisture reduction, but they had adverse effects on critical moisture content and HRY. The differences between initial and critical moisture contents were in the range of 4.5–8.0%d.b. and increasing with increases in initial moisture content.
4. From a product quality viewpoint, two-stage drying incorporating an intermediate tempering process appears suitable for a spouted bed paddy drying system. The commencement of drying with temperatures of 130 or 150°C for the first stage, followed by a drying temperature of 110°C for the second stage, is feasible.
5. A comparison of spouted bed paddy drying in the present study and fluidized bed paddy drying in the literature shows that for single-stage drying, the spouted bed provided significantly better product quality in terms of HRY than fluidized bed drying. The specific drying rates (kg water evaporated h^{-1} m^{-3}) of both techniques were comparable. Finally, the spouted bed consumed more energy than the fluidized bed when drying paddy with an intermediate initial moisture content, but the result was opposite with low initial moisture content. The SECsth of the spouted bed were almost the same at any level of moisture content and were in the range 5.5–5.7 MJ(kg water evaporated)$^{-1}$.

ACKNOWLEDGMENTS

This research was supported by a grant from Thailand Research Fund (TRF). We would like to gratefully acknowledge the contribution of Viboon Thepent (Post Harvest Engineering Research Group,